

UNIVERSITY OF CALIFORNIA,
IRVINE

Electron Affinity in Approximate Density Functional Theory and
the Role of Semiclassics in Orbital-Free Potential-Density Functional Theory

DISSERTATION

submitted in partial satisfaction of the requirements
for the degree of

DOCTOR OF PHILOSOPHY

in Chemistry

by

Dong Hyung Lee

Dissertation Committee:
Professor Kieron Burke, Chair
Professor Craig Martens
Professor Vladimir Mandelshtam

2010

Chapter 3 © 2010 American Chemical Society
Chapter 4 © 2009 American Institute of Physics
All other materials © 2010 Dong Hyung Lee

TABLE OF CONTENTS

	Page
LIST OF FIGURES	iv
LIST OF TABLES	vi
ACKNOWLEDGMENTS	viii
CURRICULUM VITAE	ix
ABSTRACT OF THE DISSERTATION	xii
1 Introduction	1
2 Background	4
2.1 Hohenberg-Kohn theorem	4
2.2 Kohn-Sham equation	7
2.3 Green's function	9
2.4 Uniform semiclassics in 1D	10
3 Accuracy of Electron Affinities of Atoms in Approximate DFT	13
3.1 Introduction	13
3.2 Computational details	18
3.3 Results and discussion	19
3.4 Why do limited basis sets work?	22
4 Condition on the Kohn-Sham Kinetic Energy	26
4.1 Introduction	26
4.2 Theory and Illustration	27
4.3 Large Z Methodology	31
4.4 Results and Interpretation	34
4.5 Modern Parametrization of Thomas-Fermi Density	43
4.6 Summary	52
5 Semiclassical Orbital-Free Potential-Density Functional Theory	54
5.1 Uniform semiclassical density	54
5.1.1 The leading term	56
5.1.2 Quantum corrections	59

5.1.3	The evanescent region	61
5.2	Uniform kinetic energy density	62
5.3	Different limit	64
5.4	Summary of equations	66
5.5	1D Applications	68
5.5.1	Harmonic potential	68
5.5.2	Morse potential	72
5.6	Is this variational?	73
5.7	Spherically symmetric 3D potential	76
5.7.1	Isotropic 3D harmonic potential	79
5.7.2	Bohr atom	81
5.8	Real atoms	86
5.8.1	Single-point calculation	86
5.8.2	Semiclassical orbital-free potential-density functional	89
6	Conclusion	94
	Bibliography	97
	Appendices	101
A	Construction of modified GEA	101

LIST OF FIGURES

	Page
3.1 Comparison of KS potentials of Li^- . The black line is essentially exact, using a density from quantum Monte Carlo. The red (dashed) line is the LDA potential on that density. The horizontal lines mark the HOMO (2s orbital) energies.	14
3.2 Comparison of errors (Δ) in ionization potentials and electron affinities in first 2 rows of periodic table. Energies are evaluated with B3LYP density functional(33; 34) evaluated on HF densities and on self-consistent densities within AVDZ basis set.	20
3.3 Comparison of errors (Δ) in IP's and EAs (in eV). Energies are evaluated with PBE density functional evaluated on the AVDZ basis set, except the square symbols, where the densities are found from a HF calculation.	21
3.4 Shifted exact $v_s(r)$ potential (eV). The HOMO from QMC is -0.62 eV, and the HOMO from LDA/AV5Z is 0.80 eV. We shift the exact v_s by the difference between eigenvalues.	22
3.5 Shifted exact $v_{xc}(r)$ potential (eV) in Li^- . The HOMO from QMC is -0.62 eV, and the HOMO from LDA/AV5Z is 0.80 eV. We shift the exact v_{xc} by the difference between eigenvalues.	23
3.6 Plot of the radial density errors for Li^- with various approximations. SCF densities are obtained with AVQZ. The exact density is from quantum Monte Carlo.	24
4.1 Percentage error between $c_1 Z^2 + c_2 Z^{5/3}$ and $\Delta T_s = T_s - c_0 Z^{7/3}$	29
4.2 Difference between $T_s/Z^{7/3}$ and $c_0 + c_1 Z^{-1/3} + c_2 Z^{-2/3}$ as a function of $Z^{-1/3}$	32
4.3 Percentage errors for atoms (from $Z = 1$ to $Z = 92$) using various approximations.	37
4.4 Accurate numerical $\Phi(y)$ and parametrized $\Phi(y)$ can not be distinguished.	44
4.5 Errors in the model, relative to numerical integrations.	44
4.6 Plot of the scaled radial densities of Ba and Ra using Eq.(4.33) and SCF densities. TF scaled densities of Ba and Ra are on top of each other.	50
4.7 Plot of the scaled reduced density gradient $s(r)$ (relative to the local Fermi wavelength) vs. $Z^{1/3}r$	51
4.8 Plot of the scaled reduced Laplacian $q(r)$ (relative to the local Fermi wavelength) vs. $Z^{1/3}r$	51

4.9	Plot of the reduced density gradient $t(r)$ (relative to the local screening length) vs. $Z^{1/3}r$. As $r \rightarrow \infty$, the TF $t \rightarrow 0.7071$	52
5.1	Contour of integration in the complex \mathcal{E} -plane.	55
5.2	1D systems.	65
5.3	Comparison of exact and semiclassical densities of a harmonic potential with $N = 2$	72
5.4	Comparison of exact and semiclassical KE densities of a harmonic potential with $N = 2$	72
5.5	Comparison of exact and semiclassical densities of Morse potential with $N = 2$	73
5.6	Comparison of exact and semiclassical KE densities of Morse potential with $N = 2$	74
5.7	Spherical 3D systems.	78
5.8	Comparison of exact and semiclassical densities of $l = 0$ orbitals with $N = 3$ for an isotropic 3D harmonic potential. Eq. (5.92) is used from $r = 0$ to r_I	81
5.9	Comparison of exact and semiclassical densities of $l = 1$ orbitals with $N = 3$ for an isotropic 3D harmonic potential. Eq. (5.92) is used from $r = 0$ to r_I	81
5.10	Comparison of exact and semiclassical densities of $l = 2$ orbitals with $N = 3$ for an isotropic 3D harmonic potential. Eq. (5.92) is used from $r = 0$ to r_I	82
5.11	Comparison of exact and semiclassical densities of $1s^1 2s^1 3s^1 4s^1$	84
5.12	Comparison of exact and semiclassical densities of $2p^1 3p^1 4p^1$	85
5.13	Comparison of exact and semiclassical densities of $3d^1 4d^1$	85
5.14	Comparison of exact and semiclassical densities of $4f^1$	86
5.15	Comparison of SCF-LDA and semiclassical densities of Kr. Eq. (5.93) is used from $r = 0$ to r_I . $(l + 1/2)^2$ is used for all orbitals instead of $l(l + 1)$	88
5.16	Comparison of SCF-LDA and semiclassical densities of Kr. Eq. (5.93) is used from $r = 0$ to r_I . $(l + 1/2)^2$ is used for all orbitals instead of $l(l + 1)$	89
5.17	SCF procedures for KS-DFT (left) and orbital-free potential-density functional theory (right).	90
5.18	Comparison of LDA-SCF and semiclassical SCF densities of Ar.	92
5.19	Convergence of total energies in each iterations	92

LIST OF TABLES

	Page
3.1 Errors in EAs (eV). Total energies for both neutral and negative atoms are evaluated on HF-SCF densities with aug-cc-pVDZ basis set.	19
3.2 Errors in EAs (eV). Total energies for both neutral and negative atoms are calculated by SCF procedure with aug-cc-pVDZ basis set.	21
4.1 The coefficients in the asymptotic expansion of the KS kinetic energy and various local and semilocal functionals. The fit was made to $Z=24$ (Cr), 25 (Mn), 30 (Zn), 31 (Ga), 61 (Pm), and 74 (W). The functionals of the last two rows are defined in section 4.4.	34
4.2 KS kinetic energy (T) in hartrees and various approximations for alkali-earth atoms.	36
4.3 Non-interacting kinetic energy (in hartrees) for molecules, and errors in approximations. All values are evaluated on the converged KS orbitals and densities obtained with B88-PW91 functionals, and the MGEA4 kinetic energies are evaluated using the TF and the GEA data from Ref. (57).	38
4.4 Jellium surface kinetic energies (erg/cm^2) and % error, which is $(\sigma_s^{app} - \sigma_s^{ex})/\sigma_s^{ex}$, of each approximation.	39
4.5 $10^4 \times (\gamma_s^{eff}(\mathbf{r}_s, N) - \gamma_s^{TF}(\mathbf{r}_s, N))$ in atomic units vs. $N = Z$ for neutral jellium spheres with $r_s = 3.93$ with various functionals. As $N = Z \rightarrow \infty$, γ_s^{eff} tends to the curvature kinetic energy of jellium, γ_s	40
4.6 KS kinetic energy (T) in hartrees and various approximations for noble atoms.	42
4.7 The values of β_i are found by fitting Eq.(4.22) to the accurate numerical solution, and those of α_i are the parameters of small- y expansion (65). B is given by 1.5880710226.	45
4.8 Various moments calculated with our model and with the models of Ref. (63; 64). Here $M_j^{(p)}$ is given by $\int dx x^p \left(\frac{\Phi(x)}{x}\right)^j$	48
5.1 The percentage errors of densities and KE densities at the turning point ($x = -\sqrt{2N}$) for a harmonic oscillator.	70
5.2 Errors of densities, kinetic energy, potential energy for a harmonic oscillator ($v(x) = x^2/2$).	71
5.3 Errors of kinetic energies and potential energies for a harmonic oscillator ($v(x) = x^2/2$). The semiclassical density is re-normalized to N to calculate kinetic energies from $t^{DF}(x)$ (Eq. (5.68)) and potential energies.	71

- 5.4 Variational principle. The trial potential, $\tilde{v}(x)$, is $x^p/2$ and the exact (target) potential is $x^4/2$. For all cases, the minimum of the total energy is at $p = 4$. 75
- 5.5 Variational principle for $N = 1$. The trial potential, $\tilde{v}(x)$, is αx^2 and the exact (target) potential is $3x^2/4$. The minimum of the total energy is at $\alpha = 3/4$. . 76

ACKNOWLEDGMENTS

I would like to thank my parents, parents-in-law, my two sisters and my brother-in-law for all the support they have given me the past 5 or 6 years.

Especially, I really thank my wife, Yumi Kim, for the dedicated support.

I would also like to thank Prof. Kieron Burke for his great advise and should acknowledge the help of co-authors Dr. Lucian A. Constantin, Prof. John P. Perdew for the paper “Condition on the Kohn-Sham kinetic energy, and modern parametrization of the Thomas-Fermi density” and Prof. Filipp U. Furche for the paper “Accuracy of Electron Affinities of Atoms in Approximate Density Functional Theory”. I also want to thank all the members in the Burke group, both past and present members and also everyone else whom I have known at Rutgers university and UCL.

Finally I acknowledge funding from NSF (CHE-0809859) and the Korea Science and Engineering Foundation Grant (No. C00063) as well as copyright permissions from American Institute of Physics (Reprinted with permission from Donghyung Lee, Lucian A. Constantin, John P. Perdew, and Kieron Burke, *J. Chem. Phys.* **130**, 034107 (2009). Copyright 2009, American Institute of Physics.) for Chapter 4 and American Chemical Society (Reproduced with permission from Donghyung Lee, Filipp Furche and Kieron Burke, *J. Phys. Chem. Lett.*, 2010, **1**, 2124 (2010). Copyright 2010 American Chemical Society.) for Chapter 3.

CURRICULUM VITAE

Dong Hyung Lee

EDUCATION

Doctor of Philosophy in Chemistry University of California, Irvine	2010 <i>Irvine, California</i>
Master of Science in Chemistry Seoul National University	2004 <i>Seoul, Korea</i>
Bachelor of Science in Chemistry Seoul National University	2002 <i>Seoul, Korea</i>

TEACHING EXPERIENCE

Teaching Assistant Teach discussion classes for general chemistry	2008, Fall quarter <i>UCI</i>
Teaching Assistant Teach general chemistry labs.	2005–2006 <i>Rutgers Univ.</i>
Teaching Assistant Teach computational chemistry labs for general chemistry.	2002 <i>Seoul Nat. Univ.</i>

CONFERENCES AND PRESENTATIONS

- Controlling Diaza-Cope rearrangement reactions with resonance assisted hydrogen bonds: Theoretical and experimental investigations
Donghyung Lee, Jik Chin, Fabrizio Mancin, Nirusha Thavarajah, Alan Lough, and Doo Soo Chung in The 227th ACS National Meeting, Anaheim, CA, 2004
- Prediction of retention factors in micellar electrokinetic chromatography using a density functional theory and a semi-empirical method
Donghyung Lee, Sungu Hwang, and Doo Soo Chung in The 227th ACS National Meeting, Anaheim, CA, 2004
- Negative ions in density functional theory
Donghyung Lee and Kieron Burke, 46th Sanibel Symposium 26 February-3 March 2006, St. Simons Island, GA, USA
- Time dependent Density-Functional Theory: Prospects and Applications, 2nd International Workshop and School, Benasque, Spain, from August 27, 2006 to September 10, 2006

- 2007 GORDON RESEARCH CONFERENCE on Time-Dependent Density-Functional Theory
- Semiclassical Origin of Density Functionals
Attila Cangi, Peter Elliott, Donghyung Lee, and Kieron Burke in APS March meeting 2008, New Orleans, Louisiana
- Semiclassical Approaches in Density Functional Theory
Peter Elliott, Attila Cangi, Donghyung Lee, and Kieron Burke in APS March meeting 2008, New Orleans, Louisiana
- A new approach to density functional theory
Kieron Burke, Peter Elliott, Attila Cangi, and Donghyung Lee in APS March meeting 2008, New Orleans, Louisiana
- Exact condition on the non-interacting kinetic energy for real matter
Donghyung Lee and Kieron Burke in APS March meeting 2008, New Orleans, Louisiana
- Density Functional Theory and Semiclassical Methods
Peter Elliott, Donghyung Lee, Attila Cangi, and Kieron Burke in APS March meeting 2009, Pittsburgh, Pennsylvania
- Towards a semiclassical theory of electronic structure
Attila Cangi, Donghyung Lee, Peter Elliott, and Kieron Burke, in APS March meeting 2009, Pittsburgh, Pennsylvania
- Semiclassics in Density Functional Theory
Donghyung Lee, Attila Cangi, Peter Elliott, and Kieron Burke, in APS March meeting 2009, Pittsburgh, Pennsylvania
- Semiclassics in Orbital-free Potential-Density Functional Theory
Donghyung Lee, Attila Cangi, Peter Elliott, and Kieron Burke, in ACS, August 22-26, 2010, Boston, MA

PUBLICATIONS

1. Controlling Diaza-Cope Rearrangement Reactions with Resonance Assisted Hydrogen Bonds J. Chin, F. Mancin, N. Thavarajah, D. Lee, A. Lough, and D. S. Chung, *J. Am. Chem. Soc.* **125**, 15276 (2003).

2. Abnormal Adsorption Behavior of Dimethyl Disulfide on Gold Surfaces J. Noh, S. Jang, D. Lee, S. Shin, Y. J. Ko, E. Ito and S. Joo, *Current Applied Physics*, **7**, 605-610 (2007).
3. Semiclassical Origins of Density Functionals P. Elliott, D. Lee, A. Cangi, and K. Burke, *Phys. Rev. Lett.* **100**, 256406 (2008).
4. Condition on the Kohn-Sham Kinetic Energy and Modern Parametrization of the Thomas-Fermi Density D. Lee, L. A. Constantin, J. P. Perdew, K. Burke, *J. Chem. Phys.* **130**, 034107 (2009).
5. Leading Corrections to Local Approximations A. Cangi, D. Lee, P. Elliott, and K. Burke, *Phys. Rev. B* **81**, 235128 (2010).
6. Accuracy of Electron Affinities of Atoms in Approximate Density Functional Theory D. Lee, F. Furche and K. Burke, *J. Phys. Chem. Lett.*, **1**, pp 2124-2129 (2010).
7. Finding Electron Affinities with Approximate Density Functionals D. Lee and K. Burke, accepted to *Mol. Phys* (2010).
8. Semiclassical Approaches to One-Dimensional Potential and Coulomb Potential D. Lee, P. Elliott, A. Cangi, and K. Burke, in preparation (2010).

ABSTRACT OF THE DISSERTATION

Electron Affinity in Approximate Density Functional Theory and
the Role of Semiclassics in Orbital-Free Potential-Density Functional Theory

By

Dong Hyung Lee

Doctor of Philosophy in Chemistry

University of California, Irvine, 2010

Professor Kieron Burke, Chair

In this dissertation I discuss the effects of the self-interaction in atomic anions and the role of semiclassics in the orbital-free (potential-)density functional theory. The first part describes how accurate electron affinities can be obtained from the traditional basis-set approaches, despite the positive highest occupied molecular orbital (HOMO) energy due to the self-interaction. I also suggest an alternative way to calculate electron affinity using approximate functionals evaluated on Hartree-Fock or exact-exchange densities for which the extra electron is bound. In the second part, I study the asymptotic expansion of the neutral-atom energy as the atomic number $Z \rightarrow \infty$. The recovery of the correct asymptotic expansion is an important condition on the Kohn-Sham kinetic energy for the accuracy of approximate kinetic energy functionals for atoms, molecules, and solids. The density and kinetic energy density as potential functionals are derived from the semiclassical Green's function. Using the density as a potential functional, I show the orbital-free potential-density functional calculation for atoms. I also present the energy potential functional in 1D and spherical 3D, where the kinetic energy is obtained from the virial theorem.

Chapter 1

Introduction

Density functional theory (DFT) has been successfully applied to many areas such as chemistry, solid-state physics, biology, and surface sciences(1). The basic theorems were proven by Hohenberg and Kohn (HK)(2) in 1964, and the practical approach to real problems was developed by Kohn and Sham(3). Kohn-Sham (KS) DFT is a rigorous way to deal with real, interacting electron problems by mapping them into non-interacting electron problems, which can be solved easily, and provides a balance between computational cost and accuracy. KS-DFT enables us to handle much larger systems in which the traditional *ab initio* methods can not. Although KS-DFT is formally rigorous, the exchange-correlation energy functional ($E_{\text{xc}}[n]$) needs to be approximated in practice. There are many approximations to E_{xc} , such as the local density approximation (LDA), generalized gradient approximation (GGA), hybrid functionals, and meta-GGAs. These approximate functionals provide suitable accuracy for many chemistry and physics areas.

Despite many successful applications, there has been an argument about the applicability of density functional approximations to atomic anions(4; 5). These approximate functionals can not remove the self-repulsion of an electron in the classical Coulomb (or Hartree) potential.

This incomplete cancellation between the Hartree and exchange potentials is called the self-interaction error (SIE). It is known that effects of the SIE decrease as the size of the system increases, due to the spatial distribution of electron density. The SIE becomes drastic in small atomic anions, making their highest occupied molecular orbital (HOMO) energies positive. This result implies the HOMO is not a bound state, and casts doubt on the reliability of DFT for electron affinity (EA) calculations.

In the original HK-DFT, the total energy is an explicit density functional and the interacting kinetic energy, $T[n]$, is also a density functional. However, in KS-DFT, the non-interacting KS kinetic energy, $T_s[n]$, is evaluated on the KS orbitals and the kinetic correlation energy ($T[n] - T_s[n]$) is contained in the exchange-correlation energy functional. Due to this limitation, we need to solve the KS differential equation to obtain the density from the orbitals. If we know T_s as a density functional with sufficient accuracy, we can construct an orbital-free density functional theory, yielding a computational method that scales linearly with the number of particles. In particular, highly accurate $T_s[n]$ is necessary for orbital-free density functional calculations, since $T_s[n] \simeq E[n]$ by the virial theorem. However, there are only a small number of known conditions on T_s (6) which approximate KS kinetic energy functional should satisfy. For the E_{xc} in KS-DFT, there are several exact conditions that E_{xc} should satisfy(7).

Despite successes achieved while focused on the density as a variable, the fundamental importance of the potential has emerged(8; 9). We recently published a paper about the semiclassical origins of density functionals(10), in which we derive the semiclassical density and kinetic energy density as potential functionals in 1D hard wall boundary systems. As discussed in Ref. (9), if we obtain $T_s[v]$ and $n[v]$ from the same semiclassical single-particle Green's function, we can find a variational equation for the total energy. Until now, we had derived the semiclassical density and kinetic energy density for box boundary conditions. However, in real systems, e.g., Coulomb potentials, there are always turning points where

the total energy is equal to the potential energy. Hence, it is necessary to study the uniform semiclassical Green's function for systems with turning points, in order to derive the density and kinetic energy density as potential functionals.

In this dissertation, I will discuss the above problems. In Chapter 2, I will give a basic background in DFT, the uniform semiclassical approximation, and the Green's function approach. In Chapter 3, I will discuss the effect of SIE in EA calculations with approximate density functionals and explain how to get reasonable EAs from traditional approaches, despite positive HOMO energies. In Chapter 4, I show that the asymptotic expansion of total energies of neutral atoms with atomic number Z can be a very important condition for high accuracy in non-interacting KS kinetic energies. In Chapter 5, I will discuss semiclassical orbital-free potential-density functional theory using a Green's function approach. Finally, I conclude with an overview and discuss the limitations encountered in these methods and their influence on electronic structure methods.

Chapter 2

Background

In this section, I will review the basics of DFT, Green's function approaches, and uniform semiclassical approximations in 1D.

2.1 Hohenberg-Kohn theorem

The first Hohenberg-Kohn (HK) theorem states that the ground state density determines the external potential $v_{\text{ext}}(\mathbf{r})$ uniquely up to an arbitrary constant. Consider the electron density $n(\mathbf{r})$ for the nondegenerate ground state of some N -electron system. It determines N by simple quadrature, as well as $v_{\text{ext}}(\mathbf{r})$ and the corresponding Hamiltonian. From this Hamiltonian, we can determine the wavefunction and hence get all properties of the system. Consider two external potentials, $v_{\text{ext}}(\mathbf{r})$ and $v'_{\text{ext}}(\mathbf{r})$, differing by more than a constant. Assume each potential gives the same $n(\mathbf{r})$ for its ground state. These two different potentials provide two different Hamiltonians, \hat{H} and \hat{H}' , respectively, whose ground state densities are the same although the normalized wavefunctions, Ψ and Ψ' , are different. Taking Ψ' as a

trial wavefunction of \hat{H} , the variational principle yields

$$\begin{aligned}
E_0 &< \langle \Psi' | \hat{H} | \Psi' \rangle \\
&= \langle \Psi' | \hat{H}' | \Psi' \rangle + \langle \Psi' | \hat{H} - \hat{H}' | \Psi' \rangle \\
&= E'_0 + \int d^3r n(\mathbf{r}) (v_{\text{ext}}(\mathbf{r}) - v'_{\text{ext}}(\mathbf{r}))
\end{aligned} \tag{2.1}$$

Similarly, taking Ψ as a trial wavefunction of \hat{H}' ,

$$\begin{aligned}
E'_0 &< \langle \Psi | \hat{H}' | \Psi \rangle \\
&= \langle \Psi | \hat{H} | \Psi \rangle + \langle \Psi | \hat{H}' - \hat{H} | \Psi \rangle \\
&= E_0 + \int d^3r n(\mathbf{r}) (v'_{\text{ext}}(\mathbf{r}) - v_{\text{ext}}(\mathbf{r}))
\end{aligned} \tag{2.2}$$

By adding Eqs. (2.1) and (2.2), we obtain a contradiction: $E_0 + E'_0 < E_0 + E'_0$. This result implies that $n(\mathbf{r})$ can come from at most one external potential $v_{\text{ext}}(\mathbf{r})$. Thus, $n(\mathbf{r})$ determines N and $v_{\text{ext}}(\mathbf{r})$ and hence all properties of the ground state. In particular, the ground state energy is a functional of the ground state electron density, and can be expressed in terms of $n_0(\mathbf{r})$:

$$\begin{aligned}
E_0 &= T[n_0] + V_{\text{ee}}[n_0] + V_{\text{ext}}[n_0] \\
&= T[n_0] + V_{\text{ee}}[n_0] + \int d^3r n_0(\mathbf{r}) v_{\text{ext}}(\mathbf{r}),
\end{aligned} \tag{2.3}$$

where subscript *ee* indicates an electron interaction. The kinetic energy and electron-electron interaction functionals are independent of the external potential, so the combination of these

two functionals is referred to as the universal functional or the Hohenberg-Kohn functional, F_{HK} .

$$E_0 = F_{\text{HK}}[n_0] + \int d^3r n_0(\mathbf{r}) v_{\text{ext}}(\mathbf{r}) \quad (2.4)$$

$$F_{\text{HK}}[n_0] = T[n_0] + V_{\text{ee}}[n_0] \quad (2.5)$$

An explicit form of either functional is not known. The electron-electron interaction energy can be divided into the classical electrostatic energy (Coulomb energy, $J[n](\mathbf{r})$) and the remaining part.

$$\begin{aligned} V_{\text{ee}}[n_0] &= \frac{1}{2} \int d^3r_1 \int d^3r_2 \frac{n(\mathbf{r}_1)n(\mathbf{r}_2)}{r_{12}} + U_{\text{xc}}[n] \\ &= J[n] + U_{\text{xc}}[n] \end{aligned} \quad (2.6)$$

where U_{xc} is the non-classical contribution, including all effects of self-interaction correction, exchange and correlation. Since we do not know the explicit form of U_{xc} , it needs to be approximated.

The second HK theorem states that $E[n]$, the functional that gives the ground state energy of the system, delivers the lowest energy if and only if the input density is the true ground state density, $n_0(\mathbf{r})$. According to the variational principle,

$$E_0 \leq E[\tilde{n}] = T[\tilde{n}] + V_{\text{ee}}[\tilde{n}] + V_{\text{ext}}[\tilde{n}] \quad (2.7)$$

For any trial density $\tilde{n}(\mathbf{r})$ that satisfies necessary boundary conditions (e.g., $\tilde{n}(\mathbf{r}) \geq 0$ with $\int d^3r \tilde{n}(\mathbf{r}) = N$), the energy $E[\tilde{n}]$ is the upper bound to the true ground state energy E_0 . Equality in Eq. (2.7) results if and only if the input density is the true ground state electron

density. For any trial density \tilde{n} , there is a corresponding external potential $\tilde{v}_{\text{ext}}(\mathbf{r})$, and hence a Hamiltonian \hat{H} and a corresponding wavefunction $\tilde{\Psi}$. For the Hamiltonian \hat{H} associated with the true external potential $v_{\text{ext}}(\mathbf{r})$,

$$\begin{aligned}
E[\tilde{n}] &= \langle \tilde{\Psi} | \hat{H} | \tilde{\Psi} \rangle \\
&= T[\tilde{n}] + V_{\text{ee}}[\tilde{n}] + \int d^3r \tilde{n}(\mathbf{r}) v_{\text{ext}}(\mathbf{r}) \\
E[n_0] &= \langle \Psi_0 | \hat{H} | \Psi_0 \rangle \\
E[\tilde{n}] &\geq E_0[n_0]
\end{aligned} \tag{2.8}$$

2.2 Kohn-Sham equation

Although the basic theory for DFT was suggested by Hohenberg and Kohn, the kinetic and exchange-correlation energy functionals are not known, and so cannot be used to solve real problems. Kohn and Sham(3) suggested a way in which the Hohenberg-Kohn theorem could be used in real calculations with acceptable accuracy. They map an interacting system into a non-interacting system that has the same density as the interacting system. For a non-interacting, non-degenerate fermion ground state, exact wavefunctions are given by Slater determinants. Thus, for the non-interacting system with a Hamiltonian including a local effective potential $v_{\text{eff}}(\mathbf{r})$:

$$\hat{H} = -\frac{1}{2} \sum_{i=1}^N \nabla_i^2 + \sum_{i=1}^N v_{\text{eff}}(\mathbf{r}_i) \tag{2.9}$$

$$\Psi_s = \frac{1}{\sqrt{N!}} \begin{vmatrix} \phi_1(\mathbf{r}_1) & \phi_2(\mathbf{r}_1) & \cdots & \phi_N(\mathbf{r}_1) \\ \phi_1(\mathbf{r}_2) & \phi_2(\mathbf{r}_2) & \cdots & \phi_N(\mathbf{r}_2) \\ \vdots & \vdots & \ddots & \vdots \\ \phi_1(\mathbf{r}_N) & \phi_2(\mathbf{r}_N) & \cdots & \phi_N(\mathbf{r}_N) \end{vmatrix} \quad (2.10)$$

where the ϕ_i are the N lowest eigenstates of the one-electron Hamiltonian \hat{f}^{KS} . These orbitals are determined by

$$\hat{f}^{\text{KS}} \phi_i = \epsilon_i \phi_i, \quad (2.11)$$

where $\hat{f}^{\text{KS}} = -\frac{1}{2}\nabla^2 + v_{\text{eff}}(\mathbf{r})$ is the one-electron Kohn-Sham operator. Because the explicit form of the true kinetic energy functional $T[n]$ is not known, they suggested using Eq. (2.12), the kinetic energy of a non-interacting system with the same density as the real, interacting system.

$$T_s[n] \equiv T_s[\Psi_s] = \langle \Psi_s | -\frac{1}{2} \sum_{i=1}^N \nabla_i^2 | \Psi_s \rangle \quad (2.12)$$

The difference between the non-interacting and true kinetic energies would then be treated approximately. Kohn and Sham defined the total energy $E[n]$ as

$$E[n] = T_s[n] + V_{\text{ext}}[n] + J[n] + E_{\text{xc}}[n], \quad (2.13)$$

where E_{xc} is the exchange-correlation energy, defined by

$$E_{\text{xc}}[n] = T[n] - T_s[n] + E_{\text{ee}}[n] - J[n]. \quad (2.14)$$

This exchange-correlation energy functional includes the effects of exchange, correlation, and the residual kinetic energy.

Using the Lagrange undetermined multiplier method with the constraint $\langle \phi_i | \phi_j \rangle = \delta_{ij}$ leads the resulting equation:

$$\begin{aligned} \left[-\frac{1}{2}\nabla^2 + v_{\text{ext}}(\mathbf{r}_1) + \int d^3r_2 \frac{n(\mathbf{r}_2)}{\mathbf{r}_{12}} + v_{\text{xc}}(\mathbf{r}_1) \right] \phi_i &= \\ \left[-\frac{1}{2}\nabla^2 + v_{\text{eff}}(\mathbf{r}_1) \right] \phi_i &= \epsilon_i \phi_i \end{aligned} \quad (2.15)$$

where $v_{\text{xc}} = \delta E_{\text{xc}}/\delta n$. According to Eq. (2.15), $v_{\text{eff}}(r)$ depends on the density through the Coulomb term and $v_{\text{xc}}[n]$. Therefore, the KS one-electron Eq. (2.15) has to be solved iteratively.

2.3 Green's function

We derive an approximation to the many-particle density $n(x)$ and the kinetic energy density $t_s(x)$ for non-interacting, spinless fermions in a one-dimensional, smooth potential $v(x)$. This system is characterized by the solutions of the static Schrödinger equation:

$$\left[p \frac{d^2\psi}{dx^2} \right] + [E - v(x)] \psi = 0, \quad (2.16)$$

where p is a constant depending on the units (i.e., in atomic units, $p = 1/2$) and E is the energy eigenvalue.

Our derivation is based on the Green's function $g(x, x'; E)$, which, analogous to Eq. (2.16), obeys

$$\left[p \frac{d^2g}{dx^2} \right] + [E - v(x)] g = \delta(x - x'). \quad (2.17)$$

The solutions of Eq. (2.17) can be expressed in terms of the independent solutions $\psi_l(x)$ and $\psi_r(x)$ satisfying the boundary conditions on the left and on the right, respectively, i.e.,

$$g(x, x'; E) = \begin{cases} \frac{\psi_l(x) \psi_r(x')}{p W(E)}, & \text{if } x \leq x' , \\ \frac{\psi_l(x') \psi_r(x)}{p W(E)}, & \text{if } x \geq x' . \end{cases} \quad (2.18)$$

where $W(E) = \psi_l(x)\partial_x\psi_r(x) - \psi_r(x)\partial_x\psi_l(x)$ is the Wronskian and $\partial_x := \partial/\partial x$. From the diagonal Green's function $g(x; \mathcal{E}) := g(x, x' = x; \mathcal{E})$ we extract the density via

$$n(x) = \frac{1}{2\pi i} \oint_C d\mathcal{E} g(x, \mathcal{E}), \quad (2.19)$$

and the (non-interacting) kinetic energy density via

$$t_s(x) = \frac{1}{2\pi i} \oint_C d\mathcal{E} [\mathcal{E} - v(x)]g(x, \mathcal{E}), \quad (2.20)$$

where \mathcal{E} denotes a complex-valued energy and C any closed contour in the complex energy-plane, enclosing all occupied poles on the real axis.

2.4 Uniform semiclassics in 1D

The Wentzel-Kramers-Brillouin (WKB) method provides approximate solutions to the 1D Schrödinger equation

$$-\frac{\hbar^2}{2m} \frac{d^2\psi(x)}{dx^2} + v(x)\psi(x) = E\psi(x), \quad (2.21)$$

which can be rearranged into

$$\frac{d^2\psi(x)}{dx^2} + \frac{p^2(x)}{\hbar^2}\psi = 0, \quad (2.22)$$

where $p(x) = \sqrt{2m(E - v(x))}$ is the semiclassical momentum. Using $\psi(x) \sim e^{if(x)/\hbar}$ in Eq. (2.22), expanding $f(x)$ as a series of \hbar , and collecting the first order of \hbar give us the WKB solution:

$$\psi(x) \simeq \frac{C}{\sqrt{p(x)}} e^{\pm \frac{i}{\hbar} \int p(x) dx} . \quad (2.23)$$

However, this WKB solution diverges at any turning points present in the system, due to the factor of $1/\sqrt{p(x)}$. Hence, uniform semiclassical approximations which give finite and accurate descriptions at turning points are crucial.

There are two popular uniform semiclassical approximations(11; 12). Miller and Good(11) developed a way to treat potentials with two turning points using a single, semiclassical wavefunction without any patching scheme. However, this uniform approximation requires us to map a given arbitrary potential into a harmonic oscillator well. Accordingly, the original semiclassical momentum should also be mapped into the modified momentum of the harmonic well. From Miller's paper(12), the uniform approximate solutions to Schrödinger equation for two-turning-point problems are given by

$$\begin{aligned} \psi_1(x) &= \frac{\theta_1^{1/6}(x)}{p^{1/2}(x)} Ai \left[- \left(\frac{3}{2} \theta_1(x) \right)^{2/3} \right] \\ \psi_2(x) &= (-1)^n \frac{\theta_2^{1/6}(x)}{p^{1/2}(x)} Ai \left[- \left(\frac{3}{2} \theta_2(x) \right)^{2/3} \right] , \end{aligned} \quad (2.24)$$

where $p(x) = \sqrt{2(E - v(x))}$ is the local wavenumber,

$$\begin{aligned} \theta_1(x) &= \int_{x_1}^x dt p(t) \\ \theta_2(x) &= \int_x^{x_2} dt p(t) , \end{aligned} \quad (2.25)$$

(x_1, x_2) are the left- and right-turning points respectively, and Ai is the Airy function. According to the continuity of wavefunctions, the solutions should satisfy the following conditions at some point x_0 :

$$\begin{aligned}\psi_1(x_0) &= \psi_2(x_0) \\ \psi'_1(x_0) &= \psi'_2(x_0).\end{aligned}\tag{2.26}$$

Given this matching condition, the quantization condition becomes

$$\Theta(E) = \theta_1(x) + \theta_2(x) = \left(N_n + \frac{1}{2}\right) \pi,\tag{2.27}$$

where the N_n is determined by

$$\begin{aligned}N_n &= \frac{4}{3\pi} A_{(n+1)/2}^{3/2} - \frac{1}{2}, & n = 1, 3, 5, \dots \\ &= \frac{4}{3\pi} B_{(n+2)/2}^{3/2} - \frac{1}{2}, & n = 0, 2, 4, \dots\end{aligned}\tag{2.28}$$

The sets of $\{A_s\}$ and $\{B_s\}$ are the roots of the following equations:

$$\begin{aligned}Ai(-A_s) &= 0, \\ Ai(-B_s) - 4B_s Ai'(-B_s) &= 0.\end{aligned}\tag{2.29}$$

The numerical results of coefficients, N_n , can be found in Ref. (12).

Chapter 3

Accuracy of Electron Affinities of Atoms in Approximate DFT

3.1 Introduction

Treating atomic anions with approximate density functional theory (DFT) has long been controversial(4; 5). The net negative charge produces strong self-interaction errors (SIE)(13), resulting in such a large upward bump in the effective potential that the last electron is unbound.

In Fig. 3.1, we show the exact Kohn-Sham (KS) potential for Li^- , found from the density of a highly accurate quantum Monte Carlo (QMC) calculation with a zero-variance zero-bias estimator(14), and by inversion of the KS equations. The HOMO is at $\epsilon_{2s} = -A$, with $A = 0.62$ eV, the electron affinity (EA). We also show the KS potential when the exchange-correlation (XC) contribution is evaluated using the local density approximation

Reproduced with permission from Donghyung Lee, Filipp Furche and Kieron Burke, J. Phys. Chem. Lett., 2010, 1, 2124 (2010). Copyright 2010 American Chemical Society.

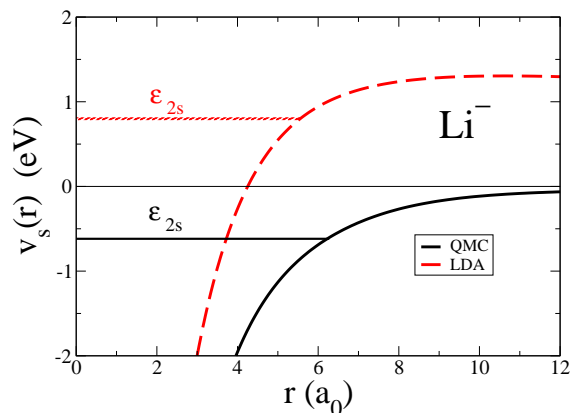


Figure 3.1: Comparison of KS potentials of Li^- . The black line is essentially exact, using a density from quantum Monte Carlo. The red (dashed) line is the LDA potential on that density. The horizontal lines mark the HOMO (2s orbital) energies.

(LDA) on this accurate density. The 2s orbital of this potential is a very sharp resonance, at approximately 0.80 eV.

Formal theorists argue that approximate DFT does “not apply to negative atomic ions if the orbital energy (is) not negative.” (15) Despite this, many have ignored these warnings, calculated EAs within DFT, and found reasonable results using reasonable basis sets(4). Because such calculations have positive HOMO energies for the anion, many authors report EAs found in this way with a note of caution. More than a decade ago, these opposing views were well-expressed in Refs (4) and (5), with the latter arguing for why such calculations should be discounted on formal grounds, and the former demonstrating that no practical problems arise, even with very large basis sets, and that useful results can be found for many small molecules (16).

The fact remains that a formally problematic procedure yields physically meaningful results. This strongly suggests that there is a systematic property to be explored. In the present letter, we use DFT calculations with exact exchange to elucidate that structure and show how the practical and formal are reconciled. Our analysis suggests a new practical solution to the problem that is as accurate as any existing DFT method with fewer formal difficulties.

We begin with our notation and formalism. The KS equations for any atom or ion are

$$\left[-\frac{1}{2}\nabla^2 + v_s^\sigma(r) \right] \phi_{i\sigma}(r) = \epsilon_{i\sigma} \phi_{i\sigma}(r) \quad (3.1)$$

where $v_s^\sigma(r)$ is a single, multiplicative spin-dependent KS potential and σ is a spin index (up and down spins). The KS potential is written as a sum of three contributions:

$$v_s^\sigma(r) = v(r) + v_H[n](r) + v_{XC}^\sigma[n_\uparrow, n_\downarrow](r) \quad (3.2)$$

where $v(r) = -Z/r$ for an atom, $v_H(r)$ is the Hartree potential, and the XC potential is

$$v_{XC}^\sigma[n_\uparrow, n_\downarrow](r) = \frac{\delta E_{XC}[n_\uparrow, n_\downarrow]}{\delta n_\sigma(r)}. \quad (3.3)$$

Thus, for either the exact or some approximate XC functional of the (spin)-densities, we have a self-consistent set of equations.

Far from a nucleus, the Hartree potential decays as N/r , where N is the electron number. The exact XC potential decays as

$$v_{XC}(r) \rightarrow -1/r, \quad r \rightarrow \infty, \quad (3.4)$$

which is a pure exchange effect(17). For a neutral atom, $Z = N$, and $v_s(r) \rightarrow -1/r$ exactly. However almost all local and gradient-corrected functional approximations to $v_{XC}(r)$ decay incorrectly with r , typically exponentially, as the density decays exponentially. This has only a small effect on the density itself, but leads to very poor HOMO levels in such calculations (errors of several eV). These are all manifestations of the infamous SIE.

A well-known cure for this problem in DFT is to use the optimized effective potential (OEP) method(18), which finds the KS potential for an *orbital*-dependent functional. The simplest

case is to include exchange alone, often denoted EXX, producing a KS potential with the correct asymptotic behavior and a HOMO energy that is close to $-I$ for neutral systems. A practical and accurate approximation to OEP, called localized Hartree-Fock (LHF), was developed by Görling and co-workers (19; 20). The total energies of EXX are practically indistinguishable from those of a standard Hartree-Fock (HF) calculation (21).

While awkward and embarrassing for DFT enthusiasts, this problem is not fatal for neutral atoms and cations, because one extracts the total energy by applying the energy functional to the self-consistent density, and need never look at the orbital energies. Such total energies (and especially energy differences) have been found to have chemically useful accuracy(22). But for anions, the problem *does* appear fatal, since the exponential decay of the approximate $v_{\text{xc}}(r)$ leaves a KS potential that behaves as

$$v_{\text{s}}(r) \rightarrow +1/r, \quad r \rightarrow \infty, \tag{3.5}$$

for an anion using an approximate XC functional. This produces a large positive bump in the potential, especially for small systems, and usually raises the HOMO above the zero of the potential (value at ∞). As we show in Fig. 3.1, the LDA HOMO energy is 0.83 eV, and the last orbital is not an eigenstate, but a very sharp resonance. The KS potential decays slowly and the classical outer turning point is at 17 Å. The true self-consistent ground state, using an approximate functional, is found when a sufficiently large fraction of an electron has escaped from the system (tunnelled to ∞), reducing the HOMO energy to zero. We avoid this sorry fate in Fig. 3.1 by evaluating the LDA approximation to the KS potential on the *exact* density, not a self-consistent density. Note that hybrid functionals mix about 25% of exact exchange with a GGA. This reduces the barrier by about 25%, but does not rectify the problem.

Long ago, Shore et al(13) studied the local density approximation for the H^- ground state.

They confined electrons in a cavity by adding a spherical hard wall and calculated HOMO and total energies, varying the position of the wall (R_B). They found that there was a plateau-like region of the energies in $15 \text{ a.u.} < R_B < 30 \text{ a.u.}$ To obtain the asymptotic solution of H^- as $R_B \rightarrow \infty$, they varied the number of core electrons at $r < 25 \text{ a.u.}$ and their wavefunction to determine the energy minimum. The energy minimum occurred when 1.7 electrons were localized near the nucleus, 0.3 electrons were delocalized in the asymptotic tail of the density, and the HOMO eigenvalue became zero. At about the same time, Schwarz(23) noted that both O^- and F^- are unstable using $X\alpha$ (24) (a precursor to LDA(3)) because HOMO eigenvalues are positive.

Galbraith and Schaefer(4) claim the applicability of approximate DFT for negative ions. If basis sets such as Dunning's augmented correlation consistent polarized valence double zeta (aug-cc-pVDZ) basis set(25; 26) or larger are used, DFT methods with GGA and hybrid functionals can be applied to negative ions such as F^- , whose outermost electron has a positive HOMO. Subsequently Rösch and Trickey (5) correctly point out that exact DFT itself has no difficulty for anions, but that the problem is with approximate functionals, as is clearly illustrated in Fig. 3.1. They claim that there are no difficulties with the physical significance of orbital eigenvalues, positive values are permissible, and that problems can be masked by finite basis sets. Although correct, none of this necessarily implies that accurate numbers cannot be extracted from finite basis sets. Later, careful calculations by Jarecki and Davidson(15) showed that, for F^- , there are two plateau regions of total energy as a function of basis-set size. On the first plateau, both total energy and HOMO appear to converge, the latter to a positive value. Beyond that, the basis set probes the outside of the barrier, some density leaks out, and the HOMO falls to zero. But the density change is so small that the total energy barely changes. Eventually, the electron completely escapes and the HOMO falls even further.

A naive solution to this difficulty is to perform HF or the DFT version, LHF, for such systems,

which produce negative HOMOs for the anions. However, for small anions, correlation effects are large, so HF total energy differences are highly inaccurate. In fact, from the total energies, many of the anions are unbound. One can also use Koopmans’ theorem, where I is estimated as $-\epsilon_{\text{HOMO}}$. While an improvement, the mean absolute errors (0.5 eV) are much larger than DFT methods including correlation with a basis set. An alternative solution to the SIE problem is to perform self-interaction corrected local spin density approximation (SIC-LSDA)(27). In Ref. (28), Cole and Perdew applied SIC-LSDA to calculate EAs for atomic systems, $Z < 86$, significantly reducing errors relative to LSDA, but much less accurate than results produced here with GGAs, hybrids, and meta-GGAs.

3.2 Computational details

In all our calculations, the total energies of neutral atoms and ions are calculated using the usual self-consistent unrestricted HF, LHF, and KS-DFT. The approximate functionals in DFT calculations are LDA (S-VWN5)(29; 30; 31), PBE(32), hybrid (B3LYP(33; 34) and PBE0(35)), and meta-GGA (TPSS(36)) functionals. We use Dunning’s augmented correlation-consistent pVXZ (aug-cc-pVXZ, X = D, T, Q, and 5, AVXZ in this paper) basis sets(25; 26). For the LHF calculations for anions, we calculate the Slater potential numerically everywhere to get accurate results. The calculations with basis sets are performed with TURBOMOLE 6.2 (37). For the special cases of H^- and Li^- we perform fully numerical DFT calculations using an OEP code(38) to calculate $v_{\text{s}}(r)$, $v_{\text{xc}}(r)$, and the densities using EXX. Since this code makes a spherical approximation, we do not use it for non-spherical cases. To calculate approximate functionals on HF densities, we perform unrestricted HF calculations on both neutral and negative atoms. Then, we evaluate the total energies of atoms using HF orbitals, so the kinetic energies are those of HF.

Table 3.1: Errors in EAs (eV). Total energies for both neutral and negative atoms are evaluated on HF-SCF densities with aug-cc-pVDZ basis set.

	EA	Δ EA				
	Exp	LDA	PBE	B3LYP	PBE0	TPSS
H	0.75	0.13	-0.11	0.03	-0.17	0.01
Li	0.62	-0.04	-0.12	-0.14	-0.14	-0.05
B	0.28	0.36	0.26	0.04	0.17	0.12
C	1.26	0.45	0.23	-0.04	0.12	0.12
O	1.46	0.41	0.14	0.01	-0.14	-0.09
F	3.40	0.59	0.12	-0.04	-0.18	-0.07
MAE ¹		0.33	0.16	0.05	0.15	0.08
Na	0.55	0.04	-0.01	-0.05	-0.05	0.03
Al	0.43	0.17	0.13	-0.08	0.10	0.06
Si	1.39	0.21	0.11	-0.13	0.09	0.07
P	0.75	0.13	0.03	0.02	-0.03	0.03
S	2.08	0.27	0.06	0.01	0.00	0.01
Cl	3.61	0.36	0.08	0.01	0.03	0.02
MAE		0.20	0.07	0.05	0.05	0.04
total		0.26	0.12	0.05	0.10	0.06

¹ Mean absolute error

3.3 Results and discussion

Our suggestion is to perform calculations that include exact exchange (either LHF or HF) for self-consistent densities, but evaluate an approximate functional on that density to obtain the energy. Such a procedure has its own drawbacks, but avoids all the pitfalls mentioned above.

In Table 3.1, we calculate EAs using HF densities for both neutral and negative atoms. The B3LYP results were used in Fig. 3.2. Our EAs are much more accurate than the corresponding ionization potentials (typically by about a factor of 2), with mean average errors below 0.1 eV. These results change little when the basis set is expanded (either larger valence space or more diffuse functions), and our new method, using HF densities, has a

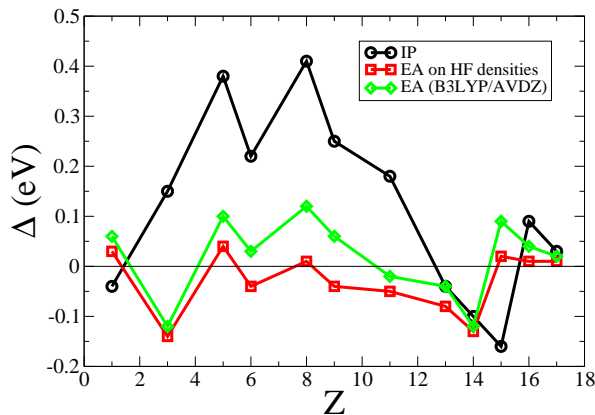


Figure 3.2: Comparison of errors (Δ) in ionization potentials and electron affinities in first 2 rows of periodic table. Energies are evaluated with B3LYP density functional(33; 34) evaluated on HF densities and on self-consistent densities within AVDZ basis set.

well-defined basis-set limit. The traditional method of limited basis sets (LBS) can only work until the basis set probes the decay of the positive barriers of the type shown in Fig. 3.1. Similarly good results are found for the PBE generalized gradient approximation(32) and its hybrid, PBE0(35). The best results are with the TPSS (36) meta-GGA with HF densities. The results for all functionals are *better* than those of ionization potentials for these elements. They also follow the usual trends for approximate functionals. The more sophisticated functionals reduce errors by a factor of 2-5 relative to LDA.

In Fig. 3.3, we repeat Fig. 3.2, but now for the PBE functional. Comparison of the two shows the more systematic (and often larger) errors of the non-empirical GGA versus the empirical hybrid B3LYP. Interestingly, with our HF method for neutral and negative atoms, PBE does as well as PBE0. B3LYP and the meta-GGA, TPSS, give the best total MAE. We find almost identical results if we use LHF instead of HF densities.

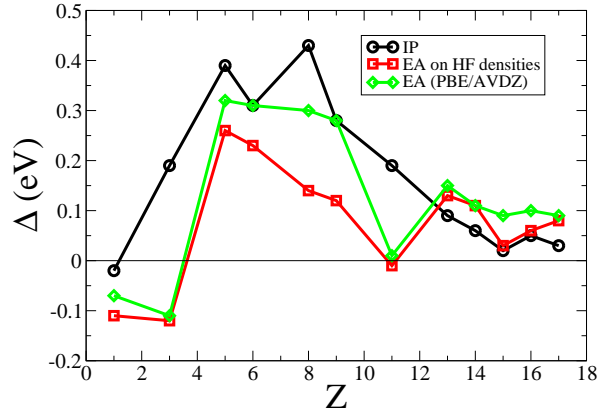


Figure 3.3: Comparison of errors (Δ) in IP's and EAs (in eV). Energies are evaluated with PBE density functional evaluated on the AVDZ basis set, except the square symbols, where the densities are found from a HF calculation.

Table 3.2: Errors in EAs (eV). Total energies for both neutral and negative atoms are calculated by SCF procedure with aug-cc-pVDZ basis set.

	EA	Δ EA				
	Exp	LDA	PBE	B3LYP	PBE0	TPSS
H	0.75	0.15	-0.07	0.06	-0.16	0.02
Li	0.62	-0.03	-0.11	-0.12	-0.13	-0.04
B	0.28	0.44	0.32	0.10	0.19	0.16
C	1.26	0.53	0.31	0.03	0.15	0.18
O	1.46	0.58	0.30	0.12	-0.07	0.03
F	3.40	0.74	0.28	0.06	-0.11	0.05
MAE	-	0.41	0.23	0.08	0.13	0.08
Na	0.55	0.07	0.01	-0.02	-0.03	0.04
Al	0.43	0.21	0.15	-0.04	0.11	0.09
Si	1.39	0.20	0.11	-0.12	0.08	0.07
P	0.75	0.25	0.09	0.09	0.00	0.07
S	2.08	0.31	0.10	0.04	0.01	0.03
Cl	3.61	0.35	0.09	0.02	0.02	0.02
MAE	-	0.23	0.09	0.06	0.04	0.05
total	-	0.32	0.16	0.07	0.09	0.07

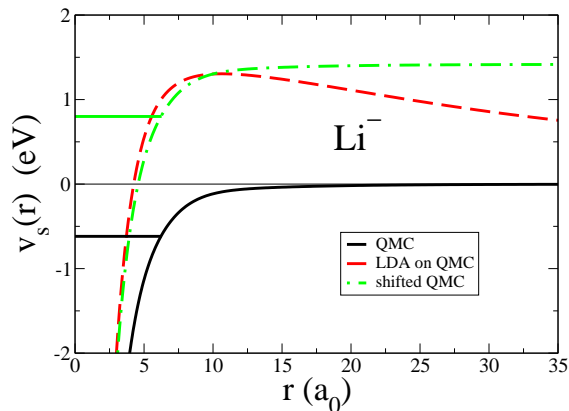


Figure 3.4: Shifted exact $v_s(r)$ potential (eV). The HOMO from QMC is -0.62 eV, and the HOMO from LDA/AV5Z is 0.80 eV. We shift the exact v_s by the difference between eigenvalues.

3.4 Why do limited basis sets work?

If the last electron is unbound in a pure DFT calculation, one can reasonably ask why limited-basis calculations yield sensible answers at all. To confirm that they do work, in Table 3.2, we report the results of using a limited basis set. The B3LYP and PBE numbers were used in Figs. 3.2 and 3.3, respectively. Without addressing the formal issues, these results are entirely sensible and very close to those of Table 3.1. MAE's are almost the same (slightly worsened), and individual differences are almost all within the MAE of the given functional. How can such sensible results and excellent agreement with Table 3.1 come from such an apparently ill-defined procedure?

The original E_{XC} defined by Kohn and Sham(3) was for fixed particle number. This means the KS potential is undefined up to an arbitrary constant. The density is unaffected by an arbitrary shift of the potential. Thus positive orbital energies *per se* do not mean a density or total energy is inaccurate. However, in real calculations with approximate XC functionals, we conventionally set $v_s(r \rightarrow \infty)$ to zero. Thus, the electron is unbound if its orbital energy is positive, as in Fig. 3.1. Consider a model in which we add to the potential $C\theta(R_c - r)$,

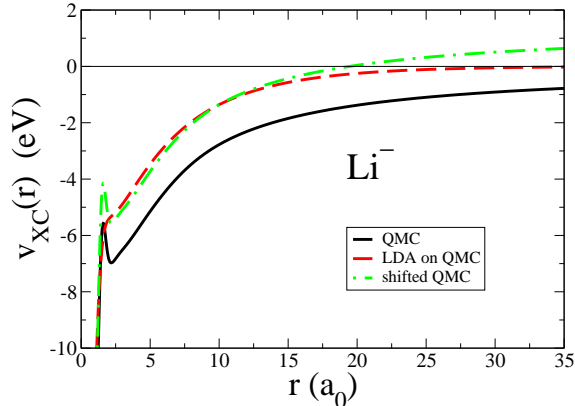


Figure 3.5: Shifted exact $v_{\text{XC}}(r)$ potential (eV) in Li^- . The HOMO from QMC is -0.62 eV, and the HOMO from LDA/AV5Z is 0.80 eV. We shift the exact v_{XC} by the difference between eigenvalues.

where $\theta(r)$ is the Heaviside step function and R_c is a very large fixed distance. As long as our basis sets do not stretch out to R_c , the anion will appear perfectly stable and have a well-defined limit for its density. If C is large enough, the HOMO will be positive. In Fig. 3.4, we have performed just such a procedure for Li^- , with $C = 1.42$ eV, and choosing $R_c = 1000\text{\AA}$, arbitrarily. This slightly inaccurate KS potential yields essentially the *exact* anionic density, produces as accurate an anionic energy as the approximate functional used to evaluate it, but has a positive HOMO of 0.80 eV.

Now then the question becomes: Do approximate functionals, complete with SIE, really accurately mimic such a shifted KS potential? The answer has long been known to be yes(39), and we show this in Fig. 3.5. Here we include only the XC portion, in order to zoom in on the region where the exact and approximate potentials differ. The LDA potential almost exactly follows the *shifted* exact potential, once the outer shell (2s) is reached. Does it converge to an accurate energy and density? The answer is generally yes, if the functional is accurate *except* for producing the wrong asymptote.

In Fig. 3.6, we show that the errors in density for the Li^- anion are only a few percent, and

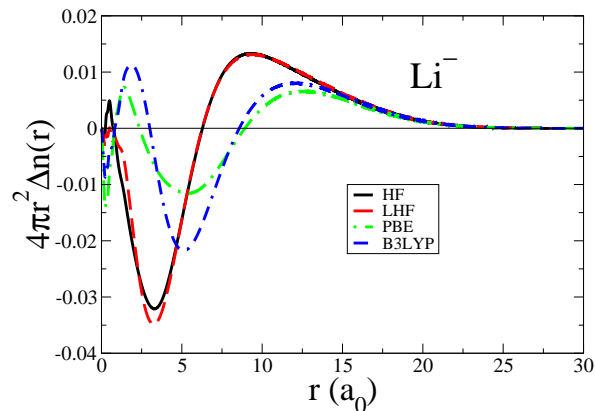


Figure 3.6: Plot of the radial density errors for Li^- with various approximations. SCF densities are obtained with AVQZ. The exact density is from quantum Monte Carlo.

are comparable for all methods.

Finally, we investigate the dependence of HOMO and total energies on basis sets by adding more diffuse functions for F^- . Moving from singly augmented to quadruply augmented AVTZ basis functions, the HOMO drops from 1.57 eV down to 0.75 eV, but the total energy of the anion changes by only 2 mH. We also checked the use of a logarithmic (diffusive) grid, but this had effects only in the 50 μH regime.

In summary, we have suggested an alternative method for calculating EAs of small anions that resolves the dilemma of positive orbital energies and has a well-defined basis set limit. By evaluating the energies on LHF or HF densities, in which the last electron is properly bound with a negative HOMO, accurate and sensible results are obtained. We have also shown that the consistency and accuracy of using limited basis sets for SCF calculations with approximate functionals can be understood, despite the positive HOMO energies of the anions. But an advantage of our method is that the basis-set limit is always well-defined. Using limited basis sets could run into difficulty if the self-interaction barrier becomes too narrow or insufficiently high, making it impossible to find a plateau region. Of course, by evaluating the potential with one functional while evaluating the energy with another, various well-known complications arise, such as in the calculation of forces. But these difficulties are

far less subtle and challenging than those of positive HOMOs.

Finally, we note that even our method will fail if the (L)HF density is insufficiently accurate or the approximate functional does not provide accurate energies. Thus we expect comparable accuracy to that found here for molecular valence anions, but the weakly bound states such as dipole- or higher multipole-bound anions(40) will be much more challenging and may require self-interaction-free energy functionals along with a correct treatment of dispersion.

Chapter 4

Condition on the Kohn-Sham Kinetic Energy, and Modern Parametrization of the Thomas-Fermi Density

4.1 Introduction

Ground-state Kohn-Sham (KS) density functional theory (DFT) is a widely-used tool for electronic structure calculations of atoms, molecules, and solids (1), in which only the density functional for the exchange-correlation energy, $E_{xc}[n]$, must be approximated. But a direct, orbital-free density functional theory could be constructed if only the non-interacting kinetic energy, T_s , were known sufficiently accurately as an explicit functional of the density (41). Using it would lead automatically to an electronic structure method that scales linearly with the number of electrons N (with the possible exception of the evaluation of the Hartree energy). Thus the KS kinetic energy functional is something of a holy grail of density

Reprinted with permission from Donghyung Lee, Lucian A. Constantin, John P. Perdew, and Kieron Burke, *J. Chem. Phys.* **130**, 034107 (2009). Copyright 2009, American Institute of Physics.

functional purists, and interest in it has recently revived (42).

In this work, we exploit the “unreasonable accuracy” of asymptotic expansions (43; 44), in this case for large neutral atoms, to show that there is a very simple condition that approximations to T_s must satisfy, if they are to attain high accuracy for total energies of matter. By matter, we mean all atoms, molecules, and solids that consist of electrons in the field of nuclei, attracted by a Coulomb potential. The condition is to recover the (known) asymptotic expansion of $T_s/Z^{7/3}$ for neutral atoms, in powers of $Z^{-1/3}$. By careful extrapolation from accurate numerical calculations up to $Z \sim 90$, we calculate the coefficients of this expansion. We find that the usual gradient expansion, derived from the slowly-varying gas, but applied to essentially exact densities, yields only a good approximation to these coefficients. Thus, all new approximations should either build in these coefficients, or be tested to see how well they approximate them. We perform several tests, using atoms, molecules, jellium surfaces, and jellium spheres, and analyze two existing approximations. In Ref. (45), a related method was used to derive the gradient coefficient in modern generalized gradient approximations (GGA’s) for exchange. Given this importance of $N = Z \rightarrow \infty$ as a condition on functionals, we revisited and improved upon the existing parametrizations of the neutral-atom Thomas-Fermi (TF) density. The second-half of the paper is devoted to testing its accuracy.

4.2 Theory and Illustration

For an N -electron system, the Hamiltonian is

$$\hat{H} = \hat{T} + \hat{V}_{\text{ext}} + \hat{V}_{\text{ee}}, \tag{4.1}$$

where \hat{T} is the kinetic energy operator, \hat{V}_{ext} the external potential, and \hat{V}_{ee} the electron-electron interaction, respectively. The electron density $n(\mathbf{r})$ yields $N = \int d^3r n(\mathbf{r})$, where N is the particle number.

To explain asymptotic exactness, we (re)-introduce the ζ -scaled potential (46) (which is further discussed in Ref. (10)), given by

$$v_{\text{ext}}^{\zeta}(\mathbf{r}) = \zeta^{4/3} v_{\text{ext}}(\zeta^{1/3}\mathbf{r}), \quad N \rightarrow \zeta N, \quad (4.2)$$

where $v_{\text{ext}}(\mathbf{r})$ is the external potential, and the Thomas-Fermi expectation value is $V_{\text{ext}}^{\zeta}[n] = \zeta^{7/3} V_{\text{ext}}[n]$. In this ζ -scaling scheme, nuclear positions \mathbf{R}_{α} and charges Z_{α} of molecules are scaled into $\zeta^{-1/3}\mathbf{R}_{\alpha}$ and ζZ_{α} respectively. In a uniform electric field, $\mathcal{E} \rightarrow \zeta^{5/3}\mathcal{E}$. For neutral atoms, scaling ζ is the same as scaling Z , producing an asymptotic expansion for the total energy of neutral atoms (43; 47; 48; 49; 50),

$$E = -c_0 Z^{7/3} - c_1 Z^2 - c_2 Z^{5/3} + \dots, \quad (4.3)$$

where $c_0 = 0.768745$, $c_1 = -1/2$, $c_2 = 0.269900$, and Z is the atomic number. This large Z -expansion gives a remarkably good approximation to the Hartree-Fock energy of the neutral atoms, with less than a 10% error for H, and less than 0.5% error for Ne. By the virial theorem for neutral atoms, $T = -E$, and $T \simeq T_{\text{s}}$ to this order in the expansion (since the correlation energy is roughly $\sim Z$). Hence, the non-interacting kinetic energy has the following asymptotic expansion.

$$T_{\text{s}} = c_0 Z^{7/3} + c_1 Z^2 + c_2 Z^{5/3} + \dots \quad (4.4)$$

We say that an approximation to the kinetic energy functional is *asymptotically exact* to the p -th degree if it can reproduce the exact c_0, c_1, \dots, c_p . The three displayed terms in Eq.

(4.3) constitute the second-order asymptotic expansion for the total energy of neutral atoms, and we expect that this asymptotic expansion is a better starting point for constructing a more accurate approximation to the kinetic energy functional than the traditional gradient expansion approximation (GEA).

The leading term in Eq. (4.4) is given exactly by a local approximation to T_s (TF theory), but the leading *correction* is due to higher-order quantum effects, and only approximately given by the gradient expansion evaluated on the exact density. However, these coefficients are *vital* to finding accurate kinetic energies. Since we know that $c_0 Z^{7/3}$ becomes exact in a relative sense as $N = Z \rightarrow \infty$, we define $\Delta T_s = T_s - c_0 Z^{7/3}$ and investigate ΔT_s as a function of Z . How accurate is the asymptotic expansion for ΔT_s ? In Fig. 4.1, we evaluate T_s for atoms (see section 4.3 for details) and plot the percentage error in ΔT_s , for all atoms and the asymptotic series with just two terms. The series is incredibly accurate, with only a 13% error for $N=2$ (He), and 14% for $N=1$. Thus, any approximation that reproduces the correct asymptotic series (up to and including the c_2 term) is likely to produce a highly accurate T_s .

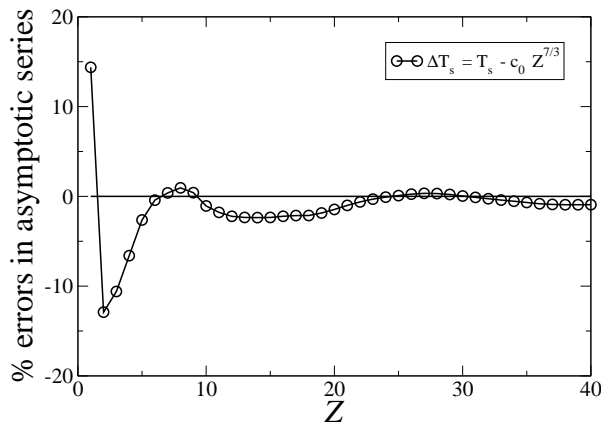


Figure 4.1: Percentage error between $c_1 Z^2 + c_2 Z^{5/3}$ and $\Delta T_s = T_s - c_0 Z^{7/3}$.

To demonstrate the power and the significance of this approach, we apply it directly to the

first term (where the answer is already known, but perhaps not yet fully appreciated in the DFT community). Using any (all-electron) electronic structure code, one calculates the total energies of atoms for a sequence running down a column in the periodic table. By sticking with a specific column, one reduces the oscillatory contributions across rows, and the alkali-earth column yields the most accurate results. By then fitting the resulting curve of $T_s/Z^{7/3}$ as a function of $Z^{-1/3}$ to a parabola, one finds $c_0 = 0.7705$. Now assume one wishes to make a local density approximation (LDA) to T_s , but knows nothing about the uniform electron gas. Dimensional analysis (coordinate scaling) yields (51)

$$T^{\text{loc}}[n] = A_s I, \quad I = \int d^3r n^{5/3}(\mathbf{r}), \quad (4.5)$$

but does not determine the constant, A_s . A similar fitting of I , based on the corresponding self-consistent densities, gives a leading term of $0.2677 Z^{7/3}$, yielding $A_s = 2.868$. Thus we have deduced the local approximation to the non-interacting kinetic energy.

A careful inspection of the above argument reveals that the uniform electron gas is never mentioned. As N grows, the wavelength of the majority of the particles becomes short relative to the scale on which the potential is changing, loosely speaking, and semiclassical behavior dominates. The local approximation is a universal semiclassical result, which is exact for a uniform gas simply because that system has a constant potential. On the basis of that argument, we know $A_s = (3/10)(3\pi^2)^{2/3} = 2.871$, demonstrating that (for this case) our result is accurate to about 0.1%. This argument tells us that the reliability of the local approximation is no indicator of how rapidly the density varies. That this argument is correct for neutral atoms was carefully proven by Lieb and Simon in 1973 (52) and later generalized by Lieb to all matter (46).

The focus of the first part of this paper is on the remaining two known coefficients (c_1 and c_2) and how well the GEA performs for them. We evaluate those gradient terms by

fitting asymptotic series and find that the traditional gradient expansion does well, but is not exact. From this information, we develop a modified gradient expansion approximation that reproduces the correct asymptotic coefficients c_1 and c_2 , merely as an illustration of the power of asymptotic exactness. We test it on a variety of systems, finding the expected behavior.

In Section 4.5, we present a parametrization of the TF density which is more accurate than previous parametrizations. The TF density has a simple scaling with Z and becomes relatively exact and slowly-varying for a neutral atom as $Z \rightarrow \infty$, breaking down only near the nucleus and in the tail. We compare various quantities of our parametrization with exact values and earlier parametrizations, and analyze the properties of the TF density.

4.3 Large Z Methodology

We begin with a careful methodology for extracting the asymptotic behavior from highly accurate numerical calculations. Fully numerical DFT calculations were performed using the OPMKS code (38) to calculate the total energies of neutral atoms using ‘exact exchange’. This is simply minimizing the Hartree-Fock energy, subject to the constraint of a multiplicative potential (18). The spin-density functional version of T_s has been used for all systems (53). We refer throughout to these as the KS results, and none of our analysis depends on which approximation we use. The coefficients c_0 , c_1 and c_2 are the same over a wide range of approximations from exact exchange-correlation to local-density exchange.

To attain maximum accuracy for c_1 and c_2 , we need to suppress the oscillations which come at the same order as the next term, $c_3 Z^{4/3}$. Consider first the KS results (T_s). We investigate the differences between $T_s/Z^{7/3}$ and $c_0 + c_1 Z^{-1/3} + c_2 Z^{-2/3}$ in Fig. 4.2. We extract 6 data points ($Z=24$ (Cr), 25 (Mn), 30 (Zn), 31 (Ga), 61 (Pm), and 74 (W)) which have the

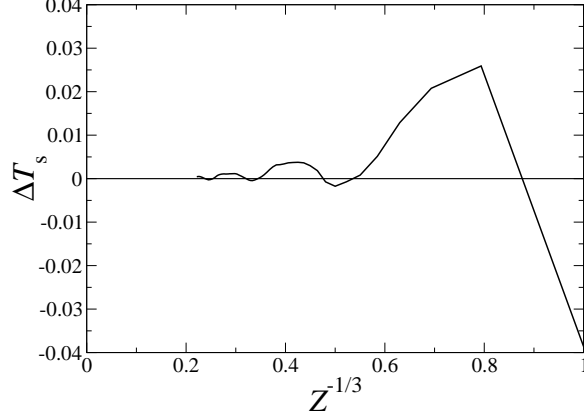


Figure 4.2: Difference between $T_s/Z^{7/3}$ and $c_0 + c_1 Z^{-1/3} + c_2 Z^{-2/3}$ as a function of $Z^{-1/3}$.

smallest differences, i.e., nearest to where the curve crosses the horizontal axis. We then make a least-squares fit with a parabolic form in $Z^{-1/3}$, ignoring the oscillation term,

$$\frac{T_s}{Z^{7/3}} = 0.768745 + c_1 Z^{-1/3} + c_2 Z^{-2/3}. \quad (4.6)$$

Effectively, we solve two linear equations for c_1 and c_2 . We explicitly include $c_0 = 0.768745$, since we don't have enough data points to extract c_0 accurately, especially in the region $Z^{-1/3} < 0.2$. It is important to control the behavior of the fitting line at $Z \rightarrow \infty$. This fitting yields an accurate estimate of $c_1 = -0.5000$ and $c_2 = 0.2702$, with error less than 1%, demonstrating the accuracy of our method for c_1 and c_2 .

We repeat the same procedure to extract c_1 and c_2 coefficients of TF and second- and fourth-order GEA's which are given by

$$T^{\text{GEA2}} = T^{\text{TF}} + T^{(2)}, \quad (4.7)$$

and (54; 41; 55):

$$T^{\text{GEA4}} = T^{\text{TF}} + T^{(2)} + T^{(4)}. \quad (4.8)$$

These gradient corrections to the local approximation are given by

$$T^{(2)} = \frac{5}{27} \int d^3r \tau^{\text{TF}}(\mathbf{r}) s^2(\mathbf{r}), \quad (4.9)$$

and

$$T^{(4)} = \frac{8}{81} \int d^3r \tau^{\text{TF}}(\mathbf{r}) \left[q^2(\mathbf{r}) - \frac{9}{8} q(\mathbf{r}) s^2(\mathbf{r}) + \frac{s^4(\mathbf{r})}{3} \right], \quad (4.10)$$

where $\tau^{\text{TF}}(\mathbf{r})$, $s(\mathbf{r})$, and $q(\mathbf{r})$ are defined as

$$\tau^{\text{TF}}(\mathbf{r}) = \frac{3}{10} k_{\text{F}}^2(\mathbf{r}) n(\mathbf{r}), \quad (4.11)$$

$$s(\mathbf{r}) = \frac{|\nabla n(\mathbf{r})|}{2k_{\text{F}}(\mathbf{r})n(\mathbf{r})}, \quad (4.12)$$

$$q(\mathbf{r}) = \frac{\nabla^2 n(\mathbf{r})}{4k_{\text{F}}^2(\mathbf{r})n(\mathbf{r})}, \quad (4.13)$$

and $k_{\text{F}}(\mathbf{r}) = (3\pi^2 n(\mathbf{r}))^{1/3}$.

We have also applied this procedure to both $T^{(2)}$ and $T^{(4)}$. Since the asymptotic expansions of these energies begin at Z^2 , we extract only a c_1 and a c_2 for each using the following equations:

$$\begin{aligned} \frac{T^{\text{GEA2}} - T^{\text{TF}}}{Z^{7/3}} &= \Delta c_1 Z^{-1/3} + \Delta c_2 Z^{-2/3}, \\ \frac{T^{\text{GEA4}} - T^{\text{GEA2}}}{Z^{7/3}} &= \Delta c_1 Z^{-1/3} + \Delta c_2 Z^{-2/3}. \end{aligned} \quad (4.14)$$

These results are also included in Table 4.1, and are of course consistent with our results from Eq. (4.6).

Table 4.1: The coefficients in the asymptotic expansion of the KS kinetic energy and various local and semilocal functionals. The fit was made to $Z=24$ (Cr), 25 (Mn), 30 (Zn), 31 (Ga), 61 (Pm), and 74 (W). The functionals of the last two rows are defined in section 4.4.

	c_1	c_2
Exact	-0.5000	0.2699
T_s	-0.5000	0.2702
T^{TF}	-0.6608	0.3854
$T^{(2)}$	0.1246	-0.0494
$T^{(4)}$	0.0162	0.0071
T^{GEA2}	-0.5362	0.3360
T^{GEA4}	-0.5200	0.3431
T^{GGA} ^a	-0.5080	0.2918
T^{LmGGA} ^a	-0.5089	0.3174

^a See section 4.4

4.4 Results and Interpretation

To understand the meaning of the above results, begin with the values of c_1 . We have combined the results of the $T^{(2)}$ and $T^{(4)}$ fits with that of the T^{TF} fit to produce the asymptotic coefficients of T^{GEA2} and T^{GEA4} . We check that these combinations produce the same coefficients in Table 4.1 which are found from the direct fitting of T^{GEA2} and T^{GEA4} using Eq. (4.6). The exact value of c_1 is $-1/2$. We see that the local approximation (TF) gives a good estimate, -0.66 . Then the second-order gradient expansion yields -0.54 , reducing the error by a factor of 5. Finally, the fourth-order gradient expansion yields -0.52 , a further improvement, yielding only a 4% error in its approximation to the Scott correction (56).

For c_2 , the gradient expansion is less useful. The exact result is 0.27, while the TF approximation overestimates this as 0.39. The GEA2 result is only slightly reduced (0.34), and the

fourth-order correction has the wrong sign.

To understand how important these results can be, we consider how exchange and correlation functionals are constructed. Often, such constructions begin from the GEA, which is then generalized to include (in an approximate way) all powers of a given gradient. For slowly varying densities, it is considered desirable to recover the GEA result. But we have seen here how this conflicts with the asymptotic expansion, and in Ref (45), it was shown how the asymptotic expansion is more significant to energies of real materials, and how successful GGA's for atoms and molecules well-approximate the large- Z asymptotic result, not the slowly-varying gas.

Atoms: To illustrate this point, we construct here a trivial modified gradient expansion, MGEA2, designed to have the correct asymptotic coefficients, in so far as is possible. Thus

$$T^{\text{MGEA2}} = T^{\text{TF}} + 1.290 T^{(2)} \tag{4.15}$$

The enhancement coefficient has been chosen to make $c_1^{\text{MGEA2}} = -1/2$. In Table 4.2, we list the results of several different approximations for the alkali-earth atoms. Because the GEA2 error passes through 0 around $Z=8$, its errors are artificially low.

Table 4.2: KS kinetic energy (T) in hartrees and various approximations for alkali-earth atoms.

Atom	Z	T_s	T^{TF}	%err	T^{GEA2}	%err	T^{MGEA2}	%err	T^{GEA4}	%err	T^{MGEA4}	%err
Be	4	14.5724	13.1290	-10	14.6471	0.5	15.0880	3.5	14.9854	2.8	14.5453	-0.2
Mg	12	199.612	184.002	-8	198.735	-0.4	203.014	1.7	201.452	0.9	199.924	0.2
Ca	20	676.752	630.064	-7	672.740	-0.6	685.136	1.2	680.286	0.5	677.433	0.1
Sr	38	3131.53	2951.89	-6	3110.44	-0.7	3156.50	0.8	3136.76	0.2	3134.48	0.09
Ba	56	7883.53	7478.27	-5	7829.36	-0.7	7931.34	0.6	7886.19	0.03	7888.14	0.06
Ra	88	23094.3	22065.8	-4	22945.9	-0.6	23201.5	0.5	23083.9	-0.05	23110.5	0.07

We can repeat this exercise for the fourth order, matching both c_1 and c_2 to exact values. Now we find:

$$T^{\text{MGEA4}}[n] = T^{\text{TF}}[n] + 1.789 T^{(2)}[n] - 3.841 T^{(4)}[n] \quad (4.16)$$

i.e., strongly modified gradient coefficients. This is somewhat arbitrary, as there are several terms in $T^{(4)}$, and there's no real reason to keep their ratios the same as in GEA (Eq. (4.10)). However, the results of Table 4.2 and Fig. 4.3 speak for themselves. The resulting functional is better than either GEA for all the alkali-earths. Of course, T_s is positive for any density, as are the terms T^{TF} , $T^{(2)}$ and $T^{(4)}$ of the GEA. Eq. (4.16) however can be improperly negative for rapidly-varying densities, and so is not suitable for general use.

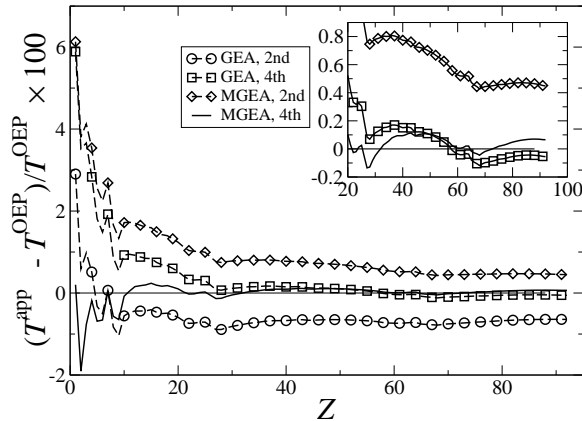


Figure 4.3: Percentage errors for atoms (from $Z = 1$ to $Z = 92$) using various approximations.

Molecules: The improvement in total kinetic energies is not just confined to atoms. Also, for non-interacting kinetic energies of molecules, using the data in Ref. (57), Eq. (4.16) gives a better average of the absolute errors in hartree (0.6) than T^{TF} (9.4), T^{GEA2} (0.9), and T^{GEA4} (0.8), shown in Table 4.3. Of greater importance are energy differences. For atomization kinetic energies, also using the data in Ref. (57), T^{TF} gives the best averaged absolute error (0.25), which is worsened by gradient corrections. Since the GEA does not have

Table 4.3: Non-interacting kinetic energy (in hartrees) for molecules, and errors in approximations. All values are evaluated on the converged KS orbitals and densities obtained with B88-PW91 functionals, and the MGEA4 kinetic energies are evaluated using the TF and the GEA data from Ref. (57).

Atom	T_s ¹	T^{TF} ¹	T^{GEA2} ¹	T^{GEA4} ¹	T^{MGEA4}
H	0.500	-0.044	0.011	0.032	-0.026
B	24.548	-2.506	-0.058	0.476	-0.177
C	37.714	-3.731	-0.154	0.600	-0.228
N	54.428	-4.993	-0.097	0.904	-0.078
O	74.867	-6.990	-0.546	0.765	-0.497
F	99.485	-9.093	-0.933	0.659	-0.609
H ₂	1.151	-0.142	-0.014	0.033	-0.094
HF	100.169	-9.016	-0.920	0.639	-0.520
H ₂ O	76.171	-7.074	-0.692	0.565	-0.484
CH ₄	40.317	-3.773	-0.140	0.619	-0.189
NH ₃	56.326	-5.292	-0.400	0.587	-0.331
BF ₃	323.678	-29.052	-2.641	2.454	-1.370
CN	92.573	-8.940	-0.687	0.978	-0.570
CO	112.877	-10.694	-0.911	1.036	-0.670
F ₂	199.023	-18.367	-2.201	0.925	-1.451
HCN	92.982	-8.925	-0.658	1.008	-0.534
N ₂	109.013	-10.487	-0.916	0.999	-0.719
NO	129.563	-12.342	-1.240	0.962	0.279
O ₂	149.834	-14.186	-1.527	0.965	-1.110
O ₃	224.697	-21.636	-2.699	1.028	-2.071
MAE ²		9.364	0.872	0.812	0.600

¹ Ref. (57)

² Mean absolute error

the right quantum corrections from the edges, turning points and Coulomb cores (10), GEA does not improve on the atomization process. However, the TF kinetic energy functional is always the dominant term. So, TF gives very good results on the atomization kinetic energies. But the error (0.29) of Eq. (4.16) is smaller than that of T^{GEA2} (0.36) and T^{GEA4} (0.44). In either case, Eq. (4.16) works better for atoms and molecules than the fourth-order gradient expansion. Thus, requiring asymptotic exactness is a useful and powerful constraint in functional design.

Jellium surfaces: We test this MGEA4 functional for jellium surface kinetic energies. As shown in Table 4.4, the $T^{(4)}$ term in T^{GEA4} improves the jellium surface kinetic energy in comparison to the results of T^{GEA2} , but Eq. (4.16) worsens the jellium surface kinetic energies due to the strongly modified coefficient of $T^{(4)}$. This is a confirmation of our general approach. By building in the correct asymptotic behavior for atoms, including the Scott correction coming from the $1s$ region, we *worsen* energetics for systems without this feature.

Table 4.4: Jellium surface kinetic energies (erg/cm^2) and % error, which is $(\sigma_s^{\text{app}} - \sigma_s^{\text{ex}})/\sigma_s^{\text{ex}}$, of each approximation.

r_s	Exact	T^{TF}	T^{GEA2}	T^{GEA4}	T^{MGEA2} ^a	T^{MGEA4} ^b	T^{LmGGA}
2	-5492.7	11	2.5	1.1	-0.9	0.73	1.3
4	-139.9	54	22	11	12	36	15
6	-3.4	660	330	180	238	675	280

^a See Eq. (4.15)

^b See Eq. (4.16)

Jellium spheres: We also investigate the kinetic energies of neutral jellium spheres (with KS densities using LDA exchange-correlation and with $r_s = 3.9$) from Ref. (58). The analysis of the results is based upon the liquid drop model of Refs. (59; 60). We write

$$T_s(r_s, N) = \frac{4}{3}\pi R^3 \tau^{\text{unif}}(r_s) + 4\pi R^2 \sigma_s + 2\pi R \gamma_s^{\text{eff}}(r_s, N), \quad (4.17)$$

where R is the radius of the sphere of uniform positive background. Since we know the bulk (uniform) kinetic energy density, τ^{unif} , and the surface kinetic energy σ_s for a given functional, we can extract $\gamma_s^{\text{eff}}(r_s, N)$ from this equation, and

$$\lim_{N \rightarrow \infty} \gamma_s^{\text{eff}}(r_s, N) = \gamma_s(r_s) \quad (4.18)$$

is the curvature energy of jellium. We calculate $\gamma_s^{\text{eff}}(r_s, N)$ using the TF, GEA, MGEA,

and a Laplacian-level meta-GGA (LmGGA) of Ref. (58), which is explained further in the following subsection. From Table 4.5, we observe that: (i) Gradient corrections in GEA

Table 4.5: $10^4 \times (\gamma_s^{\text{eff}}(\mathbf{r}_s, N) - \gamma_s^{\text{TF}}(\mathbf{r}_s, N))$ in atomic units vs. $N = Z$ for neutral jellium spheres with $r_s = 3.93$ with various functionals. As $N = Z \rightarrow \infty$, γ_s^{eff} tends to the curvature kinetic energy of jellium, γ_s .

N	Exact	T^{GEA2}	T^{GEA4}	T^{MGEA2} ^a	T^{MGEA4} ^b	T^{LmGGA}
2	-1.8	1.1	2.4	1.5	-2.8	1.9
8	-1.9	1.0	2.1	1.3	-2.3	-5.1
18	-0.5	1.2	2.0	1.6	-0.7	-6.4
58	-0.8	1.3	2.2	1.7	-1.1	-3.2
92	-1.7	1.2	2.0	1.5	-1.0	-1.9
254	-0.5	1.4	2.3	1.8	-0.9	-

^a See Eq. (4.15)

^b See Eq. (4.16)

worsen γ_s^{eff} . (ii) The LmGGA of Ref. (58) is even worse than T^{GEA4} . (iii) Eq. (4.15) (which has the right c_0 and c_1) is not so good, but better than T^{GEA4} . (iv) Eq. (4.16) (which has the right c_0 , c_1 , and c_2) gives good results.

Existing approximations: We suggest that the large- Z asymptotic expansion is a necessary condition that an accurate kinetic energy functional should satisfy, but is not sufficient. We show this by testing two kinds of semilocal approximations (GGA and meta-GGA) to the kinetic energy functionals.

Recently, Tran and Wesolowski (61) constructed a GGA-type kinetic energy functional using the *conjointness conjecture*. They found the enhancement factor by minimizing mean absolute errors of kinetic energies for closed-shell atoms. We evaluate the kinetic energies of atoms using this functional (T^{GGA}) and extract the asymptotic coefficients shown in Table 4.1. This gives a good c_1 coefficient (-0.51), with c_2 (0.29) close to the correct value (0.27), and so is much more accurate than the GEA's.

Perdew and Constantin (58) constructed a LmGGA for the positive kinetic energy density τ

that satisfies the local bound $\tau \geq \tau_W$, where τ_W is the von Weizsäcker kinetic energy density, and tends to τ_W as $r \rightarrow 0$ in an atom. It recovers the fourth-order gradient expansion in the slowly-varying limit. We calculate the asymptotic coefficients shown in Table 4.1 for this functional. These values are better than those of T^{GEA4} . The good c_1 from T^{GEA4} appears somewhat fortuitous, since there is nothing about a slowly-varying density that is relevant to a cusp in the density. The good Scott correction c_1 from the LmGGA comes from correct physics: LmGGA recovers the von Weizsäcker kinetic energy density in the $1s$ cusp, without the spurious but integrable divergences of the integrand of T^{GEA4} .

We finish by discussing other columns of the periodic table. We have also performed all these calculations on the noble gases. In fact, from studies of the asymptotic series (62), it is known that the shell-structure occurs in the next order, $Z^{4/3}$, and that the noble gases are furthest from the asymptotic curves. But Table 4.6 shows our functionals work almost as well for the noble gas series.

Table 4.6: KS kinetic energy (T) in hartrees and various approximations for noble atoms.

Atom	Z	T_s	T^{TF}	%err	T^{GEA2}	%err	T^{MGEA2}	%err	T^{GEA4}	%err	T^{MGEA4}	%err
He	2	2.86168	2.56051	-11	2.87847	0.6	2.97083	3.8	2.96236	3.5	2.80717	-1.9
Ne	10	128.545	117.761	-8	127.829	-0.6	130.753	1.7	129.737	0.9	128.447	-0.08
Ar	18	526.812	489.955	-7	524.224	-0.5	534.178	1.4	530.341	0.7	527.772	0.2
Kr	36	2752.04	2591.20	-6	2733.07	-0.7	2774.27	0.8	2756.72	0.2	2754.17	0.08
Xe	54	7232.12	6857.94	-5	7183.78	-0.7	7278.42	0.6	7236.65	0.06	7237.85	0.08
Rn	86	21866.7	20885.7	-4	21725.4	-0.6	21969.3	0.5	21857.2	-0.04	21881.7	0.07

4.5 Modern Parametrization of Thomas-Fermi Density

Our asymptotic expansion study gives new reasons for studying large Z atoms. Our approximate functionals were tested on highly accurate densities, but ultimately, self-consistency is an important and more-demanding test. Any approximate functional yields an approximate density via the Euler equation. In this section, we present a new, modern parametrization of the neutral atom TF density, which is more accurate than earlier versions (63; 64).

The TF density of a neutral atom can be written as

$$n(r) = \frac{Z^2}{4\pi a^3} \left(\frac{\Phi}{x} \right)^{3/2}, \quad (4.19)$$

where $a = (1/2)(3\pi/4)^{2/3}$ and $x = Z^{1/3}r/a$, and the dimensionless TF differential equation is

$$\frac{d^2\Phi(x)}{dx^2} = \sqrt{\frac{\Phi^3(x)}{x}}, \quad \Phi(x) > 0, \quad (4.20)$$

which satisfies the following initial conditions:

$$\Phi(0) = 1, \quad \Phi'(0) = -B, \quad B = 1.5880710226. \quad (4.21)$$

We construct a model for Φ which recovers the first eight terms of the small- x expansion and the leading term of the asymptotic expansion at large- x ($\Phi(x) \rightarrow 144/x^3$, as $x \rightarrow \infty$). Following Tal and Levy (65), we use $y = \sqrt{x}$ as the variable, because of the singularity of the TF equation. Our parametrization is

$$\Phi^{mod}(y) = \left(1 + \sum_{p=2}^9 \alpha_p y^p \right) / \left(1 + y^9 \sum_{p=1}^5 \beta_p y^p + \frac{\alpha_9 y^{15}}{144} \right) \quad (4.22)$$

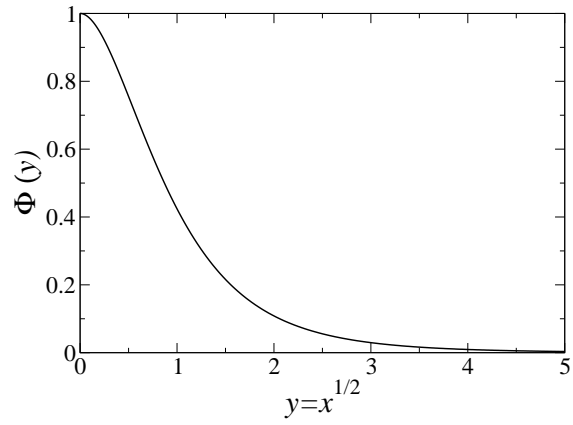


Figure 4.4: Accurate numerical $\Phi(y)$ and parametrized $\Phi(y)$ can not be distinguished.

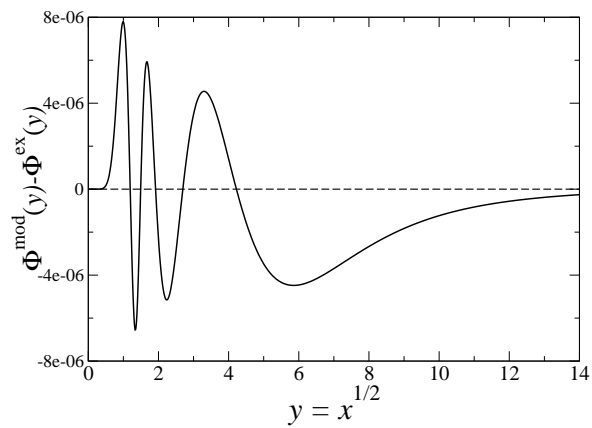


Figure 4.5: Errors in the model, relative to numerical integrations.

where α_i and β_i are coefficients given in the Table 4.7. The values of α_i are fixed by the small y -expansion, while those of β_i are found by minimization of the weighted sum of squared residuals, χ^2 , for $0 < y < 10$. The χ^2 was minimized using the Levenberg-Marquardt method (66). This method is for fitting when the model depends nonlinearly on the set of unknown parameters. 1000 points were used, equally spaced between $y = 0$ and $y = 10$. We plot

Table 4.7: The values of β_i are found by fitting Eq.(4.22) to the accurate numerical solution, and those of α_i are the parameters of small- y expansion (65). B is given by 1.5880710226.

α_2	$-B$	β_1	-0.0144050081
α_3	$4/3$	β_2	0.0231427314
α_5	$-2B/5$	β_3	-0.00617782965
α_6	$1/3$	β_4	0.0103191718
α_7	$3B^2/70$	β_5	-0.000154797772
α_8	$-2B/15$		
α_9	$2/27 + B^3/252$		

the accurate $\Phi(y)$ and our model in Fig. 4.4, and the differences between them in Fig. 4.5. These graphs illustrate the accuracy of our parametrization.

In Table 4.5 we calculate several moments using our model and existing models that were proposed by Gross and Dreizler (63) and Latter (64). The Latter parametrization is

$$\begin{aligned} \Phi^L(x) = & 1/(1 + 0.02747x^{1/2} + 1.243x - 0.1486x^{3/2} + 0.2303x^2 + 0.007298x^{5/2} \\ & + 0.006944x^3), \end{aligned} \quad (4.23)$$

and the Gross-Dreizler model (which correctly removes the \sqrt{x} term) is:

$$\Phi^{GD}(x) = 1/(1 + 1.4712x - 0.4973x^{3/2} + 0.3875x^2 + 0.002102x^3). \quad (4.24)$$

Lastly, we introduce an extremely simple model that we have found useful for pedagogical

purposes (even when N differs from Z). We write

$$n^{ped}(r) = \frac{N}{2\pi^{3/2}R^{3/2}} \frac{1}{r^{3/2}} e^{-r/R}, \quad R = \frac{\alpha N^{2/3}}{Z - \beta N}, \quad (4.25)$$

where $\alpha = (9/5\sqrt{5})(\sqrt{3}\pi/4)^{1/3}$ and $\beta = 1/2 - 1/\pi$ have been found from integration of the TF kinetic and Hartree energies, respectively, and R minimizes the TF total energy. For $N = Z$, this yields:

$$\Phi^{ped}(x) = \gamma e^{-2\alpha(1-\beta)x/3\alpha}, \quad \gamma = \frac{5\sqrt{5}}{6\sqrt{3}} \left(\frac{1}{2} + \frac{1}{\pi} \right). \quad (4.26)$$

This crude approximation does not satisfy the correct initial conditions of Eq. (4.21):

$$\begin{aligned} \Phi^{ped}(0) &= \gamma = 0.880361 (\neq 1), \\ \Phi^{ped'}(0) &= -\frac{125(2+\pi)^2}{648(4\pi^5)^{1/3}} = -0.48 (\neq -1.59). \end{aligned} \quad (4.27)$$

To compare the quality of the various parametrizations, we calculate the p -th moment of the j -th power of $\Phi(x)/x$:

$$M_j^{(p)} = \int dx x^p \left(\frac{\Phi(x)}{x} \right)^j. \quad (4.28)$$

Many quantities of interest can be expressed in terms of these moments:

1) Particle number: To ensure $\int d^3r n(\mathbf{r}) = N$, we require

$$M_{3/2}^{(2)} = 1 \quad (4.29)$$

2) TF kinetic energy: The TF kinetic energy is $c_0 Z^{7/3}$, which implies

$$M_{5/2}^{(2)} = \frac{5}{7} B. \quad (4.30)$$

3) The Hartree energy is $U = \frac{1}{2} \int \int d^3 r d^3 r' \frac{n(\mathbf{r})n(\mathbf{r}')}{|\mathbf{r}-\mathbf{r}'|} = \frac{1}{7a} M_{3/2}^{(1)} Z^{7/3}$, which implies

$$M_{3/2}^{(1)} = B. \quad (4.31)$$

4) The external energy is defined as $V_{\text{ext}} = - \int d^3 r Z n(r)/r = -\frac{1}{a} M_{3/2}^{(1)} Z^{7/3}$ for the exact TF density, which also implies Eq. (4.31).

5) The local density approximation exchange energy is defined as $E_{\text{x}}^{\text{LDA}} = A_{\text{x}} \int d\mathbf{r} n^{4/3}(\mathbf{r})$, where $A_{\text{x}} = -(3/4)(3/\pi)^{1/3}$, so for TF, $E_{\text{x}}^{\text{LDA}} = A_{\text{x}}(4\pi a^3)^{-\frac{1}{3}} M_2^{(2)} Z^{5/3}$, which implies

$$M_2^{(2)} = 0.615434679, \quad (4.32)$$

extracted from our accurate numerical solution. LDA exchange suffices (43; 45) for asymptotic exactness to the order displayed in Eqs. (4.3) and (4.4); for a numerical study, see Ref. (67; 68).

Table 4.8: Various moments calculated with our model and with the models of Ref. (63; 64). Here $M_j^{(p)}$ is given by $\int dx x^p \left(\frac{\Phi(x)}{x}\right)^j$

moment	our model	% err	Gross and Dreizler (63)	% err	Latter(64)	% err	$\Phi^{ped}(x)$	% err	exact
$M_{3/2}^{(2)}$	0.999857885	-0.01	1.008	0.8	0.999	-0.04	1	0	1
$M_{5/2}^{(2)}$	1.13426462	-0.006	1.1299	-0.4	1.137	0.2	1.11	-2	$5B/7$
$M_2^{(2)}$	0.615438208	0.001	0.6129	-0.4	0.616	0.02	0.72	16	0.615434679^1
$M_{3/2}^{(1)}$	1.58799857	-0.005	1.5844	-0.2	1.589	0.07	1.62	2	B

¹ Numerical result from the TF differential equation.

Table 4.5 shows that our modern parametrization is far more accurate than existing models by all measures, and that our simple pedagogical model is roughly correct for many features.

Finally, we make some comparisons with densities of real atoms to illustrate those features of real atoms that are captured by TF. The radial density, $s(\mathbf{r})$ (Eq. (4.12)), and $q(\mathbf{r})$ (Eq. (4.13)) are given by

$$4\pi r^2 n(r) = Z^{4/3} f(x)/a, \quad (4.33)$$

where $f(x) = \sqrt{x} \Phi^{3/2}(x)$,

$$s(r) = \frac{a_1}{Z^{1/3}} \frac{|g(x)|}{f(x)}, \quad a_1 = (9/2\pi)^{1/3}/2, \quad (4.34)$$

and

$$q(r) = \frac{a_1^2}{3Z^{2/3}} \frac{\{g^2(x) + 2x^2 \Phi(x) \Phi''(x)\}}{f^2(x)}, \quad (4.35)$$

where $g(x)$ is defined as $\Phi(x) - x\Phi'(x)$. The gradient relative to the screening length is

$$t(\mathbf{r}) = \frac{|\nabla n(\mathbf{r})|}{2k_s(\mathbf{r})n(\mathbf{r})}, \quad \text{where } k_s(\mathbf{r}) = \sqrt{4k_F(\mathbf{r})/\pi}, \quad (4.36)$$

and here

$$t(r) = \frac{a_2 |g(x)|}{(x^3 \Phi^5(x))^{1/4}}, \quad a_2 = \frac{3^{5/6} \pi^{1/3}}{2^{8/3} \sqrt{a}} = 0.6124. \quad (4.37)$$

We also show large- and small- x limit behaviors of various quantities using $\Phi(x) \rightarrow 144/x^3$

as $x \rightarrow \infty$ and $\Phi(x) \rightarrow 1 - Bx + \dots$ as $x \rightarrow 0$.

$$\frac{Z^2}{4\pi a^3} \frac{1}{x^{3/2}} \xrightarrow{x \rightarrow 0} n(r) \xrightarrow{x \rightarrow \infty} \frac{432Z^2}{a^3 \pi x^6}, \quad (4.38)$$

$$\frac{Z^{4/3}}{a} \sqrt{x} \xrightarrow{x \rightarrow 0} 4\pi r^2 n(r) \xrightarrow{x \rightarrow \infty} \frac{144Z^{4/3}}{ax^{5/2}}, \quad (4.39)$$

$$\frac{a_1}{Z^{1/3}} \frac{1}{\sqrt{x}} \xrightarrow{x \rightarrow 0} s(r) \xrightarrow{x \rightarrow \infty} \frac{a_1 x}{3Z^{1/3}}, \quad (4.40)$$

$$\frac{a_1^2}{3Z^{2/3}} \frac{1}{x} \xrightarrow{x \rightarrow 0} q(r) \xrightarrow{x \rightarrow \infty} \frac{5a_1^2 x^2}{54Z^{2/3}}, \quad (4.41)$$

$$\frac{a_2}{x^{3/4}} \xrightarrow{x \rightarrow 0} t(r) \xrightarrow{x \rightarrow \infty} \frac{2a_2}{\sqrt{3}}. \quad (4.42)$$

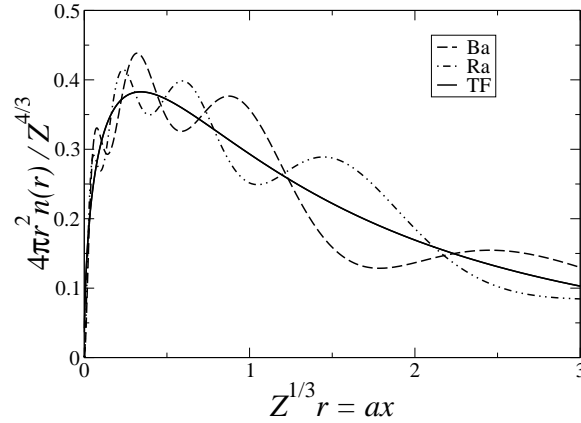


Figure 4.6: Plot of the scaled radial densities of Ba and Ra using Eq.(4.33) and SCF densities. TF scaled densities of Ba and Ra are on top of each other.

We plot the Z -scaled accurate self-consistent densities and TF radial densities of Ba ($Z = 56$) and Ra ($Z = 88$) in Fig. 4.6. Although the shell structure is missing, and the decay at a large distance is wrong, the overall shape of the TF density is relatively correct.

In Figs. 4.7, 4.8, and 4.9, we plot the scaled $s(r)$, $q(r)$, and $t(r)$ using the self-consistent and TF densities of Ba and Ra. In particular, $t(r)$ measures how fast the density changes on

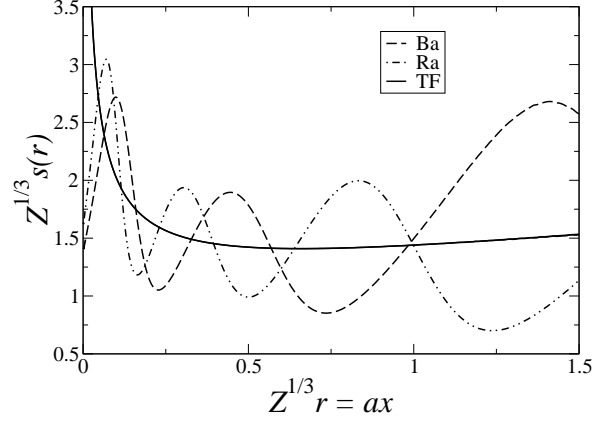


Figure 4.7: Plot of the scaled reduced density gradient $s(r)$ (relative to the local Fermi wavelength) vs. $Z^{1/3}r$.

the scale of the TF screening length, and its magnitude does not vary with Z in TF theory. From these figures, we see that $s(r)$, $q(r)$ and $t(r)$ of the TF density diverge near the nucleus, since the TF density does not satisfy Kato's cusp condition.

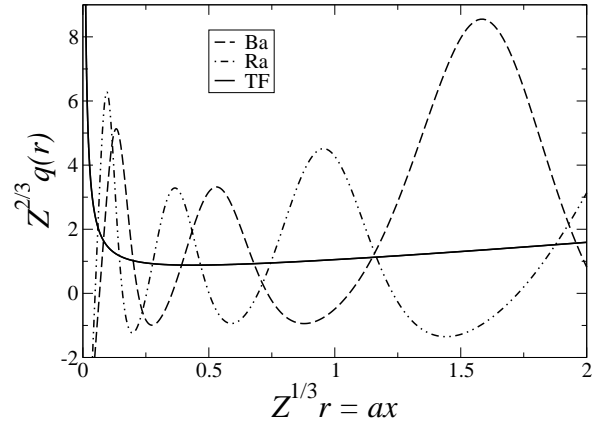


Figure 4.8: Plot of the scaled reduced Laplacian $q(r)$ (relative to the local Fermi wavelength) vs. $Z^{1/3}r$.

When $N = Z \rightarrow \infty$ for a realistic density, $s(r)$ is small except in the density tail ($s \sim Z^{-1/3}$ over most of the density), and $q(r)$ is small except in the tail and 1s core regions ($q \sim Z^{-2/3}$ over most of the density). This is why gradient expansions for the kinetic and exchange energies, applied to realistic densities, work as well as they do in this limit. The kinetic and

exchange energies have only one characteristic length scale, the local Fermi wavelength, but the correlation energy also has a different one, the local screening length. Since $t(r)$ is not and does not become small in this limit, gradient expansions do not work well at all for the correlation energies of atoms (45). The standard of “smallness” for s and q , and the more severe standard of smallness for t , are explained in Refs. (45) and (69; 70).

Finally we evaluate $T^{(0)} + T^{(2)}$ on the TF density. We find the correct c_0 in the $Z \rightarrow \infty$ expansion from $T^{(0)}$, but c_1 vanishes, due to the absence of a proper nuclear cusp, and c_2 diverges because $T^{(2)}$ diverges at its lower limit of integration.

4.6 Summary

We have shown the importance of the large- N limit for density functional construction of the kinetic energy (with the functional evaluated on a Kohn-Sham density), and also provided a modern, highly accurate parametrization of the neutral-atom TF density. Our results should prove useful in the never-ending search for improved density functionals.

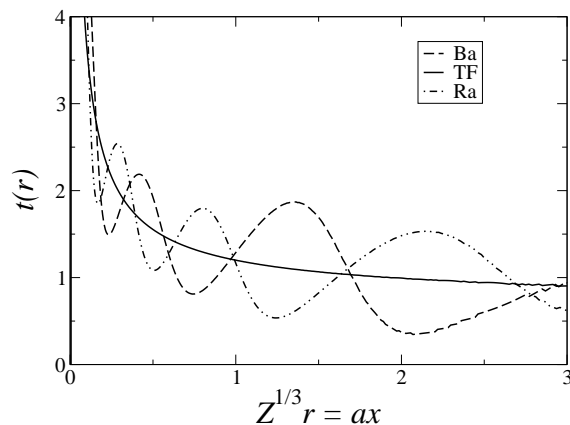


Figure 4.9: Plot of the reduced density gradient $t(r)$ (relative to the local screening length) vs. $Z^{1/3}r$. As $r \rightarrow \infty$, the TF $t \rightarrow 0.7071$.

For atoms and molecules, the large- N limit seems more important than the slowly-varying limit. On the ladder (71) of density-functional approximations, there are three rungs of semilocal approximations (followed by higher rungs of fully nonlocal ones). The LDA uses only the local density, the GGA uses also the density gradient, and the meta-GGA uses in addition the orbital kinetic energy density or the Laplacian of the density. For the exchange-correlation energy, the GGA rung cannot (45; 69) simultaneously describe the slowly-varying limit and the $N = Z \rightarrow \infty$ limit for an atom, and we have found here that the same is true (but less severely by percent error of a given energy component) for the kinetic energy. This follows because, as $N = Z \rightarrow \infty$, the reduced gradient $s(r)$ of Eq. (4.12) becomes small over the energetically important regions of the atom, as can be inferred from Fig. 4.7, so that a GGA reduces to its own second-order gradient expansion even in regions where a meta-GGA does not (45) (e.g., near a nucleus, where $q(r)$ diverges but $s(r)$ does not, as shown in Figs. 4.7 and 4.8). For the kinetic as for the exchange-correlation energy, meta-GGA's (58) can recover both the slowly-varying and large- Z limits; it remains to be seen how well fully nonlocal approximations (6; 72) can do this.

Chapter 5

Semiclassical Orbital-Free Potential-Density Functional Theory

In this chapter, we discuss how to derive a uniform semiclassical approximation to the density and kinetic energy (KE) density as a functional of the potential from the semiclassical Green's function. we apply this semiclassical scheme to 1D systems with two turning points and compare the semiclassical result to the exact answer. Also, we find that this scheme can be applied to 3D spherical systems with two turning points.

5.1 Uniform semiclassical density

Recently, we derived a semiclassical approximation to the density and KE density for systems with hard wall boundaries(10). This has been further discussed in Ref. (73). The original idea of a semiclassical Green's function approach comes from Ref. (74).

Imagine a potential $v(x)$ in 1D with hard walls at $x = 0$ and $x = L$. If the orbital energy is greater than the maximum of the bottom potential, the following WKB wavefunction

satisfies the boundary conditions:

$$\psi(x) \simeq \frac{1}{\sqrt{k(x)}} \sin \theta(x), \quad (5.1)$$

where the semiclassical momentum $k(x) = \sqrt{2(\mathcal{E} - v(x))}$ and the semiclassical phase $\theta(x) = \int_0^x dx k(x)$. Hence, we can construct the semiclassical Green's function from WKB wavefunctions using Eq. (2.18):

$$g(x; \mathcal{E}) = \frac{\cos \theta(L) - \cos (2\theta(x) - \theta(L))}{k(x) \sin \theta(L)}. \quad (5.2)$$

The Fermi energy (or chemical potential) E_F is determined by the quantization condition

$$\int_0^L dx \sqrt{2(E_F - v(x))} = \left(N + \frac{1}{2}\right) \pi, \quad (5.3)$$

where N is the number of particles, and E_F lies between the highest occupied and the lowest unoccupied levels.

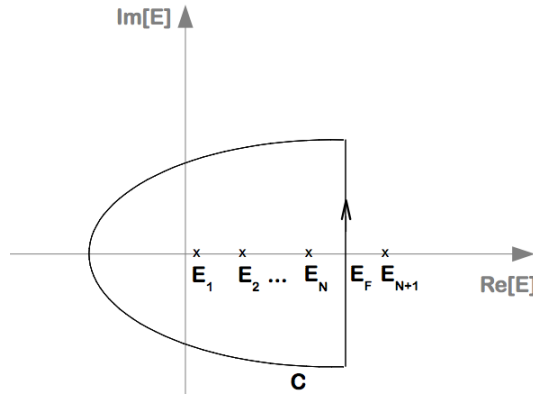


Figure 5.1: Contour of integration in the complex \mathcal{E} -plane.

Accounting for the requirement that $E_N \leq E_F \leq E_{N+1}$ we pick the contour C shown in Fig. 5.1: a vertical line along $\mathcal{E} = E_F + i\eta$ connected to a semicircle, which encloses the

N lower-lying energy-eigenvalues E_1, \dots, E_N . By choosing this particular shape for C we ensure that the lowest $|\mathcal{E}|$ used is E_F .

Via Eq. (2.19) where the contour C is chosen to pass through the real axis at E_F in Fig. 5.1, the semiclassical density for N particles is obtained

$$n^{\text{semi}}(x) = \frac{k_F(x)}{\pi} - \frac{\sin \theta_F(x)}{2T_F k_F(x) \sin \alpha(x)}, \quad (5.4)$$

where $\alpha(x) = \pi \tau_F(x)/T_F$, the semiclassical traveling time from 0 to x $\tau_F(x) = \int_0^x dx 1/k_F(x)$, and $\tau_F(L) = T_F$. Note that subscript F denotes evaluation of the given quantity at E_F . This semiclassical approximation generally gives very accurate densities (10; 73) for arbitrary bottom potentials.

However, the WKB approximation is not a good choice for construction of a uniform semiclassical Green's function for 1D systems with turning points, since the WKB wavefunction diverges at turning points due to the $1/k(x)$ factor. we use a uniform semiclassical approximation instead of WKB to avoid this problem.

5.1.1 The leading term

We construct the Green's function for a single turning point by approximating $\psi_{l,r}(x)$ by means of the uniform semiclassical solutions (12; 75)

$$\psi_l^{\text{unif}}(x) = \frac{\theta^{1/6}(x)}{\sqrt{k(x)}} Ai(-z(x)), \quad (5.5)$$

$$\psi_r^{\text{unif}}(x) = \frac{\theta^{1/6}(x)}{\sqrt{k(x)}} Ai(-e^{2\pi i/3} z(x)), \quad (5.6)$$

where the semiclassical momentum $k(x) = \sqrt{2(\mathcal{E} - v(x))}$, the semiclassical phase $\theta(x) = \int_a^x dx' k(x')$, $z(x) = (3\theta(x)/2)^{2/3}$, and a is the turning point on the left side. In this approximation, the Wronskian becomes

$$W(E) = \left(\frac{2}{3}\right)^{1/3} \frac{1}{2\pi} e^{5\pi i/6}. \quad (5.7)$$

In atomic units, $p = 1/2$ in Eq. (2.18), our semiclassical approximation to the diagonal Green's function for a single turning-point problem becomes

$$g_{\text{ST}}^{\text{semi}}(x, \mathcal{E}) = \frac{2\pi}{i} \frac{\sqrt{z(x)}}{k(x)} \text{Ai}(-z(x)) [\text{Ai}(-z(x)) - i \text{Bi}(-z(x))]. \quad (5.8)$$

As the number of particles $N \rightarrow \infty$, $E_{\text{F}} \gg \eta$ for the dominant contributions to the integral, allowing us to expand all quantities in powers of the imaginary part of the energy η

$$\frac{1}{k(x; E_{\text{F}} + i\eta)} = \frac{1}{k_{\text{F}}(x)} \left(1 - \frac{i\eta}{k_{\text{F}}^2} + \dots\right), \quad (5.9)$$

$$\theta(x; E_{\text{F}} + i\eta) = \theta_{\text{F}}(x) + i\eta\tau_{\text{F}}(x) + \dots, \quad (5.10)$$

$$\Theta(E_{\text{F}} + i\eta) = \Theta_{\text{F}} + i\eta T_{\text{F}} + \dots, \quad (5.11)$$

$$z(x; E_{\text{F}} + i\eta) = z_{\text{F}}(x) + i\eta \frac{\tau_{\text{F}}(x)}{\sqrt{z_{\text{F}}(x)}} + \dots. \quad (5.12)$$

Here, we introduce the quantities $\tau_{\text{F}}(x) = \int_{a_{\text{F}}}^x dx' 1/k_{\text{F}}(x')$, the classical time for a particle at E_{F} to travel from a_{F} to x , and $T_{\text{F}} = \tau_{\text{F}}(b_{\text{F}})$. a_{F} and b_{F} are the left and right turning points determined by E_{F} . Keeping terms up to first order in η and using the integral representation

of Airy functions (76), Eq. (2.19) yields

$$n_{\text{ST}}^{\text{semi}}(x) = -\frac{1}{\pi} \Re \int_0^\infty id\eta \left[\frac{\sqrt{z_{\text{F}}}}{k_{\text{F}}} + i\eta \left(\frac{\tau_{\text{F}}(x)}{k_{\text{F}}(x)\sqrt{z_{\text{F}}(x)}} - \frac{z_{\text{F}}(x)}{k_{\text{F}}^3(x)} \right) \right] \\ \times \frac{1}{2\pi^3} \int_0^\infty dt e^{-if(t)-t\eta\tau_{\text{F}}(x)/\sqrt{z_{\text{F}}(x)}}. \quad (5.13)$$

We make use of the semiclassical quantization condition for the two-turning-point problem, which states that Θ/π is an integer $+1/2$, i.e., $\Theta_{\text{F}} = N\pi$. Direct evaluation of the integration with respect to η gives

$$n_{\text{ST}}^{\text{semi}}(x) = \frac{2z_{\text{F}}(x)}{k_{\text{F}}(x)\tau_{\text{F}}(x)} [z_{\text{F}}(x)Ai^2(-z_{\text{F}}(x)) + Ai'(-z_{\text{F}}(x))^2]. \quad (5.14)$$

However, this semiclassical density for a single turning point system cannot recover the Thomas-Fermi (TF) density at the asymptotic limit, since the uniform semiclassical wavefunction does not know about the existence of another turning point. Hence, to recover the TF density, we set the traveling time $\tau_{\text{F}}(x)$ as

$$\tau_{\text{F}}(x) = \frac{3\theta_{\text{F}}(x)}{k_{\text{F}}^2(x)}. \quad (5.15)$$

This yields

$$n_{\text{ST}}^{\text{semi}}(x) = \frac{k_{\text{F}}(x)}{\sqrt{z_{\text{F}}(x)}} [z_{\text{F}}(x)Ai^2(-z_{\text{F}}(x)) + Ai'(-z_{\text{F}}(x))^2]. \quad (5.16)$$

Using the asymptotic form of Airy functions(76), we obtain from Eq. (5.16)

$$n_{\text{ST}}^{\text{semi}}(x) \sim \frac{k_{\text{F}}(x)}{\pi} - \frac{k_{\text{F}}(x) \cos(2\theta_{\text{F}}(x))}{6\pi\theta_{\text{F}}(x)}, \quad (5.17)$$

which recovers the TF density as the leading term.

5.1.2 Quantum corrections

The Green's function(74) for a two-turning-point system is given as

$$g^{\text{semi}}(x; \mathcal{E}) = -2\pi \frac{\sqrt{z(x)}}{k(x)} [\tan \Theta Ai^2(-z(x)) + Ai(-z(x))Bi(-z(x))]. \quad (5.18)$$

It can be split into $g_{\text{ST}}^{\text{semi}}(x; \mathcal{E})$ (Eq. (5.8)) and $g^{\text{QC}}(x; \mathcal{E})$, which arises due to the other turning point. So,

$$g^{\text{semi}}(x; \mathcal{E}) = g_{\text{ST}}^{\text{semi}}(x; \mathcal{E}) + g^{\text{QC}}(x; \mathcal{E}), \quad (5.19)$$

where

$$g^{\text{QC}}(x; \mathcal{E}) = 4\pi i \frac{\sqrt{z(x)}}{k(x)} \frac{1}{1 + e^{-2i\Theta}} Ai^2(-z(x)). \quad (5.20)$$

Hence, the density becomes

$$\begin{aligned} n^{\text{semi}}(x) &= \frac{1}{2\pi i} \oint_{C(\mu)} d\mathcal{E} g^{\text{semi}}(x; \mathcal{E}) \\ &= \frac{1}{2\pi i} \oint_{C(\mu)} d\mathcal{E} [g_{\text{ST}}^{\text{semi}}(x; \mathcal{E}) + g^{\text{QC}}(x; \mathcal{E})] \\ &= n_{\text{ST}}^{\text{semi}}(x) + n^{\text{QC}}(x), \end{aligned} \quad (5.21)$$

where $n_{\text{ST}}^{\text{semi}}(x)$ is given in Eq. (5.16). The density $n^{\text{QC}}(x)$ is

$$n^{\text{QC}}(x) = \oint_C d\mathcal{E} \frac{\sqrt{z(x)}}{k(x)} \left(\frac{2}{1 + e^{-2i\Theta}} \right) Ai^2(-z(x)). \quad (5.22)$$

By taking $\mathcal{E} \rightarrow E_F + i\eta$, expanding terms to the first order in η , and using the contour in Fig. 5.1, $n^{\text{QC}}(x)$ becomes

$$n^{\text{QC}}(x) = 4\Re \left[i \frac{\sqrt{z_{\text{F}}(x)}}{k_{\text{F}}(x)} \int_0^\infty d\eta \frac{Ai^2(-z_{\text{F}}(x) - i\eta\tau_{\text{F}}(x)/\sqrt{z_{\text{F}}(x)})}{1 + e^{2\eta T_{\text{F}}}} \right]. \quad (5.23)$$

Using the integral representation of the Airy function, $n^{\text{QC}}(x)$ can be expressed as an integral representation

$$n^{\text{QC}}(x) = \frac{2}{2\pi^{3/2}} \frac{\sqrt{z_{\text{F}}(x)}}{k_{\text{F}}(x)} \left[\int_0^\infty \frac{dt}{\sqrt{t}} \sin f(t) \int_0^\infty \frac{e^{-\eta t\tau_{\text{F}}(x)/\sqrt{z_{\text{F}}(x)}} - e^{\eta t\tau_{\text{F}}(x)/\sqrt{z_{\text{F}}(x)}}}{1 + e^{2\eta T_{\text{F}}}} d\eta \right], \quad (5.24)$$

where $f(t) = t^3/12 - z_{\text{F}}(x)t + \pi/4$. The integration with respect to η can be expressed as

$$\int_0^\infty \frac{e^{-\eta t\tau_{\text{F}}(x)/\sqrt{z_{\text{F}}(x)}} - e^{\eta t\tau_{\text{F}}(x)/\sqrt{z_{\text{F}}(x)}}}{1 + e^{2\eta T_{\text{F}}}} d\eta = \frac{\sqrt{z_{\text{F}}(x)}}{t\tau_{\text{F}}(x)} - \frac{\pi}{2T_{\text{F}}} \text{csc} \left(\frac{\pi\tau_{\text{F}}(x)}{2T_{\text{F}}\sqrt{z_{\text{F}}(x)}} t \right). \quad (5.25)$$

By setting $t = 2\sqrt{z_{\text{F}}(x)}$ via the stationary phase approximation, the above integration is simplified to yield

$$\int_0^\infty \frac{e^{-2\eta\tau_{\text{F}}} - e^{2\eta\tau_{\text{F}}}}{1 + e^{2\eta T_{\text{F}}}} d\eta = \frac{1}{2\tau_{\text{F}}} - \frac{\pi}{2T_{\text{F}}} \text{csc} \left(\frac{\pi\tau_{\text{F}}}{T_{\text{F}}} \right). \quad (5.26)$$

Hence, the density $n^{\text{QC}}(x)$ is

$$\begin{aligned} n^{\text{QC}}(x) &= \left(\frac{\sqrt{z_{\text{F}}(x)}}{k_{\text{F}}(x)\tau_{\text{F}}(x)} - \frac{\pi\sqrt{z_{\text{F}}(x)}}{k_{\text{F}}(x)T_{\text{F}}} \text{csc} \left(\frac{\pi\tau_{\text{F}}(x)}{T_{\text{F}}} \right) \right) \frac{1}{2\pi^{3/2}} \int_0^\infty \sin(f(t)) \frac{dt}{\sqrt{t}} \\ &= \left(\frac{\sqrt{z_{\text{F}}(x)}}{k_{\text{F}}(x)\tau_{\text{F}}(x)} - \frac{\pi\sqrt{z_{\text{F}}(x)}}{k_{\text{F}}(x)T_{\text{F}} \sin(\alpha(x))} \right) Ai(-z_{\text{F}}(x)) Bi(-z_{\text{F}}(x)). \end{aligned} \quad (5.27)$$

By using the asymptotic forms of Ai and Bi (76),

$$\begin{aligned} Ai(-z_F(x))Bi(-z_F(x)) &\sim \frac{1}{2\pi\sqrt{z_F(x)}} \sin(2\theta_F(x) + \pi/2) \\ &= \frac{1}{2\pi\sqrt{z_F(x)}} \cos(2\theta_F(x)) , \end{aligned} \quad (5.28)$$

Eq. (5.27) becomes

$$n^{\text{QC}}(x) = \frac{\cos(2\theta_F(x))}{2\pi k_F(x)\tau_F(x)} - \frac{\cos(2\theta_F(x))}{2k_F(x)T_F \sin(\alpha(x))} , \quad (5.29)$$

and Eq. (5.15) gives the quantum correction term corresponding to Eq. (5.16):

$$n^{\text{QC}}(x) = \frac{k_F(x) \cos(2\theta_F(x))}{6\pi\theta_F(x)} - \frac{\cos(2\theta_F(x))}{2k_F(x)T_F \sin(\alpha(x))} . \quad (5.30)$$

Combining Eq. (5.17) and Eq. (5.30) reproduces the asymptotic density formula in Ref. (74):

$$n_{\text{KS}}(x) = \frac{k_F(x)}{\pi} - \frac{\cos(2\theta_F(x))}{2k_F(x)T_F \sin(\alpha(x))} . \quad (5.31)$$

5.1.3 The evanescent region

In the evanescent region ($\mathcal{E} - v(x) < 0$), the uniform semiclassical wavefunctions are

$$\psi_l^{\text{unif}}(x) = \frac{|\theta(x)|^{1/6}}{\sqrt{|k(x)|}} Ai(|z(x)|) , \quad (5.32)$$

$$\psi_r^{\text{unif}}(x) = \frac{|\theta(x)|^{1/6}}{\sqrt{|k(x)|}} Ai(e^{2\pi i/3}|z(x)|) . \quad (5.33)$$

Using the above wavefunctions, the Green's function for a single turning-point system in this region can be constructed:

$$g_{\text{ST}}^{\text{semi}}(x, \mathcal{E}) = \frac{2\pi \sqrt{|z(x)|}}{i |k(x)|} \text{Ai}(|z(x)|) [\text{Ai}(|z(x)|) - i \text{Bi}(|z(x)|)] . \quad (5.34)$$

Using the same derivation, we find $n_{\text{ST}}^{\text{semi}}(x)$ in the evanescent region to be

$$n_{\text{ST}}^{\text{semi}}(x) = -\frac{|k_{\text{F}}(x)|}{\sqrt{|z_{\text{F}}(x)|}} [|z_{\text{F}}(x)| \text{Ai}^2(|z_{\text{F}}(x)|) - \text{Ai}'(|z_{\text{F}}(x)|)^2] . \quad (5.35)$$

The Green's function in the evanescent region for two-turning-point systems is constructed:

$$g^{\text{semi}}(x; \mathcal{E}) = -2\pi \tan \Theta \frac{\sqrt{|z(x)|}}{|k(x)|} [\text{Ai}^2(|z(x)|) - i \text{Ai}(|z(x)|) \text{Bi}(|z(x)|)] . \quad (5.36)$$

Following the logic of Eq. (5.21), we can extract $g^{\text{QC}}(x; \mathcal{E})$ in this region as

$$g^{\text{QC}}(x; \mathcal{E}) = 4\pi i \frac{\sqrt{|z(x)|}}{|k(x)|} \frac{1}{1 + e^{-2i\Theta}} [\text{Ai}^2(|z(x)|) - i \text{Ai}(|z(x)|) \text{Bi}(|z(x)|)] . \quad (5.37)$$

We then derive the quantum correction in the evanescent region, using the contour in Fig. 5.1 and find

$$n^{\text{QC}}(x) = \frac{e^{-2|\theta_{\text{F}}(x)|}}{4|k_{\text{F}}(x)| T_{\text{F}} \sinh(|\alpha(x)|)} - \frac{|k_{\text{F}}(x)| e^{-2|\theta_{\text{F}}(x)|}}{12\pi |\theta_{\text{F}}(x)|} . \quad (5.38)$$

5.2 Uniform kinetic energy density

Using the definition of Eq. (2.20) and Green's functions Eqs. (5.8) and (5.20), we derive a semiclassical approximation to the KE density in the traveling and evanescent regions. We

apply the same method as in deriving the density with the only difference that we expand the semiclassical quantities in the integrand up to the second order of η . Without going into any details of the derivations, we show the final results.

In the traveling region, the leading KE density term is given as

$$\begin{aligned}
t_{\text{ST}}^{\text{semi}}(x) &= \frac{k_{\text{F}}^3(x)}{2\sqrt{z_{\text{F}}(x)}} [z_{\text{F}}(x)Ai^2(-z_{\text{F}}(x)) + Ai'(-z_{\text{F}}(x))^2] \\
&\quad - \frac{k_{\text{F}}^3(x)}{9\theta_{\text{F}}(x)} [2z_{\text{F}}^2(x)Ai^2(-z_{\text{F}}(x)) - Ai(-z_{\text{F}}(x))Ai'(-z_{\text{F}}(x)) \\
&\quad + 2z_{\text{F}}(x)Ai'^2(-z_{\text{F}}(x))], \tag{5.39}
\end{aligned}$$

which recovers the TF KE density ($k_{\text{F}}^3(x)/6\pi$) at the asymptotic limit. The first order quantum correction to the kinetic energy density is given by

$$t_{(1)}^{\text{QC}}(x) = \frac{k_{\text{F}}^3(x) \cos(2\theta_{\text{F}}(x))}{12\pi\theta_{\text{F}}(x)} - \frac{k_{\text{F}}(x) \cos(2\theta_{\text{F}}(x))}{4T_{\text{F}} \sin(\alpha(x))}. \tag{5.40}$$

The second order KED quantum correction is given by

$$t_{(2)}^{\text{QC}}(x) = - \left(\frac{k_{\text{F}}^3(x)}{8z_{\text{F}}^{5/2}(x)} - \frac{\sqrt{z_{\text{F}}(x)}\pi^2 \cos(\alpha(x))}{2k_{\text{F}}(x)T_{\text{F}}^2 \sin^2(\alpha(x))} \right) Ai^2(-z_{\text{F}}(x)). \tag{5.41}$$

We now find analogous quantities in the evanescent region. The leading term of the KE density is

$$\begin{aligned}
t_{\text{ST}}^{\text{semi}}(x) &= \frac{|k_{\text{F}}(x)|^3}{2\sqrt{|z_{\text{F}}(x)|}} [|z_{\text{F}}(x)|Ai^2(|z_{\text{F}}(x)|) - Ai'^2(|z_{\text{F}}(x)|)] \\
&\quad - \frac{|k_{\text{F}}(x)|^3}{9|\theta_{\text{F}}(x)|} [2|z_{\text{F}}(x)|^2 Ai^2(|z_{\text{F}}(x)|) \\
&\quad - Ai(|z_{\text{F}}(x)|)Ai'(|z_{\text{F}}(x)|) - 2|z_{\text{F}}(x)|Ai'^2(|z_{\text{F}}(x)|)]. \tag{5.42}
\end{aligned}$$

If we take the asymptotic forms of Ai and Ai' , $t_{\text{ST}}^{\text{semi}}(x)$ becomes zero at the asymptotic limit in the evanescent region. The quantum corrections in this region are

$$t_{(1)}^{\text{QC}}(x) = \frac{|k_{\text{F}}(x)|^3 e^{-2|\theta_{\text{F}}(x)|}}{24\pi|\theta_{\text{F}}(x)|} - \frac{|k_{\text{F}}(x)|e^{-2|\theta_{\text{F}}(x)|}}{8T_{\text{F}}\sinh(|\alpha(x)|)}, \quad (5.43)$$

and

$$t_{(2)}^{\text{QC}}(x) = \left(\frac{|k_{\text{F}}(x)|^3}{8|z_{\text{F}}(x)|^{5/2}} - \frac{\sqrt{|z_{\text{F}}(x)|}\pi^2 \cosh(|\alpha(x)|)}{2|k_{\text{F}}(x)|T_{\text{F}}^2 \sinh^2(|\alpha(x)|)} \right) Ai^2(|z_{\text{F}}(x)|), \quad (5.44)$$

giving a set of clearly analogous expressions for the KE density in both regions.

5.3 Different limit

However, the above quantum corrections result in a discontinuity at the turning point. At the turning point, a_{F} , the magnitude of Eq. (5.30) is twice that of Eq. (5.38). For a harmonic oscillator ($v(x) = x^2/2$), Eq. (5.38) in the evanescent region is more accurate than Eq. (5.30) in the traveling region at a_{F} . (See Section 5.5.1 and Table 5.1 for the detailed discussion and the data.)

To make these equations continuous, we define the following two points, x_{I} and x_{II} , in the traveling region (see Fig. 5.2):

$$\begin{aligned} \int_{a_{\text{F}}}^{x_{\text{I}}} dx' k_{\text{F}}(x') &= \frac{\pi}{4} \\ \int_{x_{\text{II}}}^{b_{\text{F}}} dx' k_{\text{F}}(x') &= \frac{\pi}{4}. \end{aligned} \quad (5.45)$$

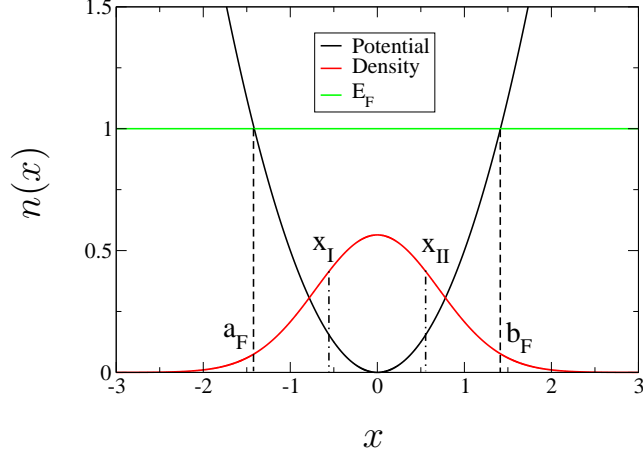


Figure 5.2: 1D systems.

At these x_I and x_{II} , $n^{\text{QC}}(x)$ (Eq. (5.30)) becomes zero since $\cos(2\theta_F(x_{I/II})) = \cos(\pi/2) = 0$. Only the leading term, $n_{\text{ST}}^{\text{semi}}(x)$, remains. So we can divide the region to make the density continuous.

With this separation of space, we obtain a continuous quantum corrections to the density:

$$n^{\text{QC}}(x) = \begin{cases} \frac{k_F(x) \cos(2\theta_F(x))}{6\pi\theta_F(x)} - \frac{\cos(2\theta_F(x))}{2k_F(x)T_F \sin(\alpha(x))}, & \text{for } x_I < x < x_{\text{mid}} \\ \frac{k_F(x) \cos(2\theta_F(x))}{12\pi\theta_F(x)} - \frac{\cos(2\theta_F(x))}{4k_F(x)T_F \sin(\alpha(x))}, & \text{for } a_F < x < x_I \\ \frac{e^{-2|\theta_F(x)|}}{4|k_F(x)|T_F \sinh(|\alpha(x)|)} - \frac{|k_F(x)|e^{-2|\theta_F(x)|}}{12\pi|\theta_F(x)|}, & \text{for } x < a_F, \end{cases} \quad (5.46)$$

where the mid-phase point, x_{mid} , is determined by

$$\int_{a_F}^{x_{\text{mid}}} dx' \theta_F(x') = \frac{N\pi}{2}. \quad (5.47)$$

These formulas give a continuous density although discontinuities in the first derivative exist at x_I , x_{II} and x_{mid} .

Using the same argument, the $t^{\text{QC}}(x)$ can also be divided into three regions:

$$t^{\text{QC}}(x) = \begin{cases} t_{(1),a}^{\text{QC}} + t_{(2),a}^{\text{QC}}, & \text{for } x_{\text{I}} < x < x_{\text{mid}} \\ \frac{1}{2}t_{(1),a}^{\text{QC}} + t_{(2),a}^{\text{QC}}, & \text{for } a_{\text{F}} < x < x_{\text{I}} \\ t_{(1),e}^{\text{QC}} + t_{(2),e}^{\text{QC}}, & \text{for } x < a_{\text{F}}. \end{cases} \quad (5.48)$$

5.4 Summary of equations

In this section, we summarize all previous results related to the semiclassical density and KE density that will be used in this paper. We define the following semiclassical quantities at E_{F} .

The semiclassical momentum:

$$k_{\text{F}}(x) = \sqrt{2|E_{\text{F}} - v(x)|}. \quad (5.49)$$

The semiclassical phase:

$$\theta_{\text{F}}(x) = \int_{a_{\text{F}}}^x k_{\text{F}}(x') dx', \quad (5.50)$$

$$z_{\text{F}}(x) = \text{Sgn}(\theta_{\text{F}}(x)) \left(\frac{3}{2} |\theta_{\text{F}}(x)| \right)^{2/3}. \quad (5.51)$$

The classical traveling time:

$$\tau_{\text{F}}(x) = \int_{a_{\text{F}}}^x \frac{1}{k_{\text{F}}(x')} dx'. \quad (5.52)$$

For the semiclassical density ($n_{\text{ST}}^{\text{semi}}$ and $n^{\text{QC}}(x)$):

$$n_{\text{ST}}^{\text{semi}}(x) = \pm \frac{k_{\text{F}}(x)}{\sqrt{\pm z_{\text{F}}(x)}} [z_{\text{F}}(x) Ai^2(-z_{\text{F}}(x)) + Ai'(-z_{\text{F}}(x))^2], \quad (5.53)$$

$$n^{\text{QC}}(x) = \begin{cases} \frac{k_{\text{F}}(x) \cos(2\theta_{\text{F}}(x))}{6\pi\theta_{\text{F}}(x)} - \frac{\cos(2\theta_{\text{F}}(x))}{2k_{\text{F}}(x)T_{\text{F}} \sin(\alpha(x))}, & \text{for } x_{\text{I}} < x < x_{\text{mid}} \\ \frac{k_{\text{F}}(x) \cos(2\theta_{\text{F}}(x))}{12\pi\theta_{\text{F}}(x)} - \frac{\cos(2\theta_{\text{F}}(x))}{4k_{\text{F}}(x)T_{\text{F}} \sin(\alpha(x))}, & \text{for } a_{\text{F}} < x < x_{\text{I}} \\ \frac{e^{-2|\theta_{\text{F}}(x)|}}{4|k_{\text{F}}(x)|T_{\text{F}} \sinh(|\alpha(x)|)} - \frac{|k_{\text{F}}(x)|e^{-2|\theta_{\text{F}}(x)|}}{12\pi|\theta_{\text{F}}(x)|}, & \text{for } x < a_{\text{F}}, \end{cases} \quad (5.54)$$

where the upper sign means the traveling region, the lower sign the evanescent region, and

$$\alpha_{\text{F}}(x) = \pi\tau_{\text{F}}(x)/T_{\text{F}}.$$

For t^{semi} , the subscript a and e mean the traveling and evanescent regions respectively. The leading term is

$$\begin{aligned} t_{\text{ST}}^{\text{semi}}(x) &= \pm \frac{k_{\text{F}}^3(x)}{2\sqrt{\pm z_{\text{F}}(x)}} [z_{\text{F}}(x) Ai^2(-z_{\text{F}}(x)) + Ai'(-z_{\text{F}}(x))^2] \\ &\mp \frac{k_{\text{F}}^3(x)}{9\theta_{\text{F}}(x)} [2z_{\text{F}}^2(x) Ai^2(-z_{\text{F}}(x)) - Ai(-z_{\text{F}}(x)) Ai'(-z_{\text{F}}(x)) \\ &\quad + 2z_{\text{F}}(x) Ai'^2(-z_{\text{F}}(x))], \end{aligned} \quad (5.55)$$

and the quantum corrections for the KE density are

$$t_{(1),a}^{\text{QC}}(x) = \frac{k_{\text{F}}^3(x) \cos(2\theta_{\text{F}}(x))}{12\pi\theta_{\text{F}}(x)} - \frac{k_{\text{F}}(x) \cos(2\theta_{\text{F}}(x))}{4T_{\text{F}} \sin(\alpha_{\text{F}}(x))} \quad (5.56)$$

$$t_{(2),a}^{\text{QC}}(x) = - \left(\frac{k_{\text{F}}^3(x)}{8z_{\text{F}}^{5/2}(x)} - \frac{\sqrt{z_{\text{F}}(x)}\pi^2 \cos(\alpha_{\text{F}}(x))}{2k_{\text{F}}(x)T_{\text{F}}^2 \sin^2(\alpha_{\text{F}}(x))} \right) Ai^2(-z_{\text{F}}(x)) \quad (5.57)$$

$$t_{(1),e}^{\text{QC}}(x) = \frac{k_{\text{F}}(x)e^{2\theta_{\text{F}}(x)}}{8T_{\text{F}}\sinh(\alpha_{\text{F}}(x))} - \frac{k_{\text{F}}(x)^3e^{2\theta_{\text{F}}(x)}}{24\pi\theta_{\text{F}}(x)} \quad (5.58)$$

$$t_{(2),e}^{\text{QC}}(x) = \left(\frac{k_{\text{F}}(x)^3}{8(-z_{\text{F}}(x))^{5/2}} - \frac{\sqrt{-z_{\text{F}}(x)}\pi^2\cosh(\alpha_{\text{F}}(x))}{2k_{\text{F}}(x)T_{\text{F}}^2\sinh^2(\alpha_{\text{F}}(x))} \right) Ai^2(-z_{\text{F}}(x)) \quad (5.59)$$

$$t^{\text{QC}}(x) = \begin{cases} t_{(1),a}^{\text{QC}} + t_{(2),a}^{\text{QC}}, & \text{for } x_{\text{I}} < x < x_{\text{mid}} \\ \frac{1}{2}t_{(1),a}^{\text{QC}} + t_{(2),a}^{\text{QC}}, & \text{for } a_{\text{F}} < x < x_{\text{I}} \\ t_{(1),e}^{\text{QC}} + t_{(2),e}^{\text{QC}}, & \text{for } x < a_{\text{F}}. \end{cases} \quad (5.60)$$

The total semiclassical density and KE density are

$$\begin{aligned} n^{\text{semi}}(x) &= n_{\text{ST}}^{\text{semi}}(x) + n^{\text{QC}}(x) \\ t^{\text{semi}}(x) &= t_{\text{ST}}^{\text{semi}}(x) + t^{\text{QC}}(x). \end{aligned} \quad (5.61)$$

5.5 1D Applications

5.5.1 Harmonic potential

The Schrödinger equation for a harmonic oscillator is

$$\left(-\frac{\hbar^2}{2m} \frac{d^2}{dx^2} + \frac{1}{2}m\omega^2x^2 \right) \psi_j(x) = \epsilon_j \psi_j(x). \quad (5.62)$$

The exact wavefunction of j-th level is given by

$$\psi_j(x) = \sqrt{\frac{1}{2^j j!}} \left(\frac{m\omega}{\pi\hbar} \right)^{1/4} e^{-m\omega x^2/2\hbar} H_j \left(\sqrt{\frac{m\omega}{\hbar}} x \right), \quad (5.63)$$

where H_j is the j -th Hermite polynomial. And the exact energy levels are

$$\epsilon_j = \left(j + \frac{1}{2}\right) \hbar\omega, \quad j=0,1,2,\dots \quad (5.64)$$

In atomic units ($m = 1, \hbar = 1$), with $\omega = 1$, the wavefunction is reduced to

$$\psi_j(x) = \sqrt{\frac{1}{2^j j!}} \left(\frac{1}{\pi}\right)^{1/4} e^{-x^2/2} H_j(x), \quad (5.65)$$

and the exact density for N particles is

$$n(x) = \sum_{j=0}^{N-1} \psi_j^2(x). \quad (5.66)$$

E_F of the harmonic oscillator for N particles is calculated by

$$\int_{-\sqrt{2E_F}}^{\sqrt{2E_F}} dx \sqrt{2(E_F - x^2/2)} = N\pi, \quad (5.67)$$

with $E_F = N$ and turning points $\pm\sqrt{2N}$. In Table 5.1, we calculate the percentage errors of the semiclassical density at the turning point (TP, $x = -\sqrt{2N}$), using Eqs. (5.53), (5.55) and (5.61). The leading terms in the density ($n_{\text{ST}}^{\text{semi}}$, Eq. (5.53)) and KE density ($t_{\text{ST}}^{\text{semi}}$, Eq. (5.55)) give relatively accurate values at the TP, and the percentage errors decrease as N becomes large. With quantum corrections, Eq. (5.61) (n^{semi} and t^{semi}) gives very good results, even for $N = 1$. The errors are less than 2% and decrease much more rapidly than those of the leading terms.

We calculate kinetic and potential energies of a harmonic oscillator ($v(x) = x^2/2$) using the semiclassical density and KE density in Table 5.2. Errors in the normalization of the semiclassical densities decrease as N increases. The magnitude of errors for the semiclassical KE increase with N , but slowly converge to a constant. The errors in potential energies are

Table 5.1: The percentage errors of densities and KE densities at the turning point ($x = -\sqrt{2N}$) for a harmonic oscillator.

N	$n_{\text{ST}}^{\text{semi}}$	n^{semi}	$t_{\text{ST}}^{\text{semi}}$	t^{semi}
1	24.0717	1.9631	13.4611	1.78836
2	14.338	1.50315	7.78502	0.799501
3	10.6836	1.20183	5.71087	0.482507
4	8.70012	1.01334	4.6052	0.334419
5	7.43109	0.884161	3.90672	0.250848
6	6.53896	0.789477	3.42032	0.198019
7	5.87216	0.716657	3.05945	0.161993
8	5.35183	0.658626	2.77952	0.136058
9	4.93263	0.611107	2.55511	0.116609
10	4.58645	0.571352	2.37056	0.101555
20	2.85266	0.365231	1.45737	0.0407332
30	2.16591	0.280327	1.10111	0.0238158
40	1.78283	0.232148	0.903817	0.0162631
50	1.53354	0.200477	0.775996	0.0120943
60	1.35623	0.177797	0.685357	0.00949334
70	1.22255	0.160614	0.617179	0.00773511
80	1.11755	0.147064	0.563717	0.00647718
90	1.03249	0.136056	0.520474	0.00553832
100	0.961952	0.126903	0.484651	0.00481425
200	0.604372	0.0801871	-	-

bigger than those in the semiclassical KE and show much slower convergence. In contrast, the percentage errors in the potential energies go to zero rapidly.

In 2003, Sim et al. derive the kinetic energy density in 1D from the virial theorem for noninteracting electrons with v -representable densities(77):

$$t^{\text{DF}}(x) = \frac{1}{2} \int_x^\infty dx' n(x') \frac{dv(x')}{dx'}. \quad (5.68)$$

We test this kinetic energy functional on the semiclassical densities for a harmonic oscillator. The kinetic energies from Eq. (5.68) have almost the same errors as the potential energies, satisfying the virial theorem. To remove the normalization errors, we re-normalize the semiclassical density to N numerically. With the re-normalized densities, we calculate the

Table 5.2: Errors of densities, kinetic energy, potential energy for a harmonic oscillator ($v(x) = x^2/2$).

N	$\int dx n^{\text{semi}}(x)$	exact KE	$\int dx t^{\text{semi}}(x)$	$\int dx t^{\text{DF}}(x)$	$\int dx n^{\text{semi}}(x)v(x)$
1	0.9856	0.25	-0.03921639	0.00076356	0.00075271
2	1.9931	1.00	-0.03546662	0.00027550	0.00027493
4	3.9943	4.00	-0.04261346	-0.00195068	-0.00195005
8	7.9960	16.00	-0.04766957	-0.00625399	-0.00629082
16	15.9974	64.00	-0.05132631	-0.01274630	-0.01273680
32	31.9983	256.00	-0.05402198	-0.02092856	-0.02159829
64	63.9989	1024.00	-0.05597217	-0.03409107	-0.03409480
128	127.9993	4096.00	-0.05753729	-0.04841689	-0.04943579
256	255.9996	16384.00	-0.05868514	-0.07050443	-0.07054575

Table 5.3: Errors of kinetic energies and potential energies for a harmonic oscillator ($v(x) = x^2/2$). The semiclassical density is re-normalized to N to calculate kinetic energies from $t^{\text{DF}}(x)$ (Eq. (5.68)) and potential energies.

N	exact KE	$\int dx t^{\text{DF}}(x)$	$\int dx n^{\text{semi}}(x)v(x)$	E
1	0.25	0.00447381	0.00441528	0.00888909
2	1.00	0.00376036	0.00375728	0.00751765
4	4.00	0.00374241	0.00373903	0.00748145
8	16.00	0.00192897	0.00173114	0.00366011
16	64.00	-0.00215785	-0.00220972	-0.00436757
32	256.00	-0.00752076	-0.00819052	-0.01571129
64	1024.00	-0.01706026	-0.01706399	-0.03412424
128	4096.00	-0.02716883	-0.02818773	-0.05535656
256	16384.00	-0.04368269	-0.04372401	-0.08740670

kinetic energies using Eq. (5.68) and the potential energies in Table 5.3. The errors in kinetic and potential energies are similar to those in Table 5.2, but the magnitude of errors is reduced as N becomes large. We plot the semiclassical (KE) densities with exact results in Figs. 5.3 and 5.4 for $N = 2$. Errors present in the semiclassical KE density decrease rapidly as N increases.

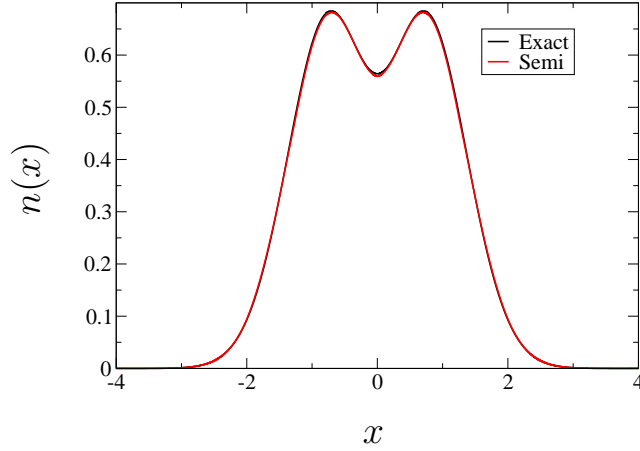


Figure 5.3: Comparison of exact and semiclassical densities of a harmonic potential with $N = 2$.

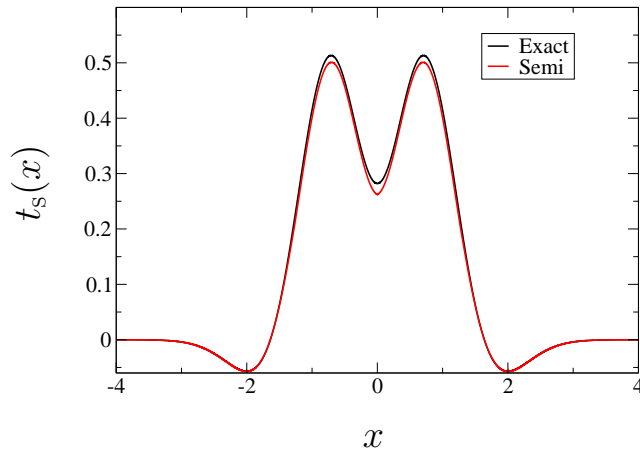


Figure 5.4: Comparison of exact and semiclassical KE densities of a harmonic potential with $N = 2$.

5.5.2 Morse potential

Then we apply the semiclassical density and KE density to a Morse potential(78). The Morse potential is an approximation to the potential energy surface of a diatomic molecule that gives the better vibrational energy levels than those found using the harmonic oscillator approximation. An exact solution can be obtained by solving the Schrödinger equation. In

this study, we use the following Morse potential:

$$v(x) = 16(e^{-x/2} - 2e^{-x/4}). \quad (5.69)$$

We obtain the exact density and KE density numerically and compare them with the semiclassical solutions for $N = 2$ in Figs. 5.5 and 5.6. The semiclassical density in Fig. 5.5

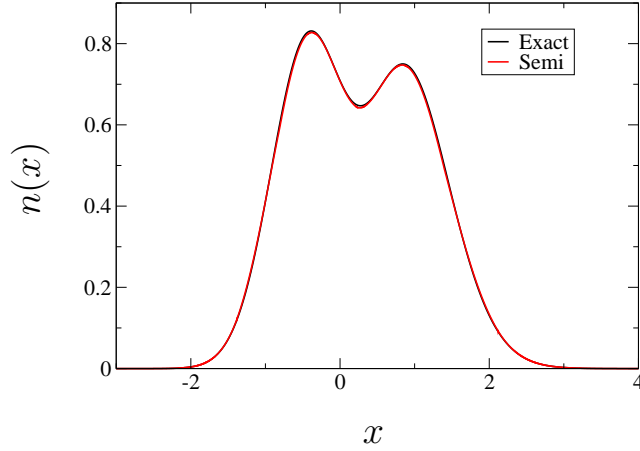


Figure 5.5: Comparison of exact and semiclassical densities of Morse potential with $N = 2$.

shows very good agreement with the exact density, but the difference of the KE densities in the traveling region is clear in Fig. 5.6. However, this difference rapidly diminishes as N increases.

5.6 Is this variational?

According to Ref. (77), we can define the total energy of a given system with the density, $n(x)$ and the potential, $v(x)$:

$$E = \frac{1}{2} \int_{-\infty}^{\infty} dx \int_x^{\infty} dx' n(x') \frac{dv(x')}{dx'} + \int_{-\infty}^{\infty} dx n(x) v(x). \quad (5.70)$$

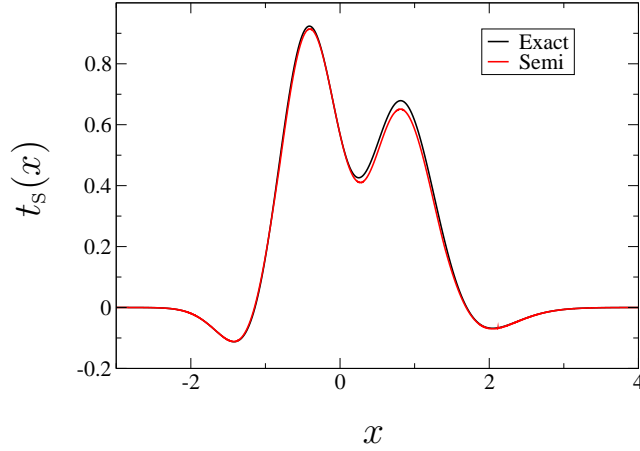


Figure 5.6: Comparison of exact and semiclassical KE densities of Morse potential with $N = 2$.

If we know the density as a functional of a given potential, the total energy will be a functional of the potential. Hence, we can rewrite the above equation as

$$E_v[v] = \frac{1}{2} \int_{-\infty}^{\infty} dx \int_x^{\infty} dx' n[v](x') \frac{dv(x')}{dx'} + \int_{-\infty}^{\infty} dx n[v](x) v(x). \quad (5.71)$$

Since the kinetic energy functional is derived from the virial theorem, the kinetic and potential energies always satisfy the virial theorem for a given potential and the density from the potential.

The question then becomes, “Is Eq. (5.71) variational?” To check this, we calculate the total energies for a given trial potential, $\tilde{v}(x)$, using

$$E_v[\tilde{v}] = \frac{1}{2} \int_{-\infty}^{\infty} dx \int_x^{\infty} dx' n[\tilde{v}](x') \frac{d\tilde{v}(x')}{dx'} + \int_{-\infty}^{\infty} dx n[\tilde{v}](x) v(x), \quad (5.72)$$

where the trial potential, $\tilde{v}(x)$, is

$$\tilde{v}(x) = \frac{1}{2} x^p, \quad p = 2, 4, 6, \text{ and } 8, \quad (5.73)$$

and the true (external) potential, $v(x)$, is

$$v(x) = \frac{1}{2}x^4. \tag{5.74}$$

In Table 5.4, we summarize the KE, PE, and total energies of $N = 1, 2, 3,$ and 4 for given trial potentials. We re-normalize the semiclassical densities numerically to N . The minimum

Table 5.4: Variational principle. The trial potential, $\tilde{v}(x)$, is $x^p/2$ and the exact (target) potential is $x^4/2$. For all cases, the minimum of the total energy is at $p = 4$.

	p	KE	PE	E	KE/PE
$N = 1$	2	0.25447381	0.38465361	0.63912742	2.00003
	4	0.36936501	0.18467997	0.55404498	
	6	0.47279080	0.13254050	0.60533129	
	8	0.56578485	0.10765556	0.67344041	
$N = 2$	2	1.00376036	2.26951144	3.27327181	2.00057
	4	1.63598630	0.81775834	2.45374464	
	6	2.11907692	0.52224034	2.64131726	
	8	2.54624093	0.40335159	2.94959252	
$N = 3$	2	2.25548094	7.16249997	9.41798091	2.00001
	4	4.12831726	2.06415038	6.19246764	
	6	5.53804028	1.18722743	6.72526771	
	8	6.69177584	0.86496638	7.55674222	
$N = 4$	2	4.00374241	16.54509916	20.54884157	2.00019
	4	8.00986449	4.00454536	12.01440985	
	6	11.14843359	2.11463851	13.26307210	
	8	13.66074179	1.46596067	15.12670246	

of the total energy for all N is always at $p = 4$.

We also test the variational principle by changing the coefficient of x^2 in Table 5.5. The trial and true potentials are, respectively,

$$\begin{aligned} \tilde{v}(x) &= \alpha x^2, \\ v(x) &= \frac{3}{4}x^2. \end{aligned} \tag{5.75}$$

We change the α from 1/2 to 1.0 and calculate the total energies using Eq. (5.72) for trial potentials. The energy minimum is found at $\alpha = 3/4$.

Table 5.5: Variational principle for $N = 1$. The trial potential, $\tilde{v}(x)$, is αx^2 and the exact (target) potential is $3x^2/4$. The minimum of the total energy is at $\alpha = 3/4$.

α	KE	PE	E	KE/PE
1.00	0.35979927	0.26984201	0.62964128	
0.95	0.35068325	0.27685260	0.62753585	
0.90	0.34148517	0.28444855	0.62593372	
0.85	0.33183181	0.29267613	0.62450794	
0.80	0.32187217	0.30169775	0.62356993	
0.75	0.31159691	0.31158810	0.62318501	1.00003
0.70	0.30225659	0.32262455	0.62488114	
0.65	0.29017028	0.33470732	0.62487760	
0.60	0.27872824	0.34836102	0.62708926	
0.55	0.26685058	0.36385248	0.63070306	
0.50	0.25447380	0.38162292	0.63609672	

5.7 Spherically symmetric 3D potential

In this section, we discuss the non-interacting, spinless fermions in spherically symmetric potentials in 3D. The Hamiltonian for the system is given in atomic units as

$$\hat{H} = -\frac{1}{2}\nabla^2 + v(\mathbf{r}). \quad (5.76)$$

The Laplacian in spherical coordinates is expressed as

$$\nabla^2 = \frac{\partial^2}{\partial r^2} + \frac{2}{r} \frac{\partial}{\partial r} - \frac{1}{r^2} \hat{L}^2. \quad (5.77)$$

We can separate the wavefunction $\psi(\mathbf{r})$ into a radial, $R(r)$, and an angular part, $Y_l^m(\theta, \phi)$:

$$\psi(\mathbf{r}) = R_{nl}(r)Y_l^m(\theta, \phi), \quad (5.78)$$

where $Y_l^m(\theta, \phi)$ is the eigenfunction of \hat{L}^2 :

$$\hat{L}^2 Y_l^m(\theta, \phi) = l(l+1)Y_l^m(\theta, \phi). \quad (5.79)$$

The radial part of Schrödinger equation becomes

$$-\frac{1}{2} \left(R_{nl}''(r) + \frac{2}{r} R_{nl}'(r) \right) + \left(\frac{l(l+1)}{2r^2} + v(r) \right) R_{nl}(r) = ER_{nl}(r), \quad (5.80)$$

where this is the eigenvalue problem in 1D. To remove the singularity at the origin, we can define the radial wavefunction as

$$R_{nl}(r) = \frac{u_{nl}(r)}{r}. \quad (5.81)$$

Then, the differential equation can be further simplified to yield

$$\left(\frac{d^2}{dr^2} + 2 \left[E - v(r) - \frac{l(l+1)}{2r^2} \right] \right) u_{nl}(r) = 0. \quad (5.82)$$

For a given spherical potential $v(r)$, the exact radial density is the sum of $u_{nl}^2(r)$:

$$4\pi r^2 n(r) = \sum_{i=1}^n \sum_{j=0}^{i-1} u_{ij}^2(r). \quad (5.83)$$

The exact centrifugal potential, $l(l+1)/2r^2$, does not give the right orbital energy or asymptotic behavior of the semiclassical wavefunctions for the Coulomb potential, $-Z/r$ (75; 79).

Thus, Langer(75) proposed the following modification of the angular contribution, which en-

sures the right energy and the asymptotic decays of semiclassical wavefunctions(79; 80; 81)

$$l(l+1) \rightarrow \left(l + \frac{1}{2}\right)^2. \quad (5.84)$$

For $l = 0$, this modification converts the single-turning-point problem into the two-turning-point problem. According to this modification, the effective potential can be rewritten as

$$v^{\text{eff}}(r) = v(r) + \frac{(l + 1/2)^2}{2r^2}, \quad (5.85)$$

and Eq. (5.82) can be written as

$$\left(\frac{d^2}{dr^2} + 2[E - v^{\text{eff}}(r)]\right) u_{nl}(r) = 0, \quad (5.86)$$

which is a 1D Schrödinger equation with two turning points. Hence, we can apply our semiclassical density formula to Eq. (5.86). Similar to the separation of space shown in Fig. 5.2, we define the necessary points for the semiclassical scheme in Fig. 5.7. r_+ and r_- are

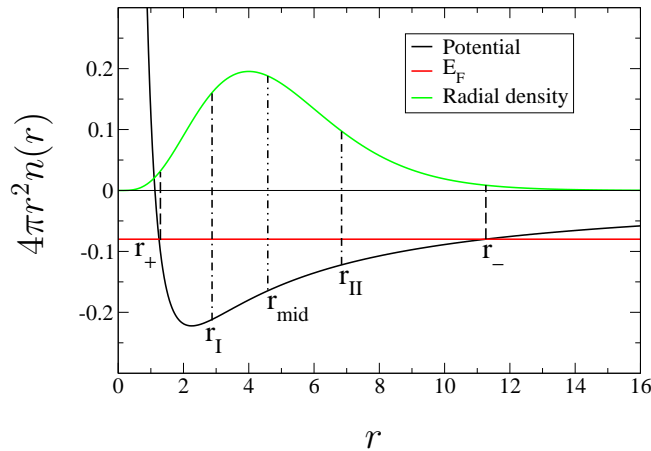


Figure 5.7: Spherical 3D systems.

the turning points at E_F and the points, r_I and r_{II} , are found by the conditions

$$\begin{aligned}\theta_F(r_I) &= \int_{r_+}^{r_I} dr k_l(r; E_F) = \pi/4, \\ \theta_F(r_{II}) &= \int_{r_{II}}^{r_-} dr k_l(r; E_F) = \pi/4.\end{aligned}\tag{5.87}$$

Our semiclassical equations give the radial density. Therefore, $4\pi r^2$ appears in front of $n_{ST}^{\text{semi}}(r)$ and $n^{\text{QC}}(r)$ to prevent confusion between these and the previous 1D results.

5.7.1 Isotropic 3D harmonic potential

The Schrödinger equation for an isotropic 3D harmonic oscillator is given by

$$-\frac{1}{2}\nabla^2\psi(\mathbf{r}) + \frac{1}{2}r^2\psi(\mathbf{r}) = E\psi(\mathbf{r}).\tag{5.88}$$

The exact radial wavefunction is

$$R_{nl}(r) = N_{nl}r^l e^{-r^2/2} L_{(n-l)/2}^{l+1/2}(r^2),\tag{5.89}$$

where $L_{(n-l)/2}^{l+1/2}(r^2)$ is an associated Laguerre polynomial and N_{nl} is the normalization constant

$$N_{nl} = \sqrt{\frac{2^{n+l+2} \left(\frac{n-l}{2}\right)! \left(\frac{n+l}{2}\right)!}{\sqrt{\pi}(n+l+1)!}}.\tag{5.90}$$

The energy levels are given by $E_n = (n + 3/2)$, which is $(n + 1)(n + 2)/2$ -fold degenerate.

With angular momentum quantum number l , the possible principle quantum number n is $l, l + 2, l + 4, \dots$. We use Langer's modification for the centrifugal potential. So the effective

potential is given by

$$v^{\text{eff}}(r) = \frac{1}{2}r^2 + \frac{(l + 1/2)^2}{2r^2}. \quad (5.91)$$

Near the origin, $4\pi r^2 n^{\text{QC}}(r)$ (Eq. (5.54)) overcorrects $4\pi r^2 n_{\text{ST}}^{\text{semi}}(r)$ (Eq. (5.53)), hence $4\pi r^2 n^{\text{semi}}(r)$ can be negative for radial densities. This becomes severe in s and p orbitals, compared to d and f orbitals, which is due to the rapid change of the centrifugal potential, $1/r^2$, near the origin. To avoid this, we use the single-turning-point formula near the origin:

$$4\pi r^2 n_{\text{app}}^{\text{semi}}(r) = \frac{2z_{\text{F}}(r)}{k_{\text{F}}(r)\tau_{\text{F}}(r)} [z_{\text{F}}(r)Ai^2(-z_{\text{F}}(r)) + Ai'(-z_{\text{F}}(r))^2]. \quad (5.92)$$

Kohn and Sham(74) suggest the linear equation around the turning point:

$$4\pi r^2 n^{\text{lin}}(r) = |2v'(a_{\text{F}})|^{1/3} (z_{\text{F}}(r)Ai^2(-z_{\text{F}}(r)) + Ai'^2(-z_{\text{F}}(r))). \quad (5.93)$$

If we take Taylor series of the potential at a_{F} , Eq. (5.93) can be derived from Eq. (5.92). However, Eq. (5.92) is not continuous with the original semiclassical approximation $4\pi r^2 n^{\text{semi}}(r)$ (Eq. 5.61). We calculate the ratio between $4\pi r^2 n_{\text{app}}^{\text{semi}}(r_1)$ of Eq. (5.92) and $4\pi r^2 n^{\text{semi}}(r_1)$ of Eq. (5.61), and multiply the radial density of Eq. (5.92) by the ratio at $r = r_1$. For $r > r_1$, we use our semiclassical approximation (Eq. (5.61)) to produce the right quantum oscillations. We apply this method to the 3D spherical harmonic oscillator in Figs. 5.8, 5.9, and 5.10, demonstrating that our semiclassical approximation produces very accurate radial densities.

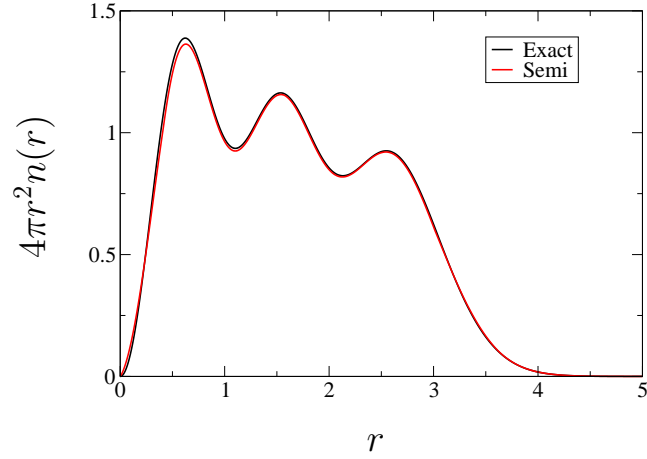


Figure 5.8: Comparison of exact and semiclassical densities of $l = 0$ orbitals with $N = 3$ for an isotropic 3D harmonic potential. Eq. (5.92) is used from $r = 0$ to r_1 .

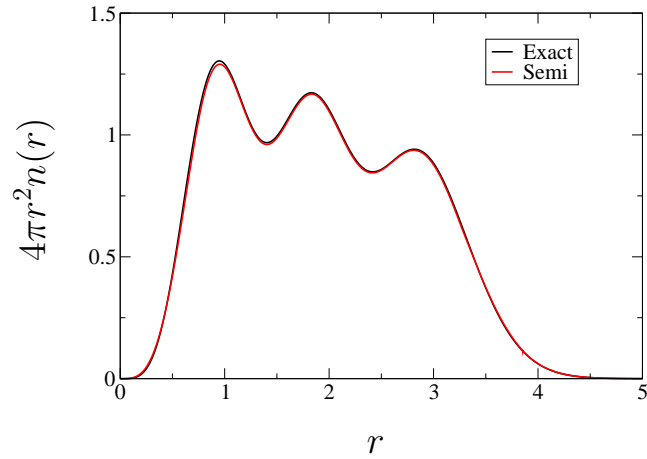


Figure 5.9: Comparison of exact and semiclassical densities of $l = 1$ orbitals with $N = 3$ for an isotropic 3D harmonic potential. Eq. (5.92) is used from $r = 0$ to r_1 .

5.7.2 Bohr atom

The Hamiltonian for a hydrogenic system is given by in atomic units

$$\hat{H} = -\frac{1}{2}\nabla^2 - \frac{Z}{r}, \quad (5.94)$$

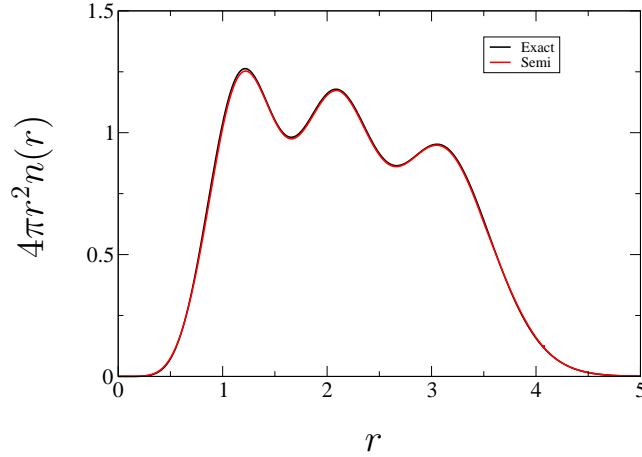


Figure 5.10: Comparison of exact and semiclassical densities of $l = 2$ orbitals with $N = 3$ for an isotropic 3D harmonic potential. Eq. (5.92) is used from $r = 0$ to r_1 .

where Z is the atomic number. We can separate the wavefunction $\psi(r)$ into a radial, $R(r)$, and an angular part, $Y_l^m(\theta, \phi)$:

$$\psi(r) = R(r)Y_l^m(\theta, \phi). \quad (5.95)$$

The radial part of Schrödinger equation becomes

$$-\frac{1}{2} \left(R''(r) + \frac{2}{r} R'(r) \right) + \left(\frac{l(l+1)}{2r^2} - \frac{Z}{r} \right) R(r) = ER(r). \quad (5.96)$$

The exact radial solution for the above equation is given as

$$R(r) = N_{nl} \left(\frac{2Zr}{n} \right)^l e^{-Zr/n} L_{n-l-1}^{2l+1} \left(\frac{2Zr}{n} \right), \quad (5.97)$$

where n is the principal quantum number, L_{n-l-1}^{2l+1} is the associated Laguerre polynomial and N_{nl} is a normalization constant,

$$N_{nl} = \sqrt{\frac{(n-l-1)! \left(\frac{2Z}{n} \right)^3}{2n(n+1)!}}. \quad (5.98)$$

We define the radial wavefunction as

$$R(r) = \frac{u(r)}{r}. \quad (5.99)$$

Then, the differential equation can be simplified to

$$\left(\frac{d^2}{dr^2} + 2 \left[E + \frac{Z}{r} - \frac{l(l+1)}{2r^2} \right] \right) u(r) = 0. \quad (5.100)$$

According to Langer's modification(75), the effective Coulomb potential can be rewritten as

$$v^{\text{eff}}(r) = -\frac{Z}{r} + \frac{(l+1/2)^2}{2r^2}, \quad (5.101)$$

and the semiclassical quantities are defined for a given angular momentum quantum number l as

$$\begin{aligned} k_l(r) &= \sqrt{2(\mathcal{E} - v^{\text{eff}}(r))} \\ \theta_l(r) &= \int_{r_+}^r dr' k_l(r') \\ \tau_l(r) &= \int_{r_+}^r dr' \frac{1}{k_l(r')}. \end{aligned} \quad (5.102)$$

The E_{F} is determined by the following quantization condition:

$$\int_{r_+}^{r_-} dr k_l(r; E_{\text{F}}) = (n-l)\pi, \quad (5.103)$$

where n and l are the valence principal and angular momentum quantum numbers respec-

tively, and the turning points at the E_F are given by

$$\begin{aligned} r_+ &= \frac{-Z + \sqrt{Z^2 + 2E_F(l + 1/2)^2}}{2E_F} \\ r_- &= \frac{-Z - \sqrt{Z^2 + 2E_F(l + 1/2)^2}}{2E_F}. \end{aligned} \quad (5.104)$$

Unlike the isotropic 3D harmonic oscillator, the potential, $v^{\text{eff}}(r)$, goes to zero as $r \rightarrow \infty$, and the E_F for given n and l is generally close to zero. In this case, the leading term, $4\pi r^2 n_{\text{ST}}^{\text{semi}}(r)$ (Eq. (5.53)), decays too rapidly compared to $4\pi r^2 n^{\text{QC}}(r)$, Eq. (5.54), after r_- , and the semiclassical radial density becomes negative in the right-side evanescent region. However, $4\pi r^2 n_{\text{app}}^{\text{semi}}(r)$ (Eq. (5.92)) decays slowly compared to $4\pi r^2 n_{\text{ST}}^{\text{semi}}(r)$. In addition, $4\pi r^2 n_{\text{ST}}^{\text{semi}}(r_-) = 4\pi r^2 n_{\text{app}}^{\text{semi}}(r_-)$ at the turning point. Hence, we use $4\pi r^2 n_{\text{app}}^{\text{semi}}(r)$ without any quantum corrections in the regions, $r < r_+$ and with quantum corrections ($4\pi r^2 n^{\text{QC}}(r)$) in the region for which $r_- < r$.

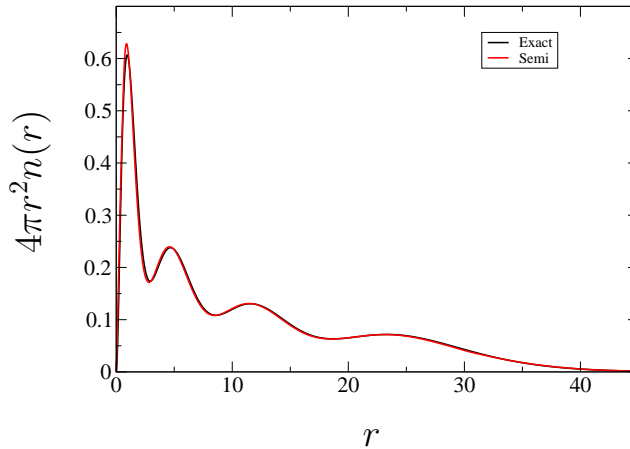


Figure 5.11: Comparison of exact and semiclassical densities of $1s^1 2s^1 3s^1 4s^1$.

We plot the exact and semiclassical radial densities with $Z = 1$ in Figs. 5.11, 5.12, 5.13 and 5.14. For example, if the valence quantum number $n = 4$ and $l = 0$, this means 4

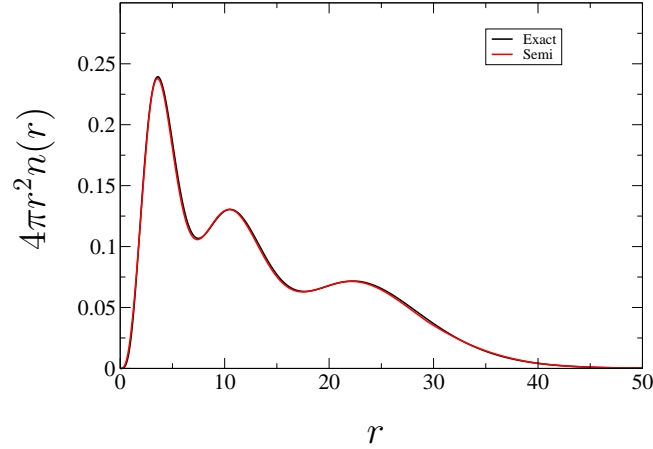


Figure 5.12: Comparison of exact and semiclassical densities of $2p^1 3p^1 4p^1$.

($=n - l$) particles, and its electronic configuration for non-interacting same spin electrons is $1s^1 2s^1 3s^1 4s^1$. The semiclassical formalism for the given potential, $v^{\text{eff}}(r)$, gives the right

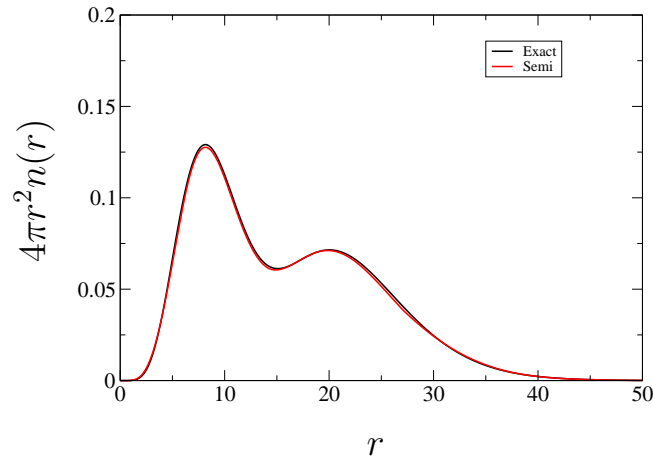


Figure 5.13: Comparison of exact and semiclassical densities of $3d^1 4d^1$.

quantum oscillations for p , d , and f orbital densities, compared to the exact radial density. However, in Fig. 5.11, a few oscillations near the origin show significant differences in the s -orbital density. Also, there is a slight phase shift for the s -orbital density which can also be seen in Fig. 9 of Ref. (74), where WKB wavefunctions were used. This is due to Langer's transformation and will be discussed in Section 5.8.

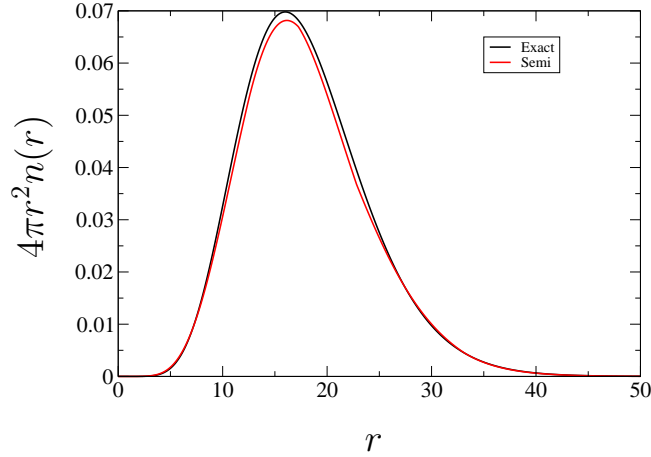


Figure 5.14: Comparison of exact and semiclassical densities of $4f^1$.

5.8 Real atoms

5.8.1 Single-point calculation

We begin with the KS formalism. The KS equations for any atoms or ions are

$$\left[-\frac{1}{2}\nabla^2 + v_{s\sigma}(\mathbf{r}) \right] \phi_{i\sigma}(\mathbf{r}) = \epsilon_{i\sigma} \phi_{i\sigma}(\mathbf{r}), \quad (5.105)$$

and the spin densities are

$$n_{\sigma}(\mathbf{r}) = \sum_{i=1}^{N_{\sigma}} |\phi_{i\sigma}(\mathbf{r})|^2, \quad (5.106)$$

where $v_{s\sigma}(r)$ is a single, multiplicative spin-dependent KS potential, and σ is the spin index (\uparrow and \downarrow). The spin-dependent KS potential is a sum of three contributions:

$$v_{s\sigma}(r) = v(r) + v_{\text{H}}[n](r) + v_{\text{XC}\sigma}[n_{\uparrow}, n_{\downarrow}](r), \quad (5.107)$$

where $v(r) = -Z/r$ for an atomic system, $v_{\text{H}}(r)$ is the Hartree potential given as

$$v_{\text{H}}(r) = \int d^3r' \frac{n(\mathbf{r}')}{|\mathbf{r} - \mathbf{r}'|}, \quad (5.108)$$

and the exchange-correlation (XC) contribution is

$$v_{\text{XC}\sigma}[n_{\uparrow}, n_{\downarrow}](r) = \frac{\delta E_{\text{XC}}[n_{\uparrow}, n_{\downarrow}]}{\delta n_{\sigma}(r)}. \quad (5.109)$$

For an atomic system, the KS equations can be separated into the radial and angular parts:

$$\left[-\frac{1}{2} \left(\frac{\partial^2}{\partial r^2} + \frac{2}{r} \frac{\partial}{\partial r} \right) + \frac{1}{2r^2} \hat{L}^2 + v_{\text{S}\sigma}(r) \right] \phi_{i\sigma}(r) = \epsilon_{i\sigma} \phi_{i\sigma}(r). \quad (5.110)$$

This can be further reduced to a 1D radial equation like Eq. (5.82). Let us define $v_{\text{S}\sigma}^{\text{eff}}(r)$ with this centrifugal potential:

$$v_{\text{S}\sigma}^{\text{eff}}(r; l) = v_{\text{ext}}(r) + v_{\text{H}}[n](r) + v_{\text{XC}\sigma}[n_{\uparrow}, n_{\downarrow}](r) + \frac{l(l+1)}{2r^2}. \quad (5.111)$$

This exact centrifugal potential does not produce the right asymptotic behavior of semiclassical wavefunctions discussed in Section 5.7. Thus we use Langer's modification instead of the exact $l(l+1)$

$$v_{\text{S}\sigma}^{\text{eff}}(r; l) = v_{\text{ext}}(r) + v_{\text{H}}[n](r) + v_{\text{XC}\sigma}[n_{\uparrow}, n_{\downarrow}](r) + \frac{(l+1/2)^2}{2r^2}, \quad (5.112)$$

where $v_{\text{S}\sigma}^{\text{eff}}(r)$ always has two turning points even for $l = 0$.

We obtain the total radial density ($4\pi r^2 n(r)$) and the KS potential ($v_{\text{S}}(r)$) of a neutral Kr atom ($Z = 36$) with the LDA XC functional using the fully numerical OPMKS code(38). The electronic configuration of Kr is $[\text{Ar}]3d^{10}4s^24p^6$. Since Kr is a spin-unpolarized, fully occupied atom, the KS potentials for up-spins and down-spins are identical. With $v_{\text{S}}^{\text{LDA}}(r)$

and Eq. (5.112), we calculate E_F for a given l :

$$\int_{r_+}^{r_-} \sqrt{2(E_F - v_{s\uparrow}^{\text{eff}}(r; l))} dr = (n - l)\pi, \quad (5.113)$$

where $\{(n, l)\} = \{(4, 0), (4, 1), (3, 2)\}$. For example, for the up-spin s -orbital density, $n = 4$ and $l = 0$. This means that the number of up-spin electrons up to $4s$ is $4(= n - l)$. With this E_F , we apply our semiclassical scheme to calculate the radial density ($4\pi r^2 n_{n,l}^{\text{semi}}(r)$) for given n and l . Degeneracy by magnetic quantum numbers (m) and spins (m_s) are handled by multiplication of the semiclassical radial density by $2(2l + 1)$. Hence, the total semiclassical radial density will be the sum of each of the radial densities for the given angular momentum quantum numbers:

$$4\pi r^2 n^{\text{semi}}(r) = \sum_{\{n,l\}} 2(2l + 1) 4\pi r^2 n_{n,l}^{\text{semi}}(r). \quad (5.114)$$

We compare the semiclassical result with SCF LDA density from OPMKS code in Fig. 5.15

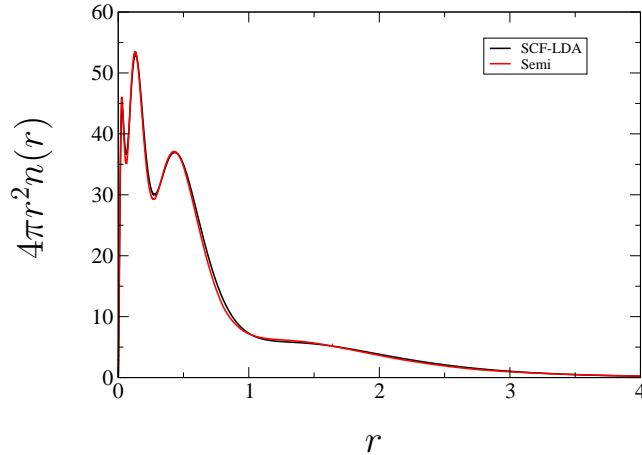


Figure 5.15: Comparison of SCF-LDA and semiclassical densities of Kr. Eq. (5.93) is used from $r = 0$ to r_1 . $(l + 1/2)^2$ is used for all orbitals instead of $l(l + 1)$.

and find they show good agreement, superficially. However, if we enlarge Fig. 5.15 and focus on the region where $r < 1.2$, we can find the phase shift and incorrect amplitude visible in

Fig. 5.16. Langer(75) stated that, “Whenever the number l is small the turning point lies

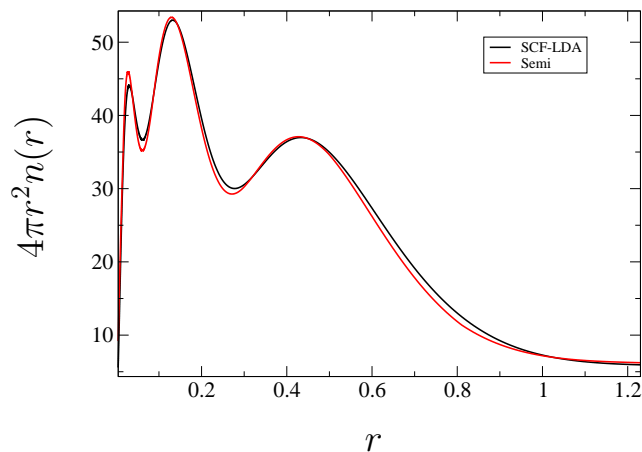


Figure 5.16: Comparison of SCF-LDA and semiclassical densities of Kr. Eq. (5.93) is used from $r = 0$ to r_t . $(l + 1/2)^2$ is used for all orbitals instead of $l(l + 1)$.

very near to the point $r = 0$, and this is true also in the case of the turning point whenever the energy is very large. The use of the formulas under such circumstances is questionable, and is generally less satisfactory than otherwise.” Also, Berry and Mount (79) mentioned “inaccuracies in Langer’s method for low l , when the turning point after the modification comes very close to the origin.”

We here adjust Langer’s modification for s and p orbitals to eliminate these effects. We use $(l + 0.53)^2$ for $l = 0$ and $(l + 0.51)^2$ for $l = 1$. Although we do not present the result in this dissertation, the semiclassical radial density becomes more accurate than the density with Langer’s original modification. This refinement seems to work for other atoms, but we need to show that this adjustment is justified.

5.8.2 Semiclassical orbital-free potential-density functional

Since $v_{s\sigma}(r)$ in Eq. (5.110) depends on the (spin)-density, we solve the KS equations iteratively and find a self-consistent solution. The flow chart of the KS-SCF procedure is depicted

in Fig. 5.17. By applying the Hohenberg-Kohn(2) theorem to the non-interacting system,

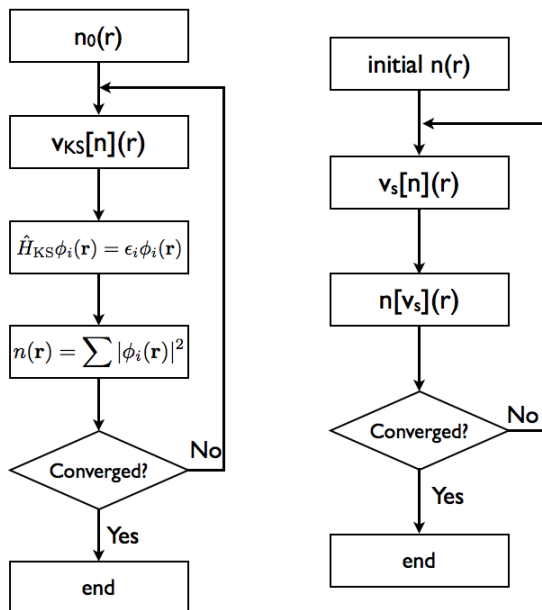


Figure 5.17: SCF procedures for KS-DFT (left) and orbital-free potential-density functional theory (right).

the KS potential, $v_{s\sigma}(r)$, which gives the ground-state spin density, $n_\sigma(r)$ for the system, is unique. If $n_\sigma(r)$ can be expressed as a functional of $v_{s\sigma}(r)$, we can state

$$n_\sigma[v_{s\sigma}](r) \xleftrightarrow{1:1} v_{s\sigma}[n_\sigma](r). \quad (5.115)$$

Using our semiclassical approximation to the density as a potential functional, we can directly obtain the radial density from a given KS potential without ever solving the KS equations. Since $v_{s\sigma}(r)$ is a density functional, we have to find a self-consistent solution. Hence we set up a new SCF procedure for orbital-free potential-density functional theory (OF-pDFT) in Fig. 5.17.

For OF-pDFT calculations, we need an initial guess for the density in order to construct $v_{s\sigma}(r)$. The initial density comes from a SCF calculation with an exact exchange (exchange-

only) (18) functional using OPMKS code(38) for Ar. In our procedure, the potential for a given l is defined as

$$v_{s\sigma}^{\text{eff}}(r; l) = v_{\text{ext}}(r) + v_{\text{H}}[n](r) + v_{\text{xc}\sigma}[n_{\uparrow}, n_{\downarrow}](r) + \frac{(l + 1/2)^2}{2r^2}, \quad (5.116)$$

where $v_{\text{xc}}(r)$ is the LDA exchange(29; 30) and correlation (VWN5)(31) functional, v_{ext} is $-Z/r$, and v_{H} is the Hartree potential. For closed-shell atoms, we use the spin-unpolarized LDA functional, and the Hartree potential can be obtained without solving the Poisson equation:

$$v_{\text{H}}(r) = \frac{Z}{r} - \frac{1}{r} \int_r^{\infty} dr' \int_{r'}^{\infty} dr'' 4\pi r'' n(r''). \quad (5.117)$$

So, from the initial density, $n_0(r)$, we calculate the LDA KS potential. Ar has $[\text{Ne}]3s^23p^6$ as its electronic configuration. To calculate the semiclassical radial density, we need $\{n, l\} = \{(3, 0), (3, 1)\}$. Then the total semiclassical radial density with the LDA KS potential will be

$$4\pi r^2 n^{\text{semi}}(r) = \sum_{\{n, l\}} 2(2l + 1) 4\pi r^2 n_{n, l}^{\text{semi}}(r). \quad (5.118)$$

The convergence criteria is the density difference (i.e., $\Delta n(r) < 10^{-5}$) between the previous and current iterations. If this condition is satisfied, then SCF is terminated and, if not, the SCF procedure will be repeated to achieve the convergence criteria.

In Fig. 5.18, we plot the LDA-SCF radial density and the converged semiclassical radial density from OF-pDFT. The semiclassical radial density still shows a slight phase shift, but this is due to the inaccuracy in Langer's method discussed in the previous Section 5.8.1.

We can also define the total energy as a potential functional. In Ref. (77), the kinetic energy for 3D spherical systems can be obtained from the virial theorem for the v -representable non-

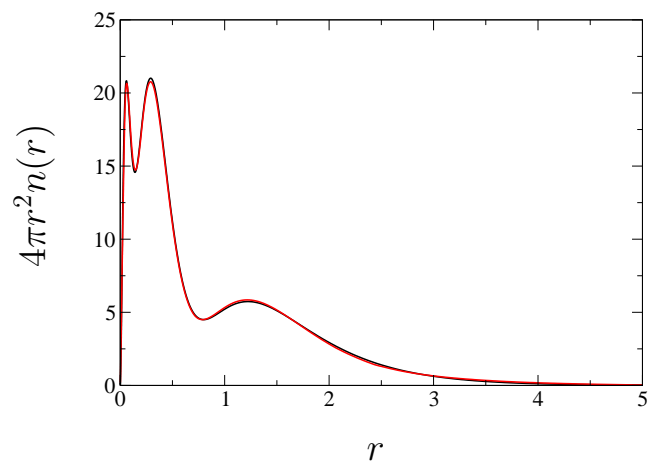


Figure 5.18: Comparison of LDA-SCF and semiclassical SCF densities of Ar.

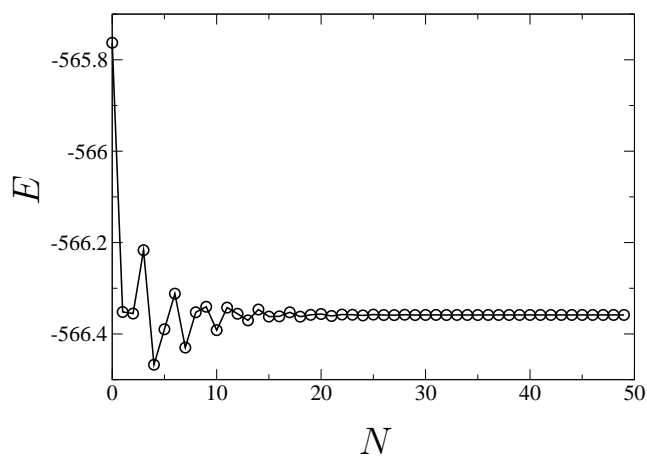


Figure 5.19: Convergence of total energies in each iterations

interacting density:

$$T_s^{\text{DF}}[v_s] = \frac{3}{2} \int d^3r \int_r^\infty dr' n[v_s](r') \frac{dv_s(r')}{dr'}. \quad (5.119)$$

So the total energy of the spherical system is

$$E[v_s] = T_s^{\text{DF}}[v_s] + E_{\text{ext}}[n[v_s]] + E_{\text{H}}[n[v_s]] + E_{\text{XC}}[n[v_s]]. \quad (5.120)$$

We plot the total energy from each iteration in Fig. 5.19. Since we use the approximate XC

(LDA) functional, the total energies are not variational. However, the total energies almost converge after 30 iterations and the energy difference is less than 4.8×10^{-6} H.

Chapter 6

Conclusion

In this dissertation, I have discussed three topics. I first explained how reasonably accurate electron affinities can be obtained via approximate density functionals. Incomplete cancellation of self-interaction in approximate density functionals results in positive HOMO energies and thus, unbound HOMO state. By studying the KS and XC potentials, I show that shifting the KS potential by a constant does not affect the total density and, therefore, the meaning of the positive HOMO becomes ambiguous. Hence, I show that an accurate density and EA can be obtained with density functional approximations, despite the positive HOMO energy. In addition, I suggest a simple and practical way to evaluate the EAs on HF and EXX densities that bind a valence electron. The results from HF and EXX densities are reasonable and slightly better than those of the traditional approaches. However, if the HF density inaccurately describes the system due to a lack of correlation, then our method will fail to get accurate EAs.

Second, I gave a condition on the KS kinetic energy. It is shown here that the asymptotic expansion of total energies with atomic number Z gives a vital condition that the non-interacting KS kinetic energy should satisfy. I construct the modified gradient expansion

approximation to the fourth order, which gives the correct asymptotic expansion coefficients. I apply this modified GEA to atoms, molecules, and the jellium surface/sphere. I find that, for atoms and molecules, our modified GEA improves the kinetic energies, when compared to those generated with TF and original GEA kinetic energy functionals. However, for the atomization process, the TF kinetic energy functional gives better mean absolute errors (0.25) than GEAs. This is because the GEA does not include quantum corrections by the turning points. I have also studied the existing kinetic energy functional approximations and found the corresponding asymptotic expansion coefficients. This modified GEA cannot be used in orbital-free density functional calculation, since if I take the functional derivative of the fourth order modified GEA to evaluate the kinetic energy potential, the derivatives of the fourth and higher terms will diverge for atoms. Furthermore, if I include the sixth order term in the GEA to improve the accuracy, the sixth order term of T^{GEA} will also diverge for atoms. Hence, the development of kinetic energy functionals based on the GEA is not appropriate.

In the final section, the uniform semiclassical Green's function using Langer's uniformization is constructed. Using a specifically chosen contour, I have derived the semiclassical density and kinetic energy density as potential functionals for 1D systems with turning points. I have demonstrated the accuracy of our semiclassical formalism for both the harmonic oscillator and the Morse potential. With the kinetic energy functional from the virial theorem, I can define the total energy as a potential functional. Since spherical 3D systems such as 3D spherical harmonic oscillators and Bohr atoms can be reduced to quasi-1D systems, I can apply our semiclassical scheme to obtain radial densities.

Also the radial part of the KS equation for real atoms is a 1D differential equation. The KS potential is a functional of the density, and the semiclassical radial density is a functional of the KS potential. Hence, I can set up a SCF procedure to find the density and the potential. For Ar, I have used the LDA XC functional for the KS potential and found the

converged, self-consistent, semiclassical radial density. The kinetic energy functional of a spherical system can also be obtained from the virial theorem, so I define the total energy potential functional for real, spherical atoms and get the converged total energy using this functional.

The semiclassical scheme is only applicable to 1D and spherical 3D systems. For general 3D problems including non-spherical systems, I need to explore other approaches, such as a path integral formalism and Gutzwillers semiclassical Green's function(82). There are many accurate approximations to $E_{xc}[n]$ such as GGAs for general 3D systems. This means that a highly accurate approximation to the density as a potential functional automatically leads to an electronic structure method that scales linearly with the number of particles, N . I will then be able to study large biological molecules with orbital-free potential-density functional theory, avoiding any QM/MM or empirical force field methods.

Bibliography

- [1] C. Fiolhais, F. Nogueira, and M. Marques, editors, *A Primer in Density Functional Theory*, Springer-Verlag, NY, 2003.
- [2] P. Hohenberg and W. Kohn, *Phys. Rev.* **136**, 864 (1964).
- [3] W. Kohn and L. J. Sham, *Phys. Rev.* **140**, 1133 (1965).
- [4] J. Morrison Galbraith and H. F. Schaefer, III, *J. Chem. Phys.* **105**, 862 (1996).
- [5] N. Rösch and S. B. Trickey, *J. Chem. Phys.* **106**, 8940 (1997).
- [6] Y. Wang and E. Carter, Orbital-free kinetic energy density functional theory, in *Theoretical Methods in Condensed Phase Chemistry (Theoretical Methods in Chemistry and Physics)*, edited by S. Schwartz, Kluwer, Dordrecht, 2000.
- [7] K. Burke, Exact conditions, in *Time-Dependent Density Functional Theory (Lecture Notes in Physics)*, edited by M. Marques et al., Springer, 2006.
- [8] W. Yang, P. W. Ayers, and Q. Wu, *Phys. Rev. Lett.* **92**, 146404 (2004).
- [9] E. K. U. Gross and C. R. Proetto, *J. Chem. Theory Comput.* **5**, 844 (2009).
- [10] P. Elliott, D. Lee, A. Cangi, and K. Burke, *Phys. Rev. Lett.* **100**, 256406 (2008).
- [11] S. C. Miller and R. H. Good, *Phys. Rev.* **91**, 174 (1953).
- [12] W. H. Miller, *J. Chem. Phys.* **48**, 464 (1968).
- [13] H. B. Shore, J. H. Rose, and E. Zaremba, *Phys. Rev. B* **15**, 2858 (1977).
- [14] J. Toulouse, R. Assaraf, and C. J. Umrigar, *J. Chem. Phys.* **126**, 244112 (2007).
- [15] A. A. Jarecki and E. R. Davidson, *Chem. Phys. Lett.* **300**, 44 (1999).
- [16] J. C. Rienstra-Kiracofe, G. S. Tschumper, H. F. Schaefer, S. Nandi, and G. B. Ellison, *Chem. Rev.* **102**, 231 (2002).
- [17] J. P. Perdew and S. Kurth, Density Functionals for Non-Relativistic Coulomb Systems in the New Century, in *Primer in density functional theory (Lecture Notes in Physics Vol.620)*, pages 1–55, Springer-Verlag, Berlin, Germany, 2003.

- [18] J. D. Talman and W. F. Shadwick, *Phys. Rev. A* **14**, 36 (1976).
- [19] F. Della Sala and A. Görling, *J. Chem. Phys.* **115**, 5718 (2001).
- [20] M. Weimer, F. Della Sala, and A. Görling, *Chem. Phys. Lett.* **372**, 538 (2003).
- [21] A. Görling and M. Ernzerhof, *Phys. Rev. A* **51**, 4501 (1995).
- [22] D. Rappoport, N. R. M. Crawford, F. Furche, and K. Burke, Approximate Density Functionals: Which Should I Choose?, in *Computational Inorganic and Bioinorganic Chemistry*, pages 159–172, Wiley, Chichester, UK, 2009.
- [23] K. Schwarz, *Chem. Phys. Lett.* **57**, 605 (1978).
- [24] J. C. Slater, *Quantum Theory of Molecules and Solids, Vol. 4*, McGraw-Hill, New York, 1974.
- [25] T. H. Dunning, Jr., *J. Chem. Phys.* **90**, 1007 (1989).
- [26] D. E. Woon and T. H. Dunning, Jr., *J. Chem. Phys.* **98**, 1358 (1993).
- [27] J. P. Perdew and A. Zunger, *Phys. Rev. B* **23**, 5048 (1981).
- [28] L. A. Cole and J. P. Perdew, *Phys. Rev. A* **25**, 1265 (1982).
- [29] P. A. M. Dirac, *Proc. R. Soc. London, Ser. A* **123**, 714 (1929).
- [30] J. C. Slater, *Phys. Rev.* **81**, 385 (1951).
- [31] S. H. Vosko, L. Wilk, and M. Nusair, *Can. J. Phys.* **58**, 1200 (1980).
- [32] J. P. Perdew, K. Burke, and M. Ernzerhof, *Phys. Rev. Lett.* **77**, 3865 (1996).
- [33] A. D. Becke, *J. Chem. Phys.* **98**, 5648 (1993).
- [34] C. Lee, W. Yang, and R. G. Parr, *Phys. Rev. B* **37**, 785 (1988).
- [35] J. P. Perdew, M. Ernzerhof, and K. Burke, *J. Chem. Phys.* **105**, 9982 (1996).
- [36] J. Tao, J. P. Perdew, V. N. Staroverov, and G. E. Scuseria, *Phys. Rev. Lett.* **91**, 146401 (2003).
- [37] TURBOMOLE V6.2 2010, a development of University of Karlsruhe and Forschungszentrum Karlsruhe GmbH, 1989-2007, TURBOMOLE GmbH, since 2007; available from <http://www.turbomole.com>.
- [38] OPMKS: Atomic DFT Program, University of Frankfurt, Germany, E. Engel.
- [39] J. P. Perdew, What Do the Kohn-Sham Orbitals Mean? How Do Atoms Dissociate?, in *Density Functional Methods in Physics*, page 265, Plenum, NY, USA, 1985.
- [40] J. Simons, *J. Phys. Chem. A* **112**, 6401 (2008).

- [41] R. M. Dreizler and E. K. U. Gross, *Density Functional Theory: An Approach to the Quantum Many-Body Problem*, Springer-Verlag, 1990.
- [42] V. Karasiev, R. Jones, S. Trickey, and F. Harris, Recent advances in developing orbital-free kinetic energy functionals, in *New Developments in Quantum Chemistry*, edited by J. Paz and A. Hernandez, chapter 2, pages 25–54, Transworld Research Network, Kerala, India, 2009.
- [43] J. Schwinger, Phys. Rev. A **22**, 1827 (1980).
- [44] J. Schwinger, Phys. Rev. A **24**, 2353 (1981).
- [45] J. P. Perdew, L. A. Constantin, E. Sagvolden, and K. Burke, Phys. Rev. Lett. **97**, 223002 (2006).
- [46] E. H. Lieb, Rev. Mod. Phys. **53**, 603 (1981).
- [47] B.-G. Englert and J. Schwinger, Phys. Rev. A **32**, 26 (1985).
- [48] C. Fefferman and L. Seco, Bull. Amer. Math. Soc. **23**, 525 (1990).
- [49] C. Fefferman and L. Seco, Adv. Math. **107**, 1 (1994).
- [50] H. Siedentop and R. Weikard, Comm. Math. Phys. **112**, 471 (1987).
- [51] M. Levy and J. P. Perdew, Phys. Rev. A **32**, 2010 (1985).
- [52] E. H. Lieb and B. Simon, Phys. Rev. Lett. **31**, 681 (1973).
- [53] G. L. Oliver and J. P. Perdew, Phys. Rev. A **20**, 397 (1979).
- [54] D. Kirzhnits, Sov. Phys. JETP **5**, 64 (1957).
- [55] C. H. Hodges, Can. J. Phys. **51**, 1428 (1973).
- [56] J. Scott, Philos. Mag. **43**, 859 (1952).
- [57] S. S. Iyengar, M. Ernzerhof, S. N. Maximoff, and G. E. Scuseria, Phys. Rev. A **63**, 052508 (2001).
- [58] J. P. Perdew and L. A. Constantin, Phys. Rev. B **75**, 155109 (2007).
- [59] J. P. Perdew, Y. Wang, and E. Engel, Phys. Rev. Lett. **66**, 508 (1991).
- [60] E. Engel, P. LaRocca, and R. M. Dreizler, Phys. Rev. B **49**, 16728 (1994).
- [61] F. Tran and T. Wesolowski, Int. J. Quant. Chem. **89**, 441 (2002).
- [62] B.-G. Englert and J. Schwinger, Phys. Rev. A **32**, 47 (1985).
- [63] E. K. U. Gross and R. M. Dreizler, Phys. Rev. A **20**, 1798 (1979).

- [64] R. Latter, Phys. Rev. **99**, 510 (1955).
- [65] Y. Tal and M. Levy, Phys. Rev. A **23**, 408 (1981).
- [66] W. Press, B. P. Flannery, S. A. Teukolsky, and W. T. Vetterling, *Numerical Recipes in FORTRAN 77*, Cambridge University Press, 1992.
- [67] S. Kotochigova, Z. H. Levine, E. L. Shirley, M. D. Stiles, and C. W. Clark, Phys. Rev. A **55**, 191 (1997).
- [68] S. Kotochigova, Z. H. Levine, E. L. Shirley, M. D. Stiles, and C. W. Clark, Phys. Rev. A **56**, 5191 (1997).
- [69] J. P. Perdew et al., Phys. Rev. Lett. **100**, 136406 (2008).
- [70] J. P. Perdew et al., Phys. Rev. Lett. **102**, 039902 (2009).
- [71] J. Perdew and K. Schmidt, Jacob's ladder of density functional approximations for the exchange-correlation energy, in *Density Functional Theory for Materials*, edited by V. Van Doren, K. Van Alsenoy, and P. Geerlings, American Institute of Physics, Melville, NY, 2001.
- [72] D. García-Aldea and J. E. Alvarellós, Phys. Rev. A **77**, 022502 (2008).
- [73] A. Cangi, D. Lee, P. Elliott, and K. Burke, Phys. Rev. B **81**, 235128 (2010).
- [74] W. Kohn and L. J. Sham, Phys. Rev. **137**, A1697 (1965).
- [75] R. E. Langer, Phys. Rev. **51**, 669 (1937).
- [76] M. Abramowitz and I. A. Stegun, *Handbook of Mathematical Functions*, Dover, 1972.
- [77] E. Sim, J. Larkin, K. Burke, and C. W. Bock, J. Chem. Phys. **118**, 8140 (2003).
- [78] P. M. Morse, Phys. Rev. **34**, 57 (1929).
- [79] M. V. Berry and K. E. Mount, Rep. Prog. Phys. **35**, 315 (1972).
- [80] M. F. Herman and R. Currier, Chem. Phys. Lett. **114**, 411 (1985).
- [81] T. Koike and H. J. Silverstone, J. Phys. A: Math. Theor. **42**, 495206 (2009).
- [82] J. Roccia and M. Brack, Phys. Rev. Lett. **100**, 200408 (2008).

Appendices

A Construction of modified GEA

To construct the modified GEA (MGEA) which gives the second and third coefficients in the asymptotic expansion exactly, we multiply the $T^{(2)}$ and $T^{(4)}$ terms of the gradient expansion by new coefficients a and b respectively, i.e. $a = 1, b = 0$ would simply be the second order GEA.

$$T^{MGEA} = T^{(0)} + aT^{(2)} + bT^{(4)} \quad (\text{A.1})$$

$$T^{MGEA} - T^{(0)} = aT^{(2)} + bT^{(4)} \quad (\text{A.2})$$

$$= (c_1^{MGEA} - c_1^{\text{TF}})Z^2 + (c_2^{MGEA} - c_2^{\text{TF}})Z^{\frac{5}{3}} \quad (\text{A.3})$$

If $a=1$ and $b=0$, then the above equation gives T_{2nd}^{GEA}

$$\begin{aligned} T^{(2)} &= T_{2nd}^{GEA} - T^{(0)} \\ &= (c_1^{GEA2} - c_1^{\text{TF}})Z^2 + (c_2^{GEA2} - c_2^{\text{TF}})Z^{\frac{5}{3}} \end{aligned} \quad (\text{A.4})$$

If a=1 and b=1, then the above equation gives T_{4th}^{GEA}

$$\begin{aligned} T^{(2)} + T^{(4)} &= T_{4th}^{GEA} - T^{(0)} \\ &= (c_1^{GEA4} - c_1^{TF})Z^2 + (c_2^{GEA4} - c_2^{TF})Z^{\frac{5}{3}} \end{aligned} \quad (A.5)$$

According to the *linearity* between the coefficients of Z-expansion and the 2nd/4th GEA, then there will be a matrix to map (a,b) into $(c_1 - c_1^{TF}, c_2 - c_2^{TF})$

$$\begin{bmatrix} c_1 - c_1^{TF} \\ c_2 - c_2^{TF} \end{bmatrix} = \begin{bmatrix} m_{11} & m_{12} \\ m_{21} & m_{22} \end{bmatrix} \begin{bmatrix} a \\ b \end{bmatrix} \quad (A.6)$$

$$\begin{bmatrix} c_1^{GEA2} - c_1^{TF} \\ c_2^{GEA2} - c_2^{TF} \end{bmatrix} = \begin{bmatrix} m_{11} & m_{12} \\ m_{21} & m_{22} \end{bmatrix} \begin{bmatrix} 1 \\ 0 \end{bmatrix} \quad (A.7)$$

$$\begin{bmatrix} c_1^{GEA4} - c_1^{TF} \\ c_2^{GEA4} - c_2^{TF} \end{bmatrix} = \begin{bmatrix} m_{11} & m_{12} \\ m_{21} & m_{22} \end{bmatrix} \begin{bmatrix} 1 \\ 1 \end{bmatrix} \quad (A.8)$$

Hence,

$$\begin{bmatrix} m_{11} & m_{12} \\ m_{21} & m_{22} \end{bmatrix} = \begin{bmatrix} c_1^{GEA2} - c_1^{TF} & c_1^{GEA4} - c_1^{GEA2} \\ c_2^{GEA2} - c_2^{TF} & c_2^{GEA4} - c_2^{GEA2} \end{bmatrix} \quad (A.9)$$

Using the coefficients in Table. 4.1, I could get the M matrix and the corresponding (a,b).

$$\begin{bmatrix} m_{11} & m_{12} \\ m_{21} & m_{22} \end{bmatrix} = \begin{bmatrix} 0.1246 & 0.0162 \\ -0.0494 & 0.0071 \end{bmatrix} \quad (A.10)$$

If (c_1^{MGEA}, c_2^{MGEA}) are chosen to give exact expansion, i.e. $(c_1^{MGEA}, c_2^{MGEA}) = (-0.5, 0.2699)$, then

$$\begin{bmatrix} c_1^{MGEA} - c_1^{TF} \\ c_2^{MGEA} - c_2^{TF} \end{bmatrix} = \begin{bmatrix} 0.1608 \\ -0.1155 \end{bmatrix} \quad (\text{A.11})$$

$$\begin{bmatrix} a \\ b \end{bmatrix} = \begin{bmatrix} 1.789 \\ -3.841 \end{bmatrix} \quad (\text{A.12})$$

Using these coefficients, we can find:

$$T^{MGEA4}[n] = T^{TF}[n] + 1.789 T^{(2)}[n] - 3.841 T^{(4)}[n]. \quad (\text{A.13})$$